

1

2 **New Insights From The Jülich Ozone-Sonde Intercomparison**  
3 **Experiments: Calibration Functions Traceable To One Ozone Reference**  
4 **Instrument**

5 Herman G.J. Smit<sup>1</sup>, Deniz Poyraz<sup>2</sup>, Roeland Van Malderen<sup>2</sup>, Anne M. Thompson<sup>3,4</sup>, David W. Tarasick<sup>5</sup>, Ryan M.  
6 Stauffer<sup>3</sup>, Bryan J. Johnson<sup>6</sup>, Debra E. Kollonige<sup>3,7</sup>

7

8 <sup>1</sup>Forschungszentrum Jülich, Institute of Energy and Climate Research, IEK-8: Troposphere, Jülich, 52425, Germany

9 <sup>2</sup>Royal Meteorological Institute of Belgium & Solar-Terrestrial Centre of Excellence, Uccle, Belgium

10 <sup>3</sup>Atmospheric Chemistry and Dynamics Laboratory, NASA/GSFC, Greenbelt, MD, USA

11 <sup>4</sup>University of Maryland Baltimore County, Baltimore, MD, USA,

12 <sup>5</sup>Environment and Climate Change Canada, Downsview, ON, Canada

13 <sup>6</sup>Global Monitoring Laboratory, NOAA Earth System Research Laboratory, Boulder, CO, USA

14 <sup>7</sup>Science Systems and Applications, Inc, Lanham, MD, USA

15

16 *Correspondence to:* Herman G.J. Smit (h.smit@fz-juelich.de)

17

18 **Abstract**

19 Although in principle the ECC (Electrochemical Concentration Cell) ozonesonde is an absolute measuring device, in  
20 practice it has several “artefacts” which change over the course of a flight. Most of the artefacts have been corrected in the  
21 recommendations of the Assessment of Standard Operating Procedures for Ozone Sondes Report (GAW Report No. 268),  
22 giving an overall uncertainty of 5-10% throughout the profile. However, the conversion of the measured cell current into the  
23 sampled ozone concentration still needs to be quantified better, using time-varying background current and more appropriate  
24 pump efficiencies. We describe an updated methodology for ECC sonde data processing that is based on JOSIE 2009/2010  
25 and JOSIE 2017-SHADOZ test chamber data. The methodology resolves the slow and fast time responses of the ECC  
26 ozonesonde and in addition apply calibration functions to make the sonde data traceable to the JOSIE ozone reference UV-  
27 photometer (OPM). The stoichiometry ( $O_3/I_2$ ) factors and their uncertainties along with fast and slow reaction pathways for  
28 the different sensing solution types used in the global ozonesonde network are determined. Experimental evidence is given  
29 for treating the background current of the ECC-sensor as the superposition of a constant ozone independent component ( $I_{B0}$ ,  
30 measured before ozone exposure in the sonde preparation protocol) and a slow time-variant ozone-dependent current  
31 determined from the initial measured ozone current using a first-order numerical convolution. The fast sensor current is  
32 refined using the time response determined in sonde preparation with a first order deconvolution scheme. Practical  
33 procedures for initializing the numerical deconvolution and convolution schemes to determine the slow and fast ECC  
34 currents are given. Calibration functions for specific ozonesondes and sensing solution type combinations were determined  
35 by comparing JOSIE 2009/2010 and JOSIE-2017-SHADOZ profiles with the JOSIE-OPM. With fast and slow currents  
36 resolved and the new calibration functions, a full uncertainty budget is obtained. The time responses correction methodology  
37 makes every ozonesonde record traceable to one standard, i.e. the OPM of JOSIE, enabling the goal of a 5% relative  
38 uncertainty to be met throughout the global ozone network.

39  
40

**Deleted:** into the measured cell current

**Deleted:** has not been fully quantified, resulting in time-varying background current and pump efficiencies

**Deleted:** the

**Deleted:** the

**Deleted:** ozone reference UV-photometer

**Deleted:** (

**Deleted:** )

49 **1 Introduction**

50 Although it is a minor trace gas constituent of the Earth’s atmosphere, ozone plays several essential roles in its chemistry and  
51 physics. In the stratosphere, where about 90% of the total ozone amount resides, ozone protects life on Earth by absorbing  
52 the harmful ultraviolet (UV) radiation from the sun, adding heat to the stratosphere. In the upper troposphere, ozone is an  
53 important absorber of infrared radiation, acting as a powerful greenhouse gas (IPCC-Climate Change, 2013, 2023). Ozone is  
54 the primary source of the hydroxyl (OH) radical in the troposphere, controlling the lifetime of hundreds of pollutants  
55 (Seinfeld and Pandis, 2016), and determining its oxidizing capacity (Thompson, 1992). The stratosphere is a natural source  
56 of tropospheric ozone but approximately half of the ozone in the troposphere is formed photochemically when combustion  
57 (vehicular, industrial or pyrogenic) processes release NO<sub>x</sub>, (NO + NO<sub>2</sub> = NO<sub>x</sub>), carbon monoxide (CO) and hydrocarbons  
58 (also referred to as volatile organic compounds (VOC)) that react through free radical cycles in the presence of UV. VOC  
59 may also originate from combustion or natural sources, the latter predominantly from vegetation and to a lesser extent from  
60 the ocean. Surface ozone is considered a pollutant with adverse impacts on human and animal health (e.g., respiratory  
61 problems) and on vegetation (Mills et al., 2018) and is a primary marker for “Air Quality,” setting the scale for Good, Fair,  
62 and Unhealthy definitions used by local Air Quality agencies (Garner and Thompson, 2013). The photochemistry of ozone  
63 pollution or “smog” was first identified by Haagen-Smit (1952) in the early 1950s and was found to typically occur at very  
64 high concentrations of VOC and NO<sub>x</sub>, whereby organic particles also playing an important role, (e.g. Seinfeld and Pandis,  
65 2016); surface ozone measurements became widespread as regions or nations enacted regulations to mitigate episodes of  
66 high ozone.

67 Measurements of stratospheric ozone gained attention in the 1960s and 1970s when it was recognized that natural levels of  
68 ozone were regulated by catalytic cycles involving nitrogen oxides (NO<sub>x</sub>, N<sub>2</sub>O<sub>5</sub>, NO<sub>3</sub> and HNO<sub>3</sub>), hydrogen oxides (with H<sub>2</sub>O  
69 vapor a source of OH and HO<sub>2</sub>, HO<sub>x</sub> = OH+HO<sub>2</sub>) and halogens (XO and XO<sub>2</sub>, where X was Cl or Br derived from oceanic  
70 methyl chloride and methyl bromide). Anthropogenic perturbations of these cycles were investigated when it was recognized  
71 that emissions of N- and Cl-containing compounds by rockets and high-altitude aircraft could threaten stratospheric ozone  
72 (Crutzen, 1970; Stolarski and Cicerone, 1974). A worse threat was hypothesized when it was realized that  
73 chlorofluorocarbons (CFCs) present in the atmosphere (Lovelock et al., 1973), but relatively inert in the troposphere could  
74 enter the stratosphere and destroy ozone photochemically there (Molina and Rowland, 1974). Perturbed stratospheric ozone  
75 chemistry by CFCs was a cause for alarm, leading to first regulations in CFC usage in the 1970s. However, it was not until  
76 ground-based total ozone monitoring (Farman et al., 1985) discovered catastrophic springtime ozone loss over Antarctica in  
77 1984-1985 that international action was taken to phase out Ozone Depleting Substances through the 1987 signing of the  
78 Montreal Protocol (UNEP-Ozone Secretariat, 14<sup>th</sup> edition, 2020). Implementation of the Montreal Protocol and its follow-on  
79 Amendments require governments to monitor ozone, reporting every four years to the World Meteorological Organization  
80 (WMO) and United Nations Environment Programme (UNEP) in Scientific Assessments on total column ozone, its vertical  
81 distribution and attribution of long-term. Since 1991 there have been nine UNEP/WMO Scientific Assessments, with the  
82 most recent report released in 2022 (WMO/UNEP, 2023).

83 Global monitoring of total ozone has relied on satellite instruments since the 1970s but ground-based instrumentation  
84 deployed on all continents still provides ground-truth. In particular, ozonesondes are essential for satellite algorithms and  
85 validation of satellite-derived profiles and reanalysis products (Wang et al., 2020; Thompson et al., 2022). Balloon-borne  
86 ozonesondes, flown together with radiosondes, make relatively inexpensive, accurate, all-weather measurements of the  
87 ozone concentrations from the ground to 30 km or higher, with ~100 m vertical resolution (Smit, 2014). The electrochemical  
88 concentration cell (ECC) ozonesonde has been deployed for more than 50 years with approximately 60 stations currently  
89 launching on all continents (global ozonesonde network shown in figure 1-2 in GAW Report No.268, 2021; Thompson et al.,  
90 2022; Stauffer et al., 2022). Ozonesonde data constitute the most important record for deriving ozone trends throughout both

Deleted:  
Deleted: was  
Deleted: worked out in the 1950s

Deleted: ~

95 [the](#) stratosphere and troposphere, particularly in the climate-sensitive altitude region near the tropopause where satellite  
96 measurements are most uncertain. Strategic ozonesonde networks like MATCH and IONS (Intensive Ozonesonde Network  
97 Studies) have been organized to support aircraft campaigns in characterizing photochemical and dynamical interactions  
98 affecting vertical and regional ozone distributions (Thompson et al., 2007a and 2011; Tarasick et al., 2010).

#### 99 **1.1 Establishing Quality Assurance/Quality Control (QA/QC) practices for ozonesondes (1996-2021)**

100 Despite the advantages of ozonesonde profiles, there is a challenge in that each ozonesonde instrument is unique, typically  
101 launched only once, and it must be carefully prepared prior to launch in order to obtain accurate data. Processing of the final  
102 measurement is carried out using certain parameters determined pre-launch. In addition, there are two manufacturers of  
103 ozonesondes that show systematic offsets relative to each other. Further biases in ozonesonde datasets can occur because  
104 three variants of the sensing solution that produce the ECC current signal from the ozone are currently in use. The  
105 ozonesonde community has created guidelines for operations and data processing applicable to the range of instrument and  
106 sensing solution types used in the global ECC-sonde network. When the guidelines are followed it is possible for  
107 consistently high-quality data to be collected across the global network.

108 The creation of guidelines or “best practices” has evolved over the past 20 years in a process referred to as the Assessment of  
109 Standard Operating Procedures (SOP) for Ozonesondes (ASOPOS) and organized through the WMO Global Atmosphere  
110 Watch (GAW). The key element of ASOPOS was the establishment of the World Calibration Centre for Ozone Sonde  
111 (WCCOS) with a custom-designed Environmental Simulation Facility (ESF) at the Research Centre in Jülich, Germany, in  
112 1995 (GAW Report No.104, 1994; Smit et al., 2000). The ESF consists of an absolute ozone measuring reference, a fast  
113 response (2s), accurate (2-3%), dual beam UV-absorption ozone photometer (OPM) (Proffitt and McLaughlin, 1983)  
114 attached to the chamber that enables control of pressure, temperature and ozone concentration simulating flight conditions of  
115 an ozone sounding up to 35 km over ~ 2 hours (Smit et al., 2007). Up to four ozonesonde instruments at once can be  
116 intercompared through this process. Simulations in the ESF included conditions of polar, midlatitude, subtropical and  
117 tropical sonde launches. Other aspects of sonde operations, e.g., response times to rapid changes in ozone concentration, are  
118 also tested in the ESF. Since 1996, nine Jülich OzoneSonde Intercomparison Experiment (JOSIE) campaigns have been  
119 conducted at WCCOS and documented in a series of publications (Smit and Kley, GAW Report No. 130, 1998) for JOSIE-  
120 1996; JOSIE-1998 (Smit and Sträter, GAW Report No. 157, 2004a), JOSIE-2000 (Smit and Sträter, GAW Report No. 158,  
121 2004b; Smit et al., 2007; Thompson et al., 2007b); JOSIE-2009/2010; JOSIE-2017 (Thompson et al., 2019). The first three  
122 JOSIEs, which tested several non-ECC instruments as well as Science Pump Corporation (SPC) and ENSCI ECC  
123 instruments, showed the ECC-sonde to be more accurate. After JOSIE-2000 only ECC-sondes were tested in the WCCOS.  
124 In 2004 a the WMO/BESOS (Balloon Experiment on Standards for OzoneSondes) field campaign, carried out in Laramie  
125 (Wyoming, USA) deployed a large gondola with 18 ozonesondes and the OPM of WCCOS (Deshler et al., 2008) with results  
126 similar to JOSIE-2000. These early experiments demonstrated that high precision and accuracy depend not only on sonde  
127 manufacturer and sensing solution strength, but also on pre-launch preparation details. Smit et al. (2007) concluded that  
128 standardisation of operating procedures for ECC sondes yields a precision better than  $\pm$  (3-5) % and an accuracy of about  
129  $\pm$ (5-10)% up to 30 km altitude.

130 In 2004 an expert team of ozonesonde operators, data providers and manufacturers formally instituted the ASOPOS to  
131 analyse the results of BESOS and the JOSIE campaigns up to that time. The ASOPOS goal was to ensure consistency of data  
132 quality across stations and within individual station time series by specifying how to prepare and operate the ozonesonde  
133 instrument and to accurately process and report profile data. The first set of SOP recommended by ASOPOS, based on the  
134 JOSIE campaigns from 1996 to 2000 and BESOS, was published online in 2012 and as GAW Report No. 201 in 2014 (Smit  
135 and ASOPOS 1.0 Panel). To make (historical) ozonesonde time series records compliant with the ASOPOS standards, an



136 OzoneSonde Data Quality Assessment (O3S-DQA) activity was initiated in 2011 within the framework of SI2N<sup>1</sup>, resulting in  
137 procedures for “homogenizing” data and estimating uncertainties (Smit and O3S-DQA Panel, 2012; [https://www.wccos-  
139 josie.org/o3s-dqa](https://www.wccos-<br/>138 josie.org/o3s-dqa)); transfer functions in support of the guidelines were documented in Deshler et al. (2017). Within several  
140 years roughly half of the global network stations had reprocessed their data (Tarasick et al., 2016; Van Malderen et al., 2016;  
141 Thompson et al., 2017; Sterling et al., 2018; Witte et al., 2017, 2018, 2019; Ancellet et al., 2022). Comparisons between  
142 ~~original and homogenized data allowed elimination of significant systematic errors~~, particularly where changes in technique  
and/or equipment had been made.

**Deleted:** original and homogenized data showed that significant systematic errors were eliminated

143 The homogenised time series were based on having raw currents from the ozonesonde cells, a prerequisite for the analysis  
144 and processing methods of the present paper. However, the ozonesonde community agreed that several issues were  
145 unresolved. These included the complexity of the so-called “background current” characterized during the preparation and  
146 the lack of traceability of the archived ozone profile to an absolute standard. A JOSIE-2017 campaign was designed to  
147 address these concerns. In addition to the tests of prior JOSIEs, the 2017 tests focused on a single regime, tropical profiles, to  
148 gather a larger set of statistics. A special challenge of tropical soundings is that near the tropopause the ozone ~~concentrations  
149 can be very low such that the signal to noise is very small (Thompson et al., 2007b), causing large relative uncertainties in  
150 the ozonesonde readings (Smit et al., 2007)~~. JOSIE-2017 (also called JOSIE-SHADOZ) was carried out with eight SHADOZ  
151 operators who supplied their home-prepared sensing solutions, following their own preparation procedures for half the  
152 simulations (Thompson et al., 2019). The other half of the simulations tested a lower-buffer variant of the sensing solution  
153 with the WMO/GAW SOP. The overall results of JOSIE-2017 resembled those of the 1996-2000 JOSIE and BESOS. In  
154 other words, the offsets of the various instrument-sensing solution types (SST) from the OPM reference and associated  
155 biases of ECC sonde instruments and SST had not changed over more than 20 years.

**Deleted:** typically

**Deleted:** giving

**Deleted:** artefact low readings

**Deleted:** Vömel

**Deleted:** 2020

156 An ASOPOS 2.0 Panel formed in 2018 to review the JOSIE-2017 campaign data along with lessons learned from  
157 reprocessed datasets and the JOSIE 2009/2010 results. ASOPOS 2.0 published GAW Report No. 268, “Ozonesonde  
158 Measurement Principles and Best Operational Practices” (Smit, Thompson and ASOPOS, 2021; hereafter referred to as  
159 GAW Report No. 268) as an update to GAW Report No. 201. The newer report gives the same recommendations as GAW  
160 Report No. 201 on sonde manufacturer-SST combinations, but stricter and more unified SOP. The latter consist of more  
161 detailed recommendations based on physical principles of the ozonesonde measurement. More explicit procedures are given  
162 for data quality indicators, hardware usage and maintenance and metadata. GAW Report No. 268 also specified for the first  
163 time how to report ozone profiles traceable to the standard OPM. However, the issues of a time-varying background current,  
164 specification of uncertainties in the ozone measurement (and related pump efficiencies) required analysis beyond GAW  
165 Report No. 268 before consensus could be reached on data-processing recommendations. That is the scope of this paper.

## 166 1.2 Addressing residual ozonesonde QA/QC issues from WMO/GAW 268. Outline of paper

167 Chapter 3 of GAW Report No. 268 draws on the Tarasick et al. (2021) review of ozonesonde performance characteristics.  
168 Both documents point out that the greatest barriers to reducing uncertainties in the final ozone measurement derive from (1)  
169 the use of improper pump efficiencies and (2) a background current that varies with ozone exposure (hence with time) over  
170 the course of the balloon ascent. The current paper revisits fundamentals of the ozonesonde measurement to overcome these  
171 two shortcomings. The here reported methodology to resolve the fast and slow time responses builds on an earlier study by  
172 Imai et al. (2013), and more recently on the work by Tarasick et al. (2021) and Vömel et al. (2020). We first give a more  
173 detailed description of the physical and chemical origin of the ECC ozonesonde signal (Section 2), illustrated with laboratory

<sup>1</sup> This is a joint initiative under the auspices of SPARC (Stratosphere–troposphere Processes And their Role in Climate), the International Ozone Commission (IO3C), the ozone focus area of the Integrated Global Atmospheric Chemistry Observations (IGACO-O3) programme, and the Network for Detection of Atmospheric Composition Change (NDACC). For simplicity, an acronym of acronyms, SI2N, was adopted.

181 measurements from the Uccle, Belgium, ozonesonde station. Section 3 first corrects for the background signal composed of  
182 (i) a constant physical component ( $I_{B0}$ ) and (ii) a small and slow varying (time constant 25 min) chemical component that  
183 varies with ozone exposure. The remaining fast component of the signal is then corrected by deconvolution with an  
184 exponential decay with a time constant between 20 and 30s. Although the approach is similar to Vömel et al. (2020), an  
185 advantage of our updated method is that it is developed from and applied to dedicated JOSIE chamber data (JOSIE  
186 2009/2010) that used consistently prepared ozonesondes, with detailed in-flight and post-flight measurements and metadata.  
187 Second, the simultaneous OPM measurements in the simulation chamber serve as reference data for determining key  
188 parameters of the method, e.g. the contribution of the slow component to the overall signal. In Section 4, the OPM reference  
189 data are used to evaluate the updated method with comparisons to the conventional method. For these analyses,  
190 measurements from all JOSIE campaigns, covering a range of simulated environments are used. Comparing residuals of the  
191 corrected ozonesonde profiles to the OPM profiles allows us to determine a set of the calibration functions for each  
192 instrument-SST combination (Section 5) and to estimate uncertainties of the updated time response correction (TRC) method  
193 (Section 6). The TRC method is implemented with actual sounding data in Section 7 for ascent and descent profiles at  
194 tropical, mid-latitude and polar (Antarctic) stations and improvements with respect to the conventional approach are  
195 quantified. A summary and outlook appear in Section 8.

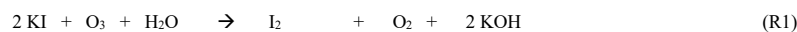
Formatted: Font: Italic

Formatted: Subscript

## 196 2 Physical and Chemical Origins of the ECC Ozonesonde Signal

### 197 2.1 Principle of Operation

198 The ECC (=Electrochemical Concentration Cell) ozonesonde, developed by Komhyr (1969), uses an electrochemical method  
199 to measure ozone which is based on the titration of ozone in a neutral buffered potassium iodide (NBKI) sensing solution  
200 according to the redox reaction (R1):



202  
203 A neutral  $\text{pH} \approx 7$  is obtained through the addition of a phosphate buffer ( $\text{NaH}_2\text{PO}_4 \cdot \text{H}_2\text{O}$  and  $\text{Na}_2\text{HPO}_4 \cdot 12\text{H}_2\text{O}$ )  
204 The titration involves a coulometric method employing electrochemical cells to determine the amount of generated “free”  
205 iodine ( $I_2$ ) per unit time through conversion into an electrical current at a depolarizing cathode electrode. The actual ECC  
206 component of the ozone sensor, made of Teflon or molded plastic, consists of two chambers. Each chamber contains a  
207 platinum (Pt) mesh electrode that serves as cathode or anode. The chambers are immersed in a KI-solution of different  
208 concentrations and linked together to provide an ion pathway and to prevent mixing of the cathode and anode concentrations.  
209

210 Continuous operation is achieved by a small nonreactive gas sampling pump (Komhyr 1967) forcing ozone in ambient air  
211 through the cathode cell that contains a lower-concentration KI-sensing solution, causing an increase of “free iodine” ( $I_2$ )  
212 according to the redox reaction (1). Transported by the stirring action of the air bubbles, the free  $I_2$  contacts the Pt-cathode  
213 and is converted to  $2 \text{I}^-$  through the uptake of two electrons. At the Pt-anode surface,  $\text{I}^-$  is converted to  $I_2$  through the release  
214 of two electrons. The overall cell reaction is:



216  
217 The electrical current  $I_M$  ( $\mu\text{A}$ ) generated in the external circuit of the electrochemical cell is directly related to the uptake rate  
218 of ozone in the sensing solution. By knowing the gas volume flow rate  $\Phi_{p0}$  [ $\text{cm}^3\text{s}^{-1}$ ] of the air sampling pump and its

221 temperature  $T_P$  (K), the electrical cell current  $I_M$  ( $\mu\text{A}$ ), after subtracting a background current  $I_B$  ( $\mu\text{A}$ ), is converted to the  
222 ozone partial pressure  $P_{O_3}$  (in mPa) (Komhyr 1969):

$$223 \quad P_{O_3} = 0.043085 * \frac{T_P}{(\eta_P * \eta_A * \eta_C * \Phi_{PO})} * (I_M - I_B) \quad (1)$$

225  
226 The constant 0.043085 is determined by the ratio of the universal gas constant, R, to twice the Faraday constant, F, (because  
227 two electrons flow in the electrical circuit from reaction (R2) (Komhyr 1969).

228 The overall efficiency of conversion consists of:

- 229 a) Pump efficiency,  $\eta_P$ , that declines at lower pressures. At reduced air pressures ( $< 100$  hPa), the pump efficiency  
230 declines due to pump leakage, dead volume in the piston of the pump, and the back pressure exerted on the pump  
231 by the cathode cell (Komhyr 1967, Steinbrecht et al., 1998, Nakano and Morofuji, 2023).
- 232 b) Absorption (i.e capture) efficiency,  $\eta_A$ , for the transfer of the sampled gaseous ozone into the liquid phase. Although  
233 evaporation reduces the amount of the sensing solution available for ozone uptake,  $\eta_A$  is not significantly affected  
234 (Komhyr, 1971). This was confirmed by Davies et al. (2003), who determined experimentally at different pressures  
235 in a vacuum tank the absorption efficiency  $\eta_A$  from the responses of two ECC-sondes connected in series. Thus,  $\eta_A$   
236 remains at 1.0, with an uncertainty of  $< \pm 1\%$  (Tarasick et al., 2021; Davies et al., 2003).
- 237 c) Conversion efficiency,  $\eta_C$ , of the absorbed ozone in the cathode solution creating iodine that leads to the measured  
238 cell current  $I_M$ . Historically, it has been assumed that  $\eta_C$  is unity at neutral pH (Saltzman and Gilbert, 1959;  
239 Komhyr, 1969; Komhyr, 1986). However, there is now a great deal of evidence that this is not quite the case, as will  
240 be discussed below.

241  
242 Currently, there are two manufacturers of ECC ozonesondes, Science Pump Corporation and Environmental Science  
243 Corporation, most recently producing the SPC-6A and EN-SCI-Z ozonesonde series, respectively. The designs of both ECC  
244 types are similar but differences include: (i) the material of the electrochemical cell (Teflon for SPC-6A and molded plastic  
245 for EN-SCI-Z); (ii) ion bridges (details are not known due to manufacturer proprietary issues); (iii) layout of the metal  
246 frame. Since 2014, a modified ECC-type ozonesonde manufactured at the Institute of Atmospheric Physics (IAP), Beijing,  
247 has been produced (Zhang et al., 2014a,b) but to date, few comparisons of the Chinese instrument with the well-  
248 characterized SPC-6A and EN-SCI models have been carried out. Thus, profiles from Chinese instruments are not included  
249 in the current study.

250  
251 Three different aqueous sensing solution types (SST) are commonly used in the ECC-sonde cathode cells: (i) SST1.0: 1.0%  
252 KI & full buffer; (ii) SST0.5: 0.5% KI & half buffer; (iii) SST0.1: 1.0% KI &  $1/10^{\text{th}}$  buffer (GAW Report No. 268),  
253 respectively. In all cases a KI saturated cathode solution is employed in the anode cell. Laboratory studies by Johnson et al.  
254 (2002) found that, depending on the concentration of the cathode sensing solution, the stoichiometric ratio of the ozone to  
255 iodine conversion reaction (1) can increase from 1.00 up to 1.05-1.20. Johnson et al. (2002) determined that this increase is  
256 caused primarily by the phosphate buffer and to a lesser extent depends on the KI concentration. No significant influence of  
257 KBr-concentration was observed, although its role is not well understood. From JOSIE 2000 (Smit et al., 2007), BESOS  
258 2004 (Deshler et al., 2008) and multiple other sounding tests (e.g. Deshler et al., 2016) it is known that there is a significant  
259 difference in the ozone readings when sondes of the same type are operated with different sensing solutions, e.g. STT0.5 and  
260 SST1.0. Both sonde types exhibit a systematic change of sensitivity, about 5-10% over the entire profile, when the sensing  
261 solution is changed from SST0.5 to SST1.0. Johnson et al. (2002) demonstrated that this offset is mostly caused by the  
262 phosphate buffer with a minor contribution from the KI- concentration. In addition, the EN-SCI sonde tends to measure  
263 about 4-5 % more ozone than the SPC-sonde when operated with the same SST for reasons that are not understood.

264 **2.2 Impact of Pump efficiency and Conversion Efficiency (Stoichiometry)**

265 The accuracy of the ECC ozonesonde depends on the extent of the ozone-iodide reaction in the cathode cell and the  
 266 efficiency of the reduction of the iodine produced, which can be expressed primarily in the overall uncertainty based on the  
 267 contribution of the individual uncertainties of each parameter expressed in Eq. (1). Tarasick et al. (2021) quantified and  
 268 reviewed the uncertainty budget of the measured partial pressure of ozone, confirming that the most critical parameters are  
 269 the (background) current for the tropospheric part of the ozone profile and the pump and conversion efficiencies used in the  
 270 post flight data processing for the stratospheric part of the ozone profile.

271  
 272 Since JOSIE 1996 (Smit and Kley, 1998) it was recognized that, if the preparation and data correction procedures prescribed  
 273 by Komhyr (1986) are used, an increase of the stoichiometric factor, presumably due to evaporation of the cathode sensing  
 274 solution in the course of the sounding, may be compensated by a too low pump flow correction in the stratosphere above 20-  
 275 25 km altitude. With new pump flow calibrations and stoichiometry investigations, Johnson et al. (2002) demonstrated that  
 276 the pump efficiency tables reported by Komhyr (1986) and Komhyr et al. (1995) indeed compensate for the increase of the  
 277 stoichiometric factor, i.e. the conversion efficiency. Commonly used pump efficiencies and their uncertainties recommended  
 278 by ASOPOS 2.0 (GAW Report No. 268) are listed in Table 1.

279  
 280 **Table 1:** Pump efficiencies ( $\eta_p$ ) as a function of air pressure for ECC ozonesondes reported by (i) Komhyr (1986), referred as  
 281 empirical effective K86-efficiency; (ii) Komhyr et al. (1995), referred as empirical effective K95-efficiency; (iii) Johnson et  
 282 al. (2002), referred as NOAA/CMDL & UWYO at Univ.Wyoming; (iv) Nakano and Morofuji, 2023, at JMA.

Pressure [hPa]	ECC (SPC-6a) Komhyr, 1986 K86-Efficiency	ECC (ENSCI) Komhyr et al., 1995 K95-Efficiency	ECC (CMDL) Johnson et al., 2002	ECC (UWYO) Johnson et al., 2002	ECC (JMA) Nakano and Morofuji, 2023
1000	1	1	1	1	1
100	0.989 ± 0.005	0.993 ± 0.005	0.968 ± 0.009	0.978 ± 0.011	0.978 ± 0.009
50	0.985 ± 0.006	0.982 ± 0.005	0.951 ± 0.011	0.964 ± 0.012	0.964 ± 0.011
30	0.978 ± 0.008	0.972 ± 0.008	0.935 ± 0.011	0.953 ± 0.015	0.948 ± 0.013
20	0.969 ± 0.008	0.961 ± 0.011	0.918 ± 0.012	0.938 ± 0.018	0.929 ± 0.014
10	0.948 ± 0.009	0.938 ± 0.021	0.873 ± 0.015	0.893 ± 0.026	0.883 ± 0.017
7	0.935 ± 0.010	0.920 ± 0.022	0.837 ± 0.019	0.858 ± 0.029	0.848 ± 0.020
5	0.916 ± 0.012	0.889 ± 0.021	0.794 ± 0.023	0.817 ± 0.034	0.807 ± 0.023

284  
 285 The pump efficiency tables reported by Johnson et al. (2002) and more recently by Nakano and Morofuji (2023) are both  
 286 based on a large number of pump calibrations using complementary and well-established methods and can therefore be  
 287 classified as true pump efficiencies. Both tables are generally consistent within statistical uncertainty, but diverge  
 288 significantly from the older Komhyr (1986) and Komhyr et al. (1995) tables. Although the Komhyr tables (K86 and K95),  
 289 have historically been called “pump efficiencies”, the Komhyr values in Table 1 are now recognized as empirical  
 290 efficiencies, which combine decreasing pump efficiency, increasing conversion efficiency, and typical memory effects in the  
 291 background current for the standard buffered solutions SST1.0 and SST0.5 (Tarasick et al., 2021). For consistency with long-  
 292 term data records, the values reported by Komhyr (1986) and Komhyr et al. (1995) are recommended by ASOPOS 2.0

Deleted: and

Deleted: to

Deleted: to

Deleted: ,

Deleted: hey

Deleted: which combine pump efficiency and conversion efficiency...

300 (GAW Report No. 268) for SPC-6A & SST1.0 and EN-SCI & SST0.5, [but now referred as empirical effective K86-](#)  
301 [Efficiency and K95-Efficiency](#), respectively.

302  
303 Normally, in the pH = 7 buffered KI sensing cathode the stoichiometry of the conversion (R1) of ozone into iodine is  
304 assumed to be 1.00 with an uncertainty of about  $\pm 0.03$  (Dietz et al., 1973), while the initial absorption efficiency of gaseous  
305 ozone into the sensing solution will be 1.00 with an uncertainty of 0.01. These values for  $\eta_A$  and  $\eta_C$  are used in the  
306 conventional method of ozonesonde data processing as recommended by ASOPOS in GAW Report No. 268 and before in  
307 GAW Report No. 201.

## 309 2.3 Perspectives on the Background Current

### 310 2.3.1 $I_{B0}$ and $I_{B1}$ Conventions for Background Currents

311 The ECC sensor background current,  $I_B$ , is defined as the residual current output by the cell when sampling ozone free air.  
312 Since the 1990s during the preparation of the ECC sensor at the day of flight, two background currents,  $I_{B0}$  and  $I_{B1}$ ,  
313 respectively, are measured: before and after exposure of a certain amount of ozone, usually about 5  $\mu\text{A}$  ozone equivalent for  
314 about 10 minutes. Both background currents are measured after flushing the cell for 10 minutes with ozone free air. (GAW  
315 Report No. 201 and GAW Report No. 268). Although small (typically  $< 0.1 \mu\text{A}$ ), the ECC sensor background current may be  
316 of appreciable magnitude compared to the [ozone](#) current when there is very low ozone such as in the tropical upper  
317 troposphere or in the stratosphere above 5 hPa but also during ozone hole conditions in polar regions.

318  
319 Background measurements of SPC-5A sondes operated with the SST 1.0 using ozone-free air, showed before about 1993,  
320 typical values of  $I_{B0} = 0.06 \pm 0.02 \mu\text{A}$  and  $I_{B1} = 0.09 \pm 0.02 \mu\text{A}$ , respectively (Smit, 2004c). After 1993  $I_{B0}$  dropped to values of  
321  $0.00\text{--}0.03 \mu\text{A}$  and [at the same time](#)  $I_{B1}$  dropped by about  $0.06 \mu\text{A}$ . This may mean that the manufacturer made changes, most  
322 likely cleaning or conditioning the electrodes or ion bridge (e.g. less leakage of  $\text{I}_2$  into the cathode solution). In the past thirty  
323 years, both SPC-6A and EN-SCI sondes [have shown](#) similar low  $I_{B0}$  and  $I_{B1}$  values when a high-quality gas filter flushes the  
324 cells with ozone free “zero” air. However, the difference of  $I_{B1}\text{--}I_{B0}$  of  $\sim 0.03\text{--}0.04 \mu\text{A}$  has stayed the same over decades. This  
325 is actually the “chemical” contribution of the overall  $\text{O}_3 + \text{KI}$  chemistry in the cathode cell to the measured background  
326 current after zero-air flushing, whereas  $I_{B0}$  is independent of ozone exposure and assumed to be an inherent property of the  
327 ECC-sensor. The latter has been demonstrated in several laboratory experiments (Smit et al., 2007; Vömel and Diaz, 2010),  
328 and in this study (Sect.2.3.3).

329  
330 Theoretically, an ECC sensor in electrochemical equilibrium will produce no current; any current in the absence of ozone or  
331 other oxidants must be due to an imbalance of tri-iodide between the anode and cathode cells (Komhyr, 1969). Possible  
332 causes of such an imbalance include (i) a leaky ion bridge, (ii) limited mass transfer of residual tri-iodide ( $\text{I}_3^-$ ) in the cathode  
333 solution (Thornton & Njazy, 1982), (iii) limited electron transfer at the cathode surface, (iv) an imbalance resulting from cell  
334 conditioning or contamination, or (v) previous exposure to ozone. The first three cases represent a background current that  
335 may be expected to remain roughly constant and should therefore be subtracted as a best approximation; however, the last  
336 two cases, (iv) and (v), should decline according to the response time of the cell (Tarasick et al., 2021).

### 338 2.3.2 Constant Background Current?

339 In the early days of the ECC there was no clear distinction between  $I_{B0}$  or  $I_{B1}$  to apply for  $I_B$  in Eq. (1). Komhyr (1969)  
340 suggested that  $I_B$  resulted largely from a residual sensitivity of the ECC sensor to oxygen, [and that](#)  $I_B$  decreased with air

Deleted: consequently

Moved (insertion) [2]

Deleted: ¶

Formatted: English (UK)

Deleted: such

344 pressure in proportion to the rate at which oxygen entered the sensor. Thornton and Niazy (1982) showed in a laboratory  
345 study that the primary source of the background current is from the removal of residual tri-iodide, normally present in the  
346 cathode solution and not from the reaction of oxygen with iodide to produce tri-iodide nor from the direct reduction of  
347 oxygen. Since 1975 the manufacturer (Science Pump Corporation) has preconditioned the ECC electrodes with iodide such  
348 that the oxygen dependence has become vanishingly small and can be neglected (Thornton and Niazy, 1982).  
349

### 350 2.3.3 Past Ozone Dependent Background Current

351 Based on simulation chamber experiments Smit et al. (1994) recommended using  $I_{B0}$  for the constant  $I_B$  subtraction, which  
352 was confirmed in a field experiment by Reid et al. (1996). However, the results could not be confirmed in later JOSIE  
353 experiments which demonstrated that the background current most likely varies with the past ozone measured, implying that  
354 two background currents operate over the sonde operation (Smit and Sträter, 2004a,b; Smit et al., 2007): (i) one background  
355 current  $I_{B0}$ , which is independent of ozone exposure and (ii) a second past ozone dependent background current that will vary  
356 in the course of the sounding. This time variant ECC background current is assumed to result from a minor, but still slowly  
357 decaying, contribution to the measured cell current. Based on laboratory experiments Johnson et al. (2002) and Vömel and  
358 Diaz (2010) suggested that its origin is related to the ECC-chemistry having a fast (20-30 s) and an additional minor pathway  
359 (reaction time constant ~20-30 min) that causes a memory effect, probably due to slow side reactions in the oxidation of  
360 iodide by  $O_3$  in the cathode sensing solution. In equilibrium this can lead to an overall stoichiometry factor,  $O_3/I_2$ , larger than  
361 1.0 as observed by Johnson et al. (2002). The magnitude of the excess stoichiometry depends strongly on the phosphate  
362 buffer concentration in the cathode sensing solution. Vömel and Diaz (2010) suggested that, instead of a measured  
363 background current, it would be better to use an appropriate solution-dependent conversion efficiency and background  
364 current values in the basic ECC-formula Eq. (1). For improved data processing the contributions of the slow (20-30 min) and  
365 fast (20-30 s) responses to the overall measured ECC ozone signal need to be considered simultaneously using an  
366 appropriate response (memory) function.

367  
368 Such a possible methodology may be the deconvolution of the measured ozone profile after determining the overall  
369 frequency response of the combined sensor and air sampling system (De Muer and Malcorps, 1984). However, the method is  
370 complicated and not practical to apply to the global ozonesonde network. More accessible are first order numerical schemes  
371 that deconvolve the fast response which were developed and tested by Imai et al. (2013) and Huang et al. (2015). Tarasick et  
372 al. (2021) further developed one simple first order numerical scheme to resolve both the fast and slow time responses of the  
373 ECC-sensor. Vömel et al. (2020) developed the methodology for quantifying the fast and slow currents in more detail but  
374 several aspects were not fully considered and their methodology was not assessed with the most comprehensive data base  
375 and for various pairs of sonde types and SSTs. This study remedies these gaps.

376  
377 To investigate the chemical origins of the slow current, laboratory response-time tests for hundreds of ECC-ozone sensors  
378 (EN-SCI, SST0.5) were made at the Uccle (Belgium) sounding station since August 2017 during every routine day-of-launch  
379 preparations to measure the two time constants in the ECC signal. In this experiment, the following steps were taken to  
380 record the ECC sensor current as function of time:

- 381 a. Before ozone exposure, flush the ECC-cell for 10 min with zero air: Record  $I_{B0}$ .
- 382 b. Expose the ECC-cell for 10 min to 5  $\mu$ A ozone equivalent.
- 383 c. Flush the ECC-cell for 10 min with zero air: Record  $I_{B1}$  and stop flushing (pump inactive, short-circuit sensor leads)
- 384 d. No Flushing until  $t=55$  min, then flush 5 min. zero air: Record  $I_{B60}$  and then stop flushing.
- 385 e. No Flushing until  $t=115$  min, then flush 5 min with zero air: Record  $I_{B120}$ .

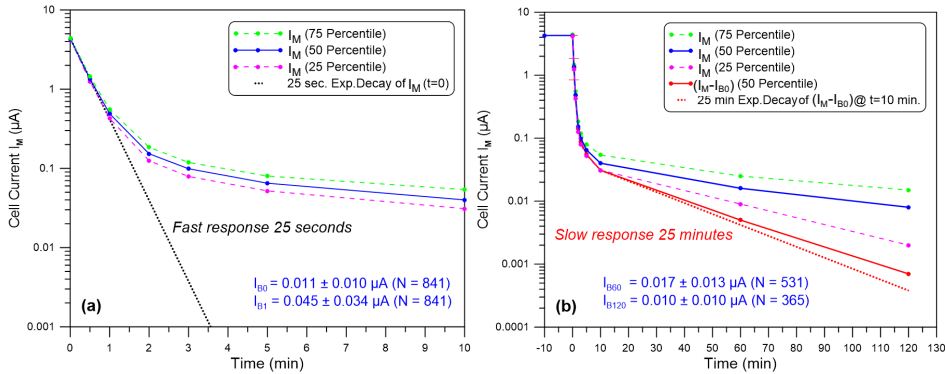
**Moved up [2]:** Theoretically, an ECC sensor in electrochemical equilibrium will produce no current; any current in the absence of ozone or other oxidants must be due to an imbalance of tri-iodide between the anode and cathode cells (Komhyr, 1969). Possible causes of such an imbalance include (i) a leaky ion bridge, (ii) limited mass transfer of residual tri-iodide ( $I_3^-$ ) in the cathode solution (Thornton & Niazy, 1982), (iii) limited electron transfer at the cathode surface, (iv) an imbalance resulting from cell conditioning or contamination, or (v) previous exposure to ozone. The first three cases represent a background current that may be expected to remain roughly constant and should therefore be subtracted as a best approximation; however, the last two cases, (iv) and (v), should decline according to the response time of the cell (Tarasick et al., 2021).

Deleted: with

Deleted:

Deleted: bc

405 The steps (a) to (c) follow exactly GAW Report No. 201 and GAW Report No. 268 SOPs. However, after these steps, most  
 406 of the time between  $t=10$  and 120 min., flushing with ozone-free air has stopped except for the 5-minute periods at  $t=55$  min  
 407 and  $t=115$  min. During the 5 minutes of flushing a short current increase was observed but it declined rapidly with a typical  
 408 “fast”  $1/e$  response time of 25 seconds. The 120-min timing was chosen because this is the typical duration of the ascent of  
 409 an ozone sounding. Summaries of the observations for the fast and slow currents appear in Figure 1.



410  
 411 **Figure 1.** Relaxation of the measured ECC-cell current  $I_M(t)$  (logarithmic scale) flushed with purified ozone free air as a  
 412 function of time after the cells have been exposed for 10 minutes with  $5 \mu\text{A}$  ozone. The sequence: (i) No flushing  $t=10$ -55  
 413 min.; (ii) Flushing  $t=55$ -60 min.; (iii) No flushing  $t=60$ -115 min.; (iv) Flushing  $t=115$ -120 min. Displayed are the medians of  
 414  $I_M(t)$  (blue solid line) and its 25 and 75 percentiles (green and pink dashed lines, respectively). Left diagram: first 10  
 415 minutes relaxation of  $I_M(t)$ ; grey dotted line:  $1/e$  decay of  $I_M(t=0)$  with 25 s. time constant. Right diagram: full two  
 416 hours of relaxation of  $I_M(t)$ ; red solid line: median of  $I_M(t)-I_{B0}$ ; red dotted line:  $1/e$  decay of  $I_{B1}-I_{B0}$  ( $t=10$  min.) with 25  
 417 min. time constant.

419 The observed relaxations in Figure 1 follow a typical superposition of two first order exponential decays of the fast and the  
 420 slow component which can be expressed here as:

$$421 \quad I_M(t) = I_{F0} \text{Exp} \left[ \frac{-t}{\tau_F} \right] + I_{S0} \text{Exp} \left[ \frac{-t}{\tau_S} \right] + I_{B0} \quad (2)$$

422 where  $I_{F0}$  and  $I_{S0}$  are the fast and slow sensor current contributions, respectively, at the start of the response test at  $t=0$ .

423  
 424 Although, after  $t=10$  min. until  $t=120$  min. for only two short periods of 5 minutes the cathode cell was flushed with ozone  
 425 free air, the results are consistent with the observations of Vömel and Diaz (2010), who flushed the cathode cell over the  
 426 entire 120 minutes relaxation period. Clearly the relaxation of the slow component of the background is independent of the  
 427 flushing, i.e. no stirring action in the cathode sensing solution, and therefore most likely has a chemical origin from a slow  
 428 reaction pathway. The  $I_{B0}$  and  $I_{B1}$  shown in Fig.1 are typical of present-day ECC sondes (e.g. GAW Report No. 268). Further,  
 429 the characteristic difference of  $I_{B1}$  and  $I_{B0}$  of about  $0.03$ - $0.04 \mu\text{A}$  has been observed over a large number of sondes ( $\approx 800$ )  
 430 and is most likely the residual of the slow reaction pathway.

431  
 432 In contrast to Vömel and Diaz (2010), based on around 25 runs, in the more than 350 Uccle experiments the cell current does  
 433 stabilize after 1-2 hours decay time to the background current before exposure to ozone,  $I_{B0}$ . As a matter of fact, assuming a  
 434 25 min  $1/e$ -decay from the mean  $I_{B1} = 0.045 \mu\text{A}$  at  $t=10$  min, the  $I_{B60}$  and  $I_{B120}$  would decay on average down to  $0.006 \mu\text{A}$   
 435 and  $0.00055 \mu\text{A}$ , after 60 and 120 minutes, respectively. Actually, we recorded mean values of  $0.017 \mu\text{A}$  and  $0.010 \mu\text{A}$ ,

Deleted: )

Deleted: )

Deleted: fairly

Formatted: Not Highlight

Formatted: Not Highlight

Formatted: Not Highlight

439 respectively. The average differences of  $I_{B60}-I_{B0}$  and  $I_{B120}-I_{B0}$  are 0.008  $\mu\text{A}$  and  $< 0.001 \mu\text{A}$ , respectively. *This indicates that*  
 440 *after correcting the measured cell current  $I_M(t)$  for the constant background current  $I_{B0}$ , the residual current  $I_M(t)-I_{B0}$  (Fig. 1:*  
 441 *red solid line) fits very well with the 25 min. 1/e-decay of the mean  $I_{B1}-I_{B0}$  starting at  $t=10$  min. (Fig. 1: Red dotted line).*  
 442 Similar observations were made in 1993 in the simulation chamber at WCCOS, whereby four ECC sondes were flushed for  
 443 more than 90 minutes with zero ozone air during the simulation of a tropical descent pressure profile. After a relaxation time  
 444 of about 70 minutes the cell currents approximate constant values which are very close to the corresponding recorded  $I_{B0}$  (for  
 445 details see Fig. S1 in the supplementary material). This means that after 1-2 hour of flushing the ECC-sensor with zero  
 446 ozone, the remaining current is identical to  $I_{B0}$ , so that during the typical duration of the ascent of an ozone sounding, the  
 447 remaining current ( $I_{B0}$ ) persists, which is not the result of a 25 min decay but has another origin. This inherent  $I_{B0}$  of the  
 448 ECC-sensor, possibly caused by a small leakage of iodine ( $\text{I}_2$ ) from the ion bridge into the cathode solution or by a mass-  
 449 transfer limit in the solution or electron transfer at the cathode surface (Thornton and Niazy, 1982, 1983), *appears to be*  
 450 constant over the 2 hours of an ozonesounding.

451  
 452 To understand the  $\text{KI}+\text{O}_3$  chemistry and the impact of the phosphate buffer on the stoichiometry of the conversion of the  
 453 sampled ozone into “free” iodine, Tarasick et al. (2019, 2021) reviewed many studies in which a variety of KI-solution  
 454 strengths with different pH-buffers were investigated. The reaction mechanism of  $\text{KI}+\text{O}_3$  in aqueous solution in presence of a  
 455 phosphate buffer as investigated by Saltzman and Gilbert (1959) may explain the observations made here and are discussed in  
 456 detail in Appendix A. In short, they proposed two reaction pathways: a primary reaction pathway without a buffer and the  
 457 secondary pathway with a buffer. Experimentally, Saltzman and Gilbert (1959) showed that the impact of the slow reactions  
 458 increases with the buffer concentration, whereas buffered solutions with no KI showed no evidence of any  $\text{O}_3$  reactions. This  
 459 means that the additional reactions with  $\text{O}_3$  are secondary reactions after the initial  $\text{O}_3 + \text{KI}$  reaction. Saltzman and Gilbert  
 460 further demonstrated that the secondary pathway *could form additional free iodine, half of it reacting very fast ( $\ll$  than 1 sec,*  
 461 *i.e. residence time of air sample in the cathode cell), the other half more slowly ( $\sim 25$  min).* This means that the secondary  
 462 reaction pathway can contribute both to the fast and slow ECC current, respectively. However, loss mechanisms may occur  
 463 too. In summary, we do not know exactly the stoichiometry of the fast and slow reaction pathways leading to “free” iodine.”  
 464 Therefore, we can only indirectly quantify these two stoichiometries that lead to the fast and slow cell current components  
 465 observed, respectively. In other words, the measured cell current  $I_M(t)$  is the superposition of

$$467 \quad I_M(t) = I_{P,F}(t) + I_{S,F}(t) + I_S(t) + I_{B0} \quad (3)$$

468 where

469  $I_{P,F}$  = sensor current contribution from fast primary reaction pathway.

470  $I_{S,F}$  = sensor current contribution from fast secondary reaction pathway.

471  $I_S$  = sensor current contribution from slow secondary reaction pathway with a typical 20-25 min time response.

472 The contribution of the fast reaction pathways that form iodine fast is lumped together in the total fast sensor current  
 473 component  $I_f(t)$  with a typical time response of 20-30 s. The measured sensor current  $I_M(t)$  is then expressed as:

$$474 \quad I_M(t) = I_f(t) + I_S(t) + I_{B0} \quad (4)$$

475 The overall stoichiometry  $S_T$  of the chemical conversion of  $\text{O}_3$  into  $\text{I}_2$  is the sum of the stoichiometry factors  $S_F$  and  $S_S$  of the  
 476 fast and slow reaction pathways, respectively.

477

#### 478 2.4 Formulating New Fast and Slow Components of the ECC Current

479 From the response tests (fast decay from  $5 \mu\text{A}$  down to  $0.1-0.5 \mu\text{A}$  within less than 1 minute) it can be concluded that  $S_F$  is  
 480 close to one (0.9-1.1) and at least a factor 10-20 larger than  $S_S$ , which is small (0.01-0.10). The time scale of the slow current

Formatted: Font: Italic

Formatted: Subscript

Formatted: Not Highlight

Formatted: Not Highlight

Deleted: is assumed

Formatted: Highlight

Deleted: an



483 component ( $\tau_s=25$  min) is about a factor of 60 slower than the dominating fast current component. This means that the slow  
 484 current acts as a slowly time-varying background current. The latter can be treated as a superposition with the ozone-  
 485 independent background  $I_{B0}$  to constitute the total background, but given now as the time varying  $I_B(t)$  in Eq. (1).

$$486 \quad I_B(t) = I_{B0} + I_S(t) \quad (5)$$

487 By substituting  $I_M(t)-I_B(t)$  into Eq. (1) the partial pressure of ozone is now expressed as Eq. (6):

$$488 \quad P_{O_3} = 0.043085 * \frac{T_P}{(\eta_P * \eta_A * \eta_C * \Phi_{P_{O_3}})} * I_F(t) \quad (6)$$

489 where the fast sensor current is expressed as:

$$490 \quad I_F(t) = I_M(t) - I_S(t) - I_{B0} \quad (7)$$

491 The conversion efficiency may depend on sonde type and sensing solution type. It is largely related to the stoichiometry of  
 492 the conversion of  $O_3$  into  $I_2$  from the primary fast reaction pathway and to a lesser degree on the secondary reaction pathway.  
 493 The partial ozone pressure can be determined from equation Eqs. (6)-(7) in two steps:

- 494 a. Determine the slow current as a function of time. Because the past ozone exposure-dependent slow current  
 495 component  $I_S(t)$  is much slower and smaller than the fast current component  $I_F(t)$ , the slow current can be  
 496 determined from the convolution of the measured current  $I_M(t)$  with the slow time constant  $\tau_s=25$  min.
- 497 b. Calculate the fast current  $I_F(t)$  and then through deconvolution of  $I_F(t)$ , resolve the time delay of the relatively fast  
 498 time constant  $\tau_f=20-30$  seconds.

499 The fast as well as the slow reaction path are determined by a first order time response and can therefore be separated in a  
 500 convolution part to determine  $I_S(t)$  and a deconvolution part to obtain the fast current component,  $I_{F,D}(t)$ , respectively. The  
 501 mathematical techniques used here to resolve the impacts of the slow and fast time constants,  $\tau_s$  and  $\tau_f$ , respectively, are  
 502 based on the numerical scheme described by Miloshevich et al. (2004) and were first applied by Imai et al (2013) to resolve  
 503 the time delay effects caused by the ECC fast response time. A first order response of a measured sensor signal  $U$  (here ECC  
 504 ozone sensor current) that is approximately proportional to a change in time of  $U$ , is described by the common "growth law  
 505 equation":

$$506 \quad \frac{dU_m}{dt} = \frac{1}{\tau} * (U_a - U_m) \quad (8)$$

507 where  $U_m$  is the instantaneous measured signal,  $U_a$  is the ambient ("true") signal that is driving the change in  $U_m$ , and  $\tau$  is the  
 508 time constant of the signal.

509 Integrating Eq.(8) over a small time step  $\Delta t_k = t_k - t_{k-1}$  gives the measured signal as a function of time:

$$510 \quad U_m(t_k) = U_a(t_k) - \{U_a(t_k) - U_m(t_{k-1})\} * \text{Exp}\left(-\frac{\Delta t_k}{\tau}\right) \quad (9)$$

511 In case the time step  $\Delta t_k$  is chosen small relative to the response time  $\tau$ , it can be assumed that the "true" (ambient) signal  $U_a$   
 512 is quasi-stationary during time step  $\Delta t_k$  such that  $U_a(t_k) = U_a(t_{k-1})$ . The exponential term is the response function.

513 Eq. (9) can be expressed in a numerical convolution or de-convolution scheme. From Eq. (9) we can obtain  $I_S(t)$  and  $I_{F,D}(t)$ ,  
 514 as follows:

515 **Case 1: Slow current component derived from convolution (time constant  $\tau_s$ ) of the ambient sensor current  $I_a$ :**

516 To obtain the slow current component ( $I_S$ ),  $U_m$  in Eq. (9) is substituted by the slow fraction of  $I_a$ , represented here by the  
 517 stoichiometry  $S_S$  multiplied with the ambient ("true") ozone sensor current  $I_a$ . Eq. (9) can now be re-written into the  
 518 integrating form:

$$519 \quad I_S(t_k) = S_S * I_a(t_k) - \{S_S * I_a(t_k) - I_S(t_{k-1})\} * X_S \quad (10)$$

520 whereby the slow response function  $X_S$  is:

$$521 \quad X_S = \text{Exp}\left(-\frac{\Delta t_k}{\tau_S}\right) \quad (11)$$

522

Deleted: to

Deleted: ,

Deleted: exponentially

Deleted: This assumes that

Deleted: .

Deleted: Further, it is

529 **Case 2: Deconvolution (time constant  $\tau_F$ ) of the fast signal  $I_F$  with  $\tau_F$ :**

530 To obtain the deconvolved fast current component  $I_{F,D}$ , Eq. (9) should be solved to obtain  $U_a (=I_{F,D})$ , and  $U_m$  is substituted by  
531 the fast fraction  $I_F$ . Eq. (9) can then be re-written into the differentiating form:

$$532 \quad I_{F,D}(t_k) = \frac{I_F(t_k) - I_F(t_{k-1}) \cdot X_F}{(1 - X_F)} \quad (12)$$

533 where the fast response function  $X_F$  is:

$$534 \quad X_F = \text{Exp} \left( -\frac{\Delta t_k}{\tau_F} \right) \quad (13)$$

535  
536 Compared to Vömel et al. (2020), the recursive numerical convolution scheme proposed here (Eq.11) is the same, while the  
537 deconvolution scheme (Eq.12) differs through the inclusion of the exponential fast response function  $X_F$  (Eq. 13) itself,  
538 rather than its first order approximation. The latter allows larger time steps  $\Delta t_k$ , which may become significant for older  
539 ozone sounding records that had data with resolution of 10 seconds or more.

### 540 3 Resolving Slow- and Fast-Response Signals using JOSIE 2009/2010

541 To resolve the slow and fast time responses of the measured ECC sensor current, the JOSIE measurements conducted in  
542 several campaigns between 1996 and 2017 form an ideal dataset, because of several reasons. Firstly, all the ozonesonde  
543 preparations and the measurements were carried out in a controlled environment. Secondly, the availability of simultaneous  
544 reference measurements from a fast-response photometer OPM with high precision and accuracy provides an absolute  
545 reference for the derived ozone profiles. Further, in the course of the simulation several response tests are performed in  
546 which the ozonesondes and the OPM are exposed to zero-ozone air for a five minute period (see Fig. 2). These response tests  
547 enable us to determine the stoichiometry of the slow reaction pathway and subsequently the slow sensor current  $I_S(t)$  as a  
548 function of time. In this sense, the JOSIE 2009 and 2010 campaigns dataset is of particular interest, because all experiments  
549 included four of those response tests in the simulation profiles themselves.

550  
551 For the sake of clarity, it is to be noted that the here reported ozone readings of the OPM are already based on the new UV-  
552 absorption cross-section, referred to as the CCQM.O3.2019 (BIPM, 2022; Hodges et al., 2019) value that is about 1.23%  
553 lower than the former cross-section (Hearn et al., 1961) that was mostly used before in the global ozone ground based  
554 monitoring networks. In 2024-2025 the new cross-section will be introduced into the global ozone observation networks  
555 using UV-photometry (BIPM, 2022). Consequently, all  $P_{O_3}$  measurements of the OPM reported here are about 1.23% larger  
556 than the values reported before in earlier JOSIE-publications.

#### 557 3.1 JOSIE 2009/2010

558 The JOSIE 2009 and 2010 protocols are similar to the JOSIE 1998 campaign (Smit and Sträter, 2004a; Smit et al., 2007). In  
559 2009 a set of 40 brand new ECC sondes (20 SPC6A and 20 ENSCI) were tested; in 2010 the same set of ECC sondes, re-  
560 refurbished and tested under the same conditions, were evaluated against the same OPM reference. One aim of these  
561 campaigns was to test the performance of brand new and refurbished ozonesondes. It was found that the re-used sondes  
562 agree within 1%–2% with brand new sondes, although with a slightly lower precision of ~5% (see Fig. 3.1 in GAW Report  
563 No. 268). The JOSIE 2009/2010 ozonesondes were prepared by only three operators, strictly following the same preparation  
564 protocols, including the use of purified air from the same cylinders for the ozone-free air source. It can therefore be  
565 considered as an ideal data set for well-prepared ozonesondes. All ozonesonde data were processed according to the  
566 guidelines of GAW Report No. 268, which we denote as the “conventional” method hereafter. That means: (i) subtracting the  
567 constant background current  $I_{B1}$ ; (ii) correcting the pump flow rate for the moistening effect; (iii) using the empirical

Deleted:

Deleted: s

Formatted: Not Highlight

570 ~~effective efficiency tables by~~ Komhyr (1986) and Komhyr et al. (1995) for SPC and EN-SCI ozonesondes respectively; (iv)  
 571 converting the measured pump temperature to the internal pump body temperature, with an additional small pressure  
 572 dependent correction (GAW Report No. 268); and (v) no total ozone normalisation. Note also that all simulations were  
 573 identical in representing a typical mid-latitude ozone profile (Smit et al., 2007).  
 574 During both campaigns, a total of 26 simulation runs were made, of which all but one had 4 ozonesondes simultaneously in  
 575 the simulation chamber, giving a total amount of 103 ozonesonde profiles. However, 17 of those profiles were gathered  
 576 using research-mode SSTs and are not included here. Fourteen simulations were carried out in December 2009, 2 in January  
 577 2010, and 10 in August 2010.

Deleted: pump flow rate

Deleted: correction

### 578 3.2 Determination of Slow Current $I_s(t)$

#### 579 3.2.1 Determination of Stoichiometry $S_s$

580 To determine the relative contribution  $S_s$  of the slow component in the ECC ozonesonde signal, in other words, the  
 581 stoichiometry factor of the slow reaction pathway of conversion of  $O_3$  into  $I_s$ , the response tests of the JOSIE 2009/2010  
 582 dataset are used. Four time response tests are included during these simulations at four different pressure levels, (RT1: 475-  
 583 375 hPa, RT2: 100-85hPa, RT3: 20-15 hPa, RT4: 6-5 hPa), during which ozone-free air is provided in the simulation  
 584 chamber for 5 minutes. A typical example of a JOSIE 2009 simulation run is given in Figure 2. After 5 minutes the fast  
 585 sensor current has declined by more than 16  $1/e$  relaxation times and is ~~negligible~~. This means that at the end of this time  
 586 response test, the only contribution to the overall measured current  $I_M(t)$ , after correction for  $I_{B0}$ , comes from the remaining  
 587 slow current component. At this moment, the fast co-existing OPM data (red in Fig. 2) provide the true value of the  
 588 ozonesonde signal. The next paragraphs outline the different practical steps.

Deleted: vanishing small

Deleted: s

Deleted: measure of the

589 To obtain a direct measure of the true ECC-ozone sensor current, the OPM ozone partial pressure is converted to the generic  
 590 OPM current ( $I_{OPM}$ ) for each individual ozonesonde using sonde pump temperature, sonde pump flow rate and true pump  
 591 efficiency values of JMA (Nakano and Morofuji, 2023, See Table 1), as in Eq. (1).

$$592 \quad I_{OPM} = \frac{(\eta_P \cdot \eta_A \cdot \eta_C \cdot \Phi_{PO})}{T_P + 0.043085} * P_{O3,OPM} \quad (14)$$

593  
 594 In other words, we are calculating the generic sensor current corresponding to the ozone equivalent measured by the OPM,  
 595 as if it were the true ECC ozone current. This means that the generic  $I_{OPM}$  is taken as the actual reference (“true”) current for  
 596 determining the slow stoichiometry factor  $S_s$ .

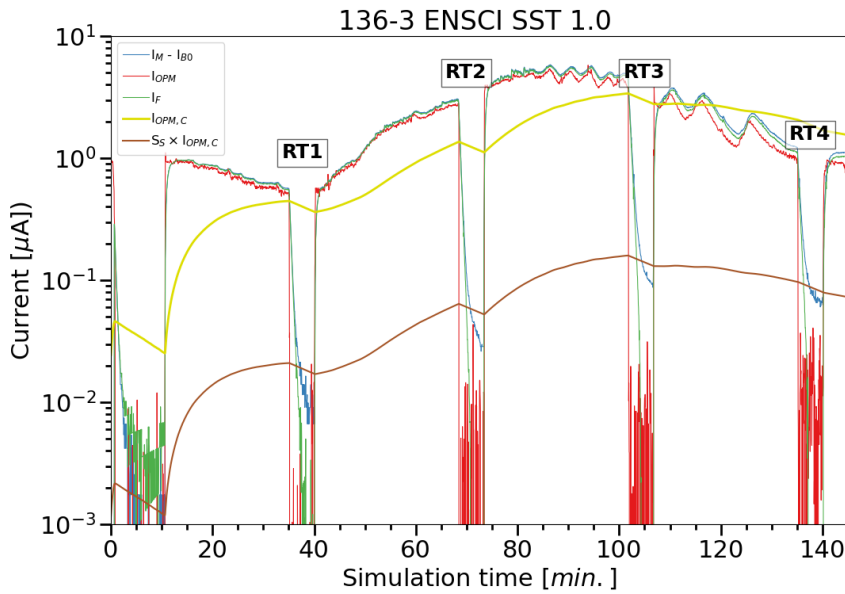
597  
 598 Additionally, the generic OPM current  $I_{OPM}$  (red in Fig. 2) is convolved into  $I_{OPM,C}$  with an exponential time response with  $\tau_s$   
 599 = 25 minutes using Eq. 9, to obtain a slow time response into the generic OPM current signal (yellow in Fig. 2).

$$600 \quad I_{OPM,C}(t_k) = I_{OPM}(t_k) - \{I_{OPM}(t_k) - I_{OPM,C}(t_k - 1)\} * X_S \quad (15)$$

601 Finally, the slow stoichiometry factor  $S_s$  is obtained by taking the ratio of the remaining ECC sensor current  $I_M$  minus the  
 602 constant background current  $I_{B0}$  and the convolved OPM signal ( $I_{OPM,C}$ ), at the end of the time response test intervals RT1,  
 603 RT2, RT3, RT4, when only the slow component is expected to contribute to the sonde signal, such that

$$604 \quad S_s = \frac{(I_M(ECC) - I_{B0})}{I_{OPM,C}} \quad (16)$$

605  
 606



612  
613

614 **Figure 2.** Example of a simulation run during JOSIE 2009 as a function of the simulation time, with the measured ECC  
615 current  $I_M$  minus  $I_{B0}$  (blue line), the generic OPM current  $I_{OPM}$  (red line), the 25 min convolved  $I_{OPM,C}$  (yellow line) and the  
616 25 min convolved  $I_{OPM}$  adapted to  $I_M - I_{B0}$  after the determination of the slow stoichiometry factor  $S_S$  or slow current  $I_S (= S_S \times$   
617  $I_{OPM,C})$  (brown line) and the fast sensor current  $I_F$  (green line), obtained after correction of the measured sensor current  $I_M$  for  
618 the constant background current  $I_{B0}$  and the slow current contribution  $I_S$

619

620 The ratios used to obtain the slow stoichiometry factor ( $S_S$ ) values are calculated during the final 50 seconds of each time  
621 response test, RT1, RT2, RT3, RT4, respectively. Those values, obtained for all ozone profiles within each sonde type and  
622 SST combination, are shown in Fig. 3, together with median, 25th and 75th percentile values. The median  $S_S$  values and their  
623 Median Absolute Deviation (MAD) uncertainties are given in Table 2. Note that the determination of the median  $S_S$  values  
624 (and their uncertainties) is very robust, and does not depend on the time response test interval or the slow time lag constant.  
625 We will come back to this in Sect. 6.2. Further it showed that by varying  $\tau_S = 25$  min. by  $\pm 5$  min. the corresponding  $S_S$   
626 values only changed by less than 5%, which is small compared to the MAD uncertainty of  $S_S$  (Table 2).

627

628 The most striking feature is that  $S_S$  only depends on the SST, not on the sonde type. This confirms our hypothesis on the  
629 origin of this slow component, as described in Section 2.4. For SST0.5 and SST1.0 there is an almost proportional relation  
630 between the magnitude of  $S_S$  and the buffer strength. Johnson et al. (2002) have demonstrated that increase of the  
631 stoichiometry is primarily caused by the buffer strength with only a minor contribution by the KI-concentration. This result  
632 might be explained by the secondary reaction pathway of the reaction mechanism after Saltzman and Gilbert (1959),  
633 whereby the extra slow stoichiometry contribution is caused by the buffer (Appendix A). However, a comparable result does  
634 not hold for SST0.1 (Table 2). One would expect that for the low buffered case (SST0.1)  $S_S$  should be much smaller than for  
635 the SST0.5. This is not true;  $S_S$  is even slightly larger. It seems that for the SST0.1, other competing reaction mechanisms

Deleted: ion

Deleted: ,

Deleted: , independent of the KI concentration (or percentage...

Deleted: has been

Deleted:

642 may occur, which do depend on the KI concentration, and may generate free iodine on a 25-minute time scale. Such a  
 643 hypothetical mechanism may also explain the fact that for low or no buffered SST we still measure  $I_{B1}$  background currents  
 644 with values of 0.01-0.03  $\mu\text{A}$  larger than  $I_{B0}$  as measured in JOSIE 2000 (no buffer SST; Smit and Sträter, 2004b) and JOSIE  
 645 2017 (SST0.1; Thompson et al., 2019). A speculative mechanism is that the electronically excited oxygen singlet molecule  
 646 formed in (R3) of the primary reaction pathway of the  $\text{O}_3+\text{KI}$  chemistry (Appendix A) may, in addition to de-activation in  
 647 (R4), react with  $\text{H}_2\text{O}$  and produce hydrogen peroxide ( $\text{H}_2\text{O}_2$ ) (e.g. Xu et al., 2002). The formed  $\text{H}_2\text{O}_2$  would oxidize KI to  
 648 produce free iodine, but on a time scale of 25 minutes which could contribute to the slow current  $I_s(t)$ . Further studies are  
 649 required to understand the underlying chemical processes.

650  
 651 **Table 2:** Median and their Median Absolute Deviation (MAD) uncertainty values of the slow stoichiometry factor  $S_s$   
 652 obtained from JOSIE 2009 and 2010 for SPC and EN-SCI ozonesondes operated with the sensing solution types SST0.5 and  
 653 SST1.0. The stoichiometry factor  $S_s$  for EN-SCI/SST0.1 has been determined with the same approach but using laboratory  
 654 measurements at Uccle with an ozone reference instrument (see Appendix B). \*: the same value for SPC/SST0.1 has been  
 655 adopted as for EN-SCI 1.0%-0.1B.  $N_s$  is the number of sonde profiles.

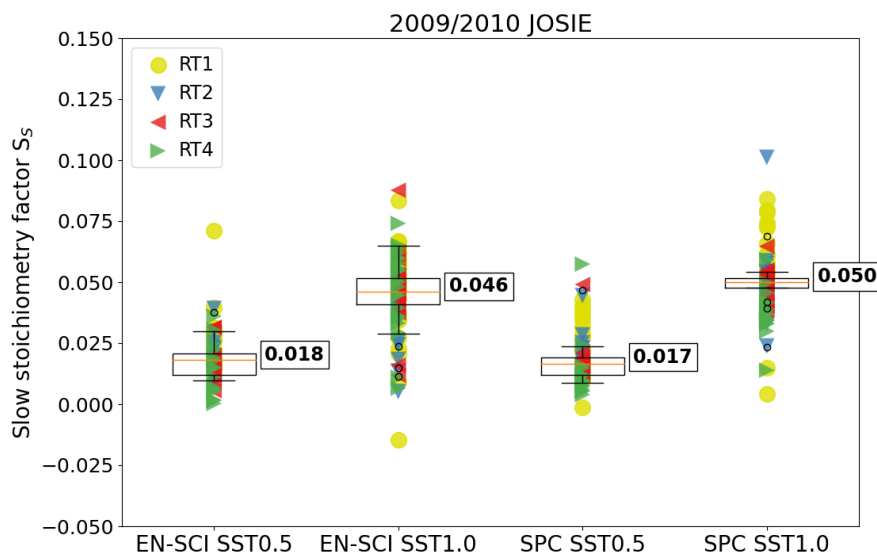
Sonde Type	SST1.0	SST0.5	SST0.1
SPC	$0.050 \pm 0.002$ ( $N_s = 16$ )	$0.017 \pm 0.004$ ( $N_s = 21$ )	$0.023 \pm 0.005^*$
EN-SCI	$0.046 \pm 0.006$ ( $N_s = 23$ )	$0.018 \pm 0.004$ ( $N_s = 15$ )	$0.023 \pm 0.005$ ( $N_s = 8$ )

657  
 658 The stoichiometry factors  $S_s$  (Table 2) to determine the slow current  $I_s(t)$  are substantially lower than the so-called “steady  
 659 state bias factors” applied by Vömel et al. (2020). These steady state bias factors were determined as the overall excess  
 660 stoichiometry to one from laboratory experiments with a fixed ozone exposure during several hours (Figs. 3 & 4 in Vömel  
 661 and Diaz, 2010). In this study we derived for SST1.0  $S_s = 0.046$ -0.050 which is only half the 0.09 value of Vömel et al.  
 662 (2020). For SST0.5 and SST0.1, our respective  $S_s = 0.017$ -0.018 and 0.023 values are also smaller than their 0.024 and 0.031  
 663 steady-state bias factors. Using the same laboratory procedures as Vömel et al. (2010), Johnson et al. (2002) reported an  
 664 excess overall stoichiometry of  $\sim 0.07$  for SST1.0. The lower factors obtained in this study, particularly for SST1.0, might  
 665 also be related to the different methodology followed for determining  $S_s$ . Here,  $S_s$  values are determined from the response  
 666 of a downward step under zero-ozone conditions. In Johnson et al. (2002), and Vömel and Diaz (2010) the excess  
 667 stoichiometry factors were determined from the relatively small differences observed between the ECC sonde and a  
 668 reference UV-photometer after a 60-min upward step ozone exposure. The latter requires very accurate generation of ozone  
 669 values with a precision better than 1% to determine the relatively small excess stoichiometry factors involved. Also note that  
 670 for the earlier studies reference ozone readings are based on older UV absorption cross sections that are now corrected by  
 671 1.23% to be compatible with the new UV absorption cross-section applied to the OPM. Accordingly, the steady state bias  
 672 factors of Johnson et al. (2002) and Vömel et al. (2020) should be decreased by subtracting 0.012. The resulting  $S_s$  values  
 673 would then approach the  $S_s$  values obtained here for SST0.1 and SST0.5, and better approximate the SST1.0  $S_s$  values.  
 674

Deleted:

Deleted: N

Deleted: also



678

679 **Figure 3.** Box-Whisker plots of the slow stoichiometry factor  $S_s$  as the ratio of the measured  $I_M$  minus  $I_{B0}$  to the 25 min  
 680 convolved OPM current ( $I_{OPM,C}$ ) obtained from JOSIE 2009 and 2010 for EN-SCI and SPC ozonesondes operated with the  
 681 SST0.5 and SST1.0. The yellow dots and triangle symbols (blue, red and green) represent the individual values obtained  
 682 from the four response tests RT1, RT2, RT3 and RT4, respectively. Thus, every ozonesonde profile is represented four times  
 683 in the graph. The Box-Whisker plots are represented by the median plus the 25th and 75th percentiles (respectively, orange  
 684 and black horizontal lines for each pair of instrument-SST combination).

Formatted: Font: Italic

Deleted: Whisker

Deleted:

685

686 Another difference between the new methodology and that of Vömel & Diaz (2010) is that we subtract  $I_{B0}$  from the  
 687 ozonesonde signal prior to determining the stoichiometry. However, we also determined the  $S_s$  values without correction of  
 688  $I_{B0}$ ; the results appear in Fig. S2 in Supplementary Material. It is noted that these  $S_s$  values increase for all sensing solution  
 689 types by only 0.005-0.009. For SST0.5 and SST0.1, they approach the Vömel & Diaz (2010) values, but the substantially  
 690 lower  $S_s$  values for SST1.0, as derived here (Table 2) cannot be explained exclusively by subtracting  $I_{B0}$ . Furthermore,  
 691 comparing Fig. 3 with Fig. S2, also demonstrates that the subtraction of the  $I_{B0}$  value makes the determination of the  $S_s$   
 692 values even more independent of the selected RT intervals, which is not the case without this prior subtraction (e.g. the RT1  
 693 values being significantly larger than the other RT values).

694

695 The factors reported by Johnson et al. (2002) and Vömel & Diaz (2010) are based on a limited sample of experiments (three  
 696 different sondes using three different solutions for a total of 22 runs in Vömel & Diaz, 2010) in contrast to the large  
 697 statistical sample in this study (Table 2). The difference between the two approaches – in terms of exposure to ozone or not –  
 698 may be then explained by assuming that when the overall excess stoichiometry originates from the secondary reaction  
 699 pathway, only half of it contributes to the slow cell current  $I_s(t)$  and with the other half contributing to the fast cell current  
 700  $I_f(t)$ . For SST05 and this SST1.0 this can be understood by the type of reaction mechanisms of the secondary reaction  
 701 pathway as proposed by Saltzman and Gilbert (1959): in this case, about half of the extra stoichiometry caused by the buffer

704 could be still contributing to the relatively fast signal (R7) and ~~the other half~~ to the slow signal (R8) (see Appendix A). This  
705 would mean that the stoichiometry of the secondary reaction pathway could be two times the stoichiometry factor  $S_S$  of the  
706 slow ECC current  $I_S(t)$  determined here from the response tests RT1 to RT4 after  $I_F(t) = 0$ . However, for the  $S_S$  values for the  
707 SST0.1, even slightly larger than for SST0.5, explanations would be more speculative. More analysis and new JOSIE trials  
708 might be required to find the cause of varying factors among the different studies and SSTs.

Deleted: for 50%

Deleted: 50%

Formatted: English (US)

Deleted: , for example in the JOSIE simulation chamber,

### 710 3.2.2 Initial Condition of Slow Current $I_S(t)$

711 With the derived  $S_S$  values, the slow component of the sonde signal ( $I_S$ ) is computed by convolution with the slow time  
712 constant  $\tau_s = 25$  min., as in Eq. (10) (brown line in Fig. 2). Note that, in practice, to determine  $I_S(t)$ , the measured current  $I_M(t)$   
713 minus  $I_{B0}$  can be taken instead of the true generic ozone current  $I_{OPM}(t)$ , because their differences are rather small (less than  
714 5-10%), at the same time the slow stoichiometry factors  $S_S$  are also smaller than 0.1. From here on, we will use the measured  
715 current  $I_M(t)$  minus  $I_{B0}$  to determine the slow current  $I_S(t)$  along with the  $S_S$  values listed in Table 2.

Deleted: s

716 As Eq. (10) is a recursive expression, the initial conditions of  $I_S$  reflect prior ozone exposure during pre-launch preparations,  
717 although decaying exponentially in time. Exposure to ozone values during pre-launch will cause non-zero  $I_S$  values at the  
718 beginning of the simulation, impacting the boundary layer ozone profile (e.g., Fig. 10 in Vömel et al., 2020). Ideally, the  
719 convolution of the slow component of the sonde signal is computed taking the pre-launch measurements into account. These  
720 pre-launch measurements are available for JOSIE 2009/2010 (as in Fig. 4), but this is often not the case for operational  
721 soundings. Using those JOSIE 2009/2010 pre-launch simulation data (with negative simulation times in Fig. 4), we found  
722 that the best approximation of the true  $I_S$  (red dashed line in Fig. 4, taking all the pre-launch measurements into account) is  
723 obtained if  $I_S(t_0)$  equals  $(I_{B1} - I_{B0})$  multiplied with the exponential decay factor  $X_S = \text{Exp}[-\Delta t / \tau_s]$ , where  $\Delta t$  is the time interval  
724 between the measurement of  $I_{B1}$  and the start of the launch (green dashed line in Fig. 4). It is important to mention here the  
725 good agreement of the measured  $I_{B1}$  value (yellow horizontal line in Fig. 4, subtracted by  $I_{B0}$ ) with the convolved, pre-  
726 launch, slow component  $I_S$  (dashed red line) at  $t = -2500$  seconds (time mark No.2 in Fig. 4). This reinforces the selection of  
727 the  $I_{B1} - I_{B0}$  measurement as a good pre-launch representation of the slow component of the ECC signal.

729 To apply this method in the ozonesonde network, it is essential to record the time difference between the  $I_{B1}$  measurement  
730 and the sonde launch. In GAW Report No. 268, the recording of the  $I_{B1}$  timestamp is included in the SOP for ozonesonde  
731 preparations. For the JOSIE 2009/2010 data, we will use this exponential decay method for the initial condition of the  
732 convolved slow component at  $t=0$ . For the initial condition of the slow component  $I_S(t_0)$  we investigated two other  
733 alternatives:

- 735 •  $I_S(t_0) = I_{B1} - I_{B0}$ , denoted by the horizontal yellow line in Fig. 4, which results in a slow component  $I_S$  marked by the  
736 purple solid line, which clearly overestimates the true  $I_S$  in the beginning of the profile (up to about 3500 s).
- 737 •  $I_S(t_0) = 0$ , for which the corresponding  $I_S$ , represented by the brown solid line in Fig. 4, underestimates the true  $I_S$   
738 up to about a simulation time of 2200s for the JOSIE 2009/2010 representative example here.

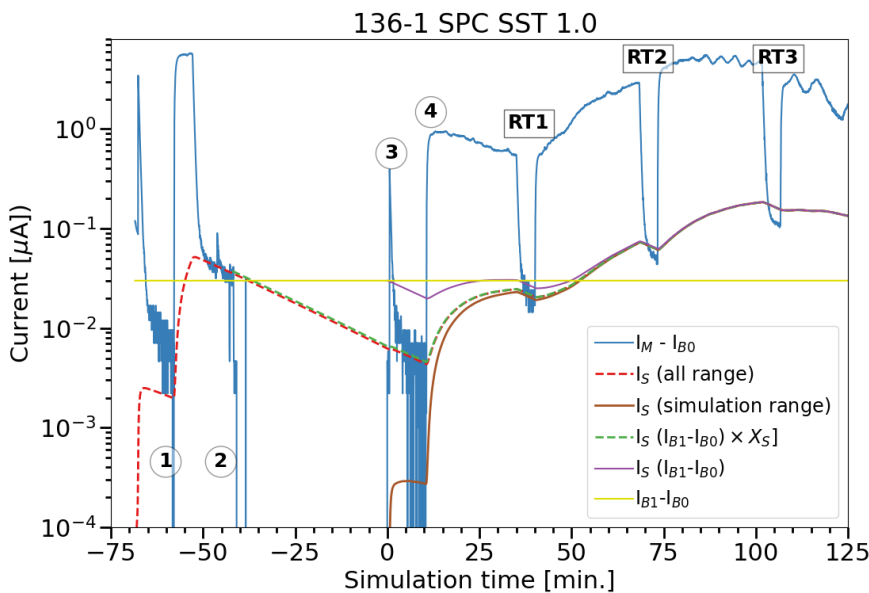
739 For stations with a time gap of several hours between the  $I_{B1}$  measurement and the launch time, the current will have been  
740 fallen back to the  $I_{B0}$  (see the Uccle example in Fig. 1), resulting, after subtraction of  $I_{B0}$ , in this particular case  $I_S(t_0) = 0$ .

741 A better understanding of the ECC time response provided a justification for quality control indicators on the  $I_{B0}$  ( $< 0.03 \mu\text{A}$ )  
742 and  $I_{B1}$  ( $< 0.07 \mu\text{A}$ ) in GAW Report No. 268. In practice, often higher background currents  $I_{B0}$  and  $I_{B1}$  are recorded at the  
743 sounding sites at the day of the launch. These high background currents are typically caused by the use of an inadequate gas  
744 filter in the test unit, e.g. the filter provides ozone free air, but does not trap water vapour and contaminants in the laboratory  
745

750 air that is filtered into the preparation equipment. A poor filter combined with a leaky photolysis cuvette producing ozone by  
 751 UV-photodissociation of oxygen with a Hg-discharge lamp can contaminate the air flow to produce high background current  
 752 measurements. It appears that UV irradiation can produce substances that cause reactions similar to KI and O<sub>3</sub>. There are  
 753 some indications (Newton et al., 2016) that high backgrounds may be due to processes with 1/e-decay times ~ 25 minutes  
 754 like the slow cell current  $I_S(t)$ . Nevertheless, more research is necessary to investigate the cause and the time behaviour of  
 755 these high background currents in the course of the sounding in order to correct for this artifact properly. As stated by  
 756 ASOPOS 2.0 (WMO/GAW Report No. No. 268) the use of proper gas filters to provide ozone free, dry and purified air in  
 757 practice at the sounding site, is very essential in general, but also when applying the data processing proposed here.

Deleted: in

Deleted: display



758  
759

760 **Figure 4.** Convolved slow ECC current obtained from different initialization scenarios as function of the simulation time.  
 761 (details see text). The dashed red line is the convolved ECC current obtained from the measured  $I_M$  minus  $I_{B0}$ , hereby  
 762 including all pre-launch measurements (with negative simulation times). Time stamps 1-4: 1= record  $I_{B0}$ ; 2= record  $I_{B1}$ ;  
 763 3=turn on pump motor (at simulation time  $t=0$ ); 4= start ozone profile of simulation. RT1, RT2, RT3 are the first three in-  
 764 flight time response tests. **Slow current  $I_S(t)$  derived with four different start scenarios: (i) all range ( $I_S = 0$  at  $t = -67$  min., red  
 765 dashed line); (ii) simulation range ( $I_S = 0$  at  $t = 0$  min., brown solid line); (iii)  $I_S = I_{B1} - I_{B0}$  at time stamp 2 with 25 min.  
 766 exponential decay  $X_S$  (green dashed line); (iv)  $I_S = I_{B1} - I_{B0}$  at time stamp 3 (purple solid line).**

Formatted: Font: Italic

Formatted: Font: Italic, Subscript

Formatted: Font: Italic

Formatted: Subscript

Formatted: Font: Italic

Formatted: Font: Italic

Formatted: Subscript

Formatted: Font: Italic

Formatted: Subscript

Formatted: Font: Italic

Formatted: Subscript

Formatted: Subscript

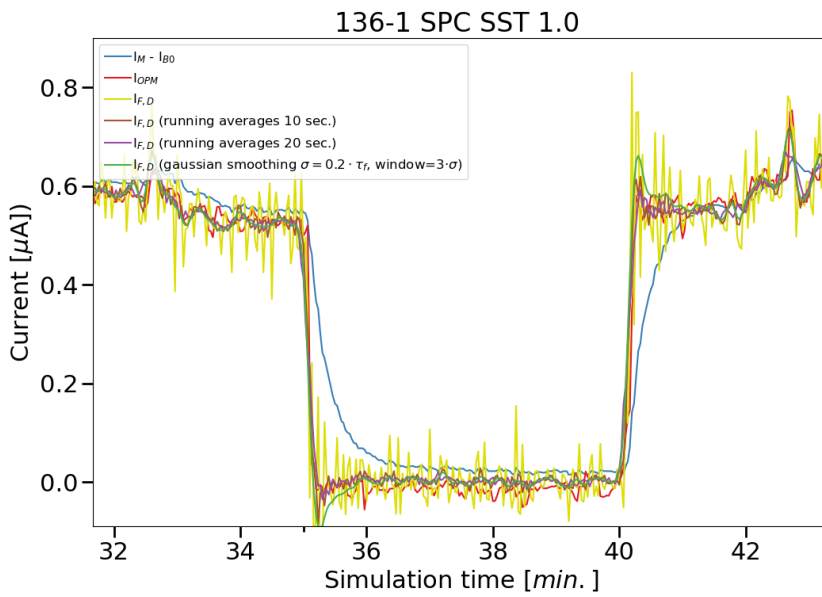
### 768 3.3 Determination of the Fast ECC Ozone Sensor Current, $I_F(t)$

769 After determining the slow component of the signal due to the secondary reaction pathway, we can subtract it from the  
 770 overall measured current  $I_M - I_{B0}$  to end up with the fast component  $I_F$  (Eq. 7), as shown by the green line in Fig. 2. From the  
 771 fast component  $I_F(t)$ , we can remove the time lag introduced by the 1/e time response of about 20-30 seconds through  
 772 deconvolution of  $I_F(t)$  according to Eq. (12). In this paper, we use  $\tau_F = 25 \pm 4$  seconds for EN-SCI, and  $\tau_F = 21 \pm 4$  seconds



775 for SPC ozonesondes, which are the average fast time responses determined from all the simulation time response tests (RT1,  
 776 RT2, RT3, RT4) during JOSIE 2009/2010. The response times of the EN-SCI sondes are typically about 4 seconds larger  
 777 than the SPC-6A sondes due to the slightly lower pump flow rates and slightly larger volume of the cathode cell of the EN-  
 778 SCI sondes (Smit and Sträter, 2004a). In general, we found that the fast response times in upward as well as in downward  
 779 direction agree within 1-2 seconds. Moreover,  $\tau_F$  only varies marginally in flight with a slight decrease of less than 5-10 %  
 780 between the surface (RT1) and the upper part of the sounding (RT4). The in-flight  $\tau_F$  values also agree very well with the  $\tau_F$   
 781 values determined from the response tests made during the pre-flight preparation of the ECC sensor, which confirmed earlier  
 782 observations made during JOSIE (Smit and Sträter, 2004a). A close-up of the first time response interval RT1 is provided in  
 783 Fig. 5, in which also the deconvolved fast component is shown in yellow.

Deleted:



784  
 785  
 786 **Figure 5.** Example of a downward and upward response of a simulation run in the tropospheric part of the vertical profile to  
 787 show the impact of resolving the fast response effects on the measured cell current  $I_M$  minus  $I_{B0}$  ( $I_M - I_{B0}$ : blue solid line). The  
 788 fast, deconvolved current  $I_{F,D}$ , without smoothing, is shown in yellow, and with a moving average smoothing over a time  
 789 interval of 10 and 20s in brown and purple, respectively. The Gaussian smoothing applied on  $I_{F,D}$  and used in this paper is  
 790 marked by the green line. For reference, the OPM current is shown in red.

Formatted: Font: Italic

Formatted: Font: Italic

791  
 792 Note that the deconvolution procedure introduces a substantial amount of noise in the data. To reduce this noise, the  
 793 deconvolved current signal should be smoothed. We therefore used a smoothing with a Gaussian filter with width equal to  
 794 20% of the time lag constant  $\tau_F$  as in Vömel et al. (2020), their equations (10) and (11). Compared to other common  
 795 smoothing techniques, e.g. running averages with a time window of 10 seconds (see brown line in Fig. 5), this Gaussian  
 796 filter still has a slight phase shift with respect to the true signal ( $I_{OPM}$ , in red in Fig. 5), but outperforms other tested  
 797 smoothing algorithms in terms of reducing the noise level. The final smoothed deconvolved signal is shown in green in Fig.  
 798 5. It is obvious that, after correcting for the slow and the fast times responses in the signal, the resulting current better agrees

800 with the OPM current than the original measured current. It even exhibits small-scale features that are also present in the  
801 fast(er) response OPM measurements. ~~The remaining small differences indicate that~~ the conversion efficiency, i.e.  
802 stoichiometry of the fast reaction, slightly deviates from one.

**Deleted:** S

**Deleted:** still remain that

**Deleted:** s

#### 803 4. Comparison of Ozone Profiles Based on the Conventional Versus Updated Time Responses Correction Method

804 To test the Time Responses Correction (abbreviated here as TRC) methodology as described in the previous ~~section~~ and a  
805 first version in Vömel et al. (2020), we apply the methodology on individual ozonesonde profiles of the different JOSIE  
806 simulations and compare those corrected profiles with the corresponding OPM measurements. This method involves the use  
807 of the stoichiometry factors  $S_s$  from Table 2 for the different ozonesonde-SST pairs and the application of the measured ~~true~~  
808 pump efficiency factors of Nakano and Morofuji (2023) (Table 1). ~~In contrast to this TRC method, ozone partial pressures~~  
809 from profiles are determined according to the “conventional method”, as recommended in ASOPOS (GAW Report No. 201;  
810 GAW Report No. 268), e.g. using the constant background  $I_{B1}$  correction with the Komhyr et al. (1986, 1995) ~~empirical~~  
811 ~~effective~~ efficiency factors (Table 1). ~~The comparisons are made for two different JOSIE campaigns: (i) JOSIE 2009/2010~~  
812 with mid-latitude profiles and well-established ozonesonde preparation procedures, and (ii) the JOSIE 2017 campaign with  
813 mostly tropical profiles and good ozonesonde preparation procedures.  
814 All ~~comparisons of the TRC with the conventional method~~ are processed as a function of flight time. However, to present the  
815 results as vertical profiles, they are mapped on a pressure grid with successive pressure levels of  $P_i=0.98 \times P_{i-1}$  between 1000  
816 and 5-6 hPa. Hereby, all presented JOSIE experiments are based on a pressure, temperature and ozone profile simulating a  
817 balloon ascent velocity of about 5 m/s, such that a quasi-realistic linking between the simulated flight time and pressure scale  
818 is obtained.

**Deleted:** chapter

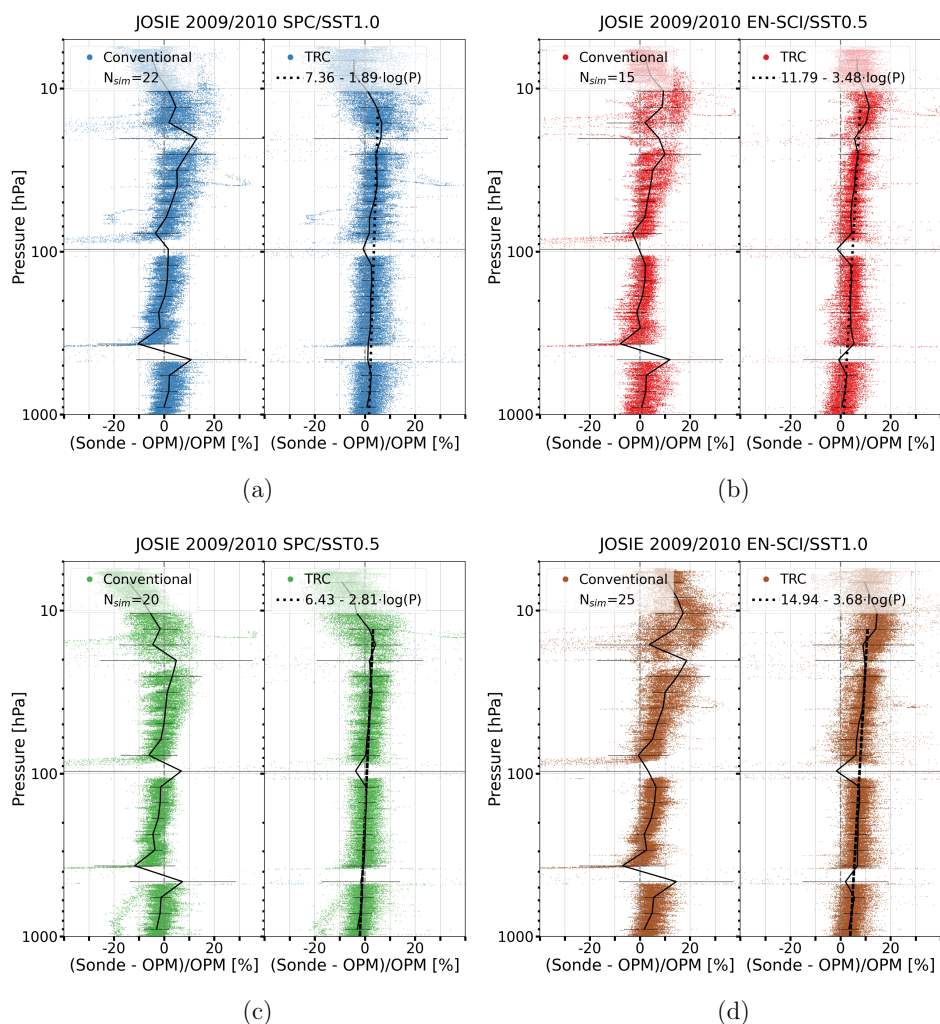
**Deleted:** As opposed

**Deleted:** Both sets of processed profiles are compared to the OPM reference values which are enhanced by 1.23% compared to earlier JOSIE publications due to the newly revised ozone absorption cross-section at 254 nm wavelength (Hodges et al., 2019). In 2024-2025 the new cross-section will be introduced into the global ozone observation networks using UV-photometry (BIPM, 2022).

**Deleted:** here presented

#### 819 4.1 Ozone Profiles from JOSIE 2009-2010 for SST1.0 and SST0.5

820 In Figure 6, the relative differences with the OPM for the conventionally (left diagrams) and TRC (right diagrams) processed  
821 ozonesonde profiles of JOSIE 2009/2010, respectively, are shown for each pair of sonde (SPC6A or EN-SCI) and solution  
822 type (SST0.5 or SST1.0), respectively, including the mean (black solid lines) and its  $1\sigma$ -standard deviation. The absolute  
823 ozone partial pressure differences are presented in the supplementary material (Fig. S3).  
824



838  
 839 **Figure 6** JOSIE 2009/2010: Relative differences with the OPM for the conventional (left diagrams) and TRC (right  
 840 diagrams) processed ozonesonde profiles for four pairs of sonde type and SST shown as scatter plots in four different colors  
 841 in the panels a-d: SPC6A/SST1.0 (a: blue dots), EN-SCI/SST0.5 (b: red dots), SPC6A/SST0.5 (c: green dots), and EN-  
 842 SCI/SST1.0 (d: brown dots), respectively. In each diagram for both methods the mean and  $1\sigma$ -standard deviation of the  
 843 relative differences are included (solid black line). The black dashed lines in the TRC-diagrams are the linear regressions of  
 844 the difference of the ozonesonde to the OPM as function of the pressure (on a  $\log$  scale). A summary plot is provided in  
 845 Fig. S4, and absolute differences are available in Fig. S3 of the Supplementary material.

846  
 847 For the conventional method, large relative deviations from the OPM exist in the pressure intervals response-time tests (in  
 848 particular RT1, RT2, RT3) ~~included in a simulation~~. This can be explained by the difference in response time between the  
 849 OPM and the ozonesondes and the fact that when ozone concentrations are close to zero, the relative differences will be

**Deleted:** arithmic

**Formatted:** Superscript

**Deleted:** take place during

852 magnified. The TRC method is able to correct well for the time response differences, as illustrated by the small relative  
853 differences, although with higher uncertainty ( $1\sigma$ -standard deviation) compared to adjacent pressure levels. A major  
854 improvement of the TRC methodology compared to the conventional corrections is the fact that the relative differences with  
855 respect to the OPM are almost pressure-independent, hence past ozone exposures. Up to about 13 hPa ( $Z\approx 30$  km), only a  
856 slightly increasing bias with decreasing pressure exists between the overall mean of the TRC-corrected ozonesondes and  
857 OPM for the JOSIE 2009/2010 sample (black dashed linear regression lines in Fig. 6).

858  
859 At pressures lower than 13 hPa the SPC sondes exhibit a declining behaviour, which is discussed in the next section. Overall,  
860 both EN-SCI SST0.5 and SPC SST1.0 agree very well within a few percent, with the TRC methodology using the correct  
861 pump efficiencies (see also Fig. S4). Consistent with earlier JOSIE and BESOS campaigns (Smit et al., 2007; Deshler et al.,  
862 2008), for both sonde types, SST0.5 gives around 3-5% lower ozonesonde readings than SST1.0, whereas, for both SSTs,  
863 SPC ozonesondes read  $\sim 3$ -5% lower than EN-SCI.  
864

#### 865 4.2 Ozone Profiles from JOSIE 2017 for SST1.0, SST0.5, and SST0.1

866 During the JOSIE 2017 campaign, tropical ozone profiles were simulated for three different SSTs: SST1.0, SST0.5 and  
867 SST0.1 (Thompson et al., 2019). No time-response tests were performed during these simulations. Therefore, for SST1.0 and  
868 SST0.5, the stoichiometry factors,  $S_s$ , derived from the JOSIE2009/2010 data have been applied. However, the SST0.1  
869 solution was not tested during the JOSIE 2009/2010 campaign. Therefore, for this SST, we determined the stoichiometry  
870 factors  $S_s$  with the same method as described in Sect. 3.2.1, but with time-response tests during ozonesonde laboratory  
871 measurements with a calibrated ozone analyser (details in Appendix B). The derived  $S_s$  factor is  $0.023 \pm 0.005$ . For the  
872 JOSIE 2017 campaign data, the initial value of the slow current component  $I_s$  at the start of the simulation at  $t=0$  (Sect.  
873 3.2.2) has been chosen to equal 0 (i.e. equal to  $I_{B0}$  before subtracting  $I_{B0}$ ), as there were usually a few hours between the end  
874 of the day of launch preparations and the start of the simulation, such that  $I_{B1}$  has decayed to  $I_{B0}$ .

875  
876 The differences of the JOSIE 2017 ozonesonde profiles with the corresponding OPM profile using the conventional and TRC  
877 data processing methodologies are shown in Figure 7; the absolute differences appear in Fig. S5. The most prominent feature  
878 for the conventional corrections, sonde type-SST combinations, is the dependence of the sonde to OPM differences on  
879 pressure or measured ozone amounts: the mean relative differences are largest (as well as the corresponding standard  
880 deviations) just below the tropopause at  $\sim(100-200)$  hPa, where the ozone partial pressures are minimal. The mean relative  
881 differences increase with decreasing pressure in both troposphere and stratosphere (also obvious in Fig. S6) and are most  
882 pronounced in the Tropics, where the ozone concentrations can be very low near the tropopause. In contrast, when the TRC-  
883 method is applied to the data, the pressure/ozone amount dependence of the relative difference almost completely disappears.  
884 For the standard EN-SCI/SST0.5 and SPC/SST1.0, there remains a slightly increasing bias with decreasing pressure (black  
885 dashed lines), while for the SST0.1 ozonesonde simulations, there is a tendency for decreasing (negative) relative differences  
886 with decreasing pressure. For both SPC and EN-SCI, SST0.1 ozone readings are slightly lower than the OPM measured  
887 ozone concentrations in the stratosphere, and up to 10% lower than the ozone values measured with the SOP recommended  
888 solutions (SPC/SST1.0 and EN-SCI/SST0.5).

**Deleted:** The Uccle experiments (Fig. 1) illustrated that the measured current with a zero-air source falls after two hours back to the  $I_{B0}$  value measured at the beginning of the preparation. ...

**Deleted:** t

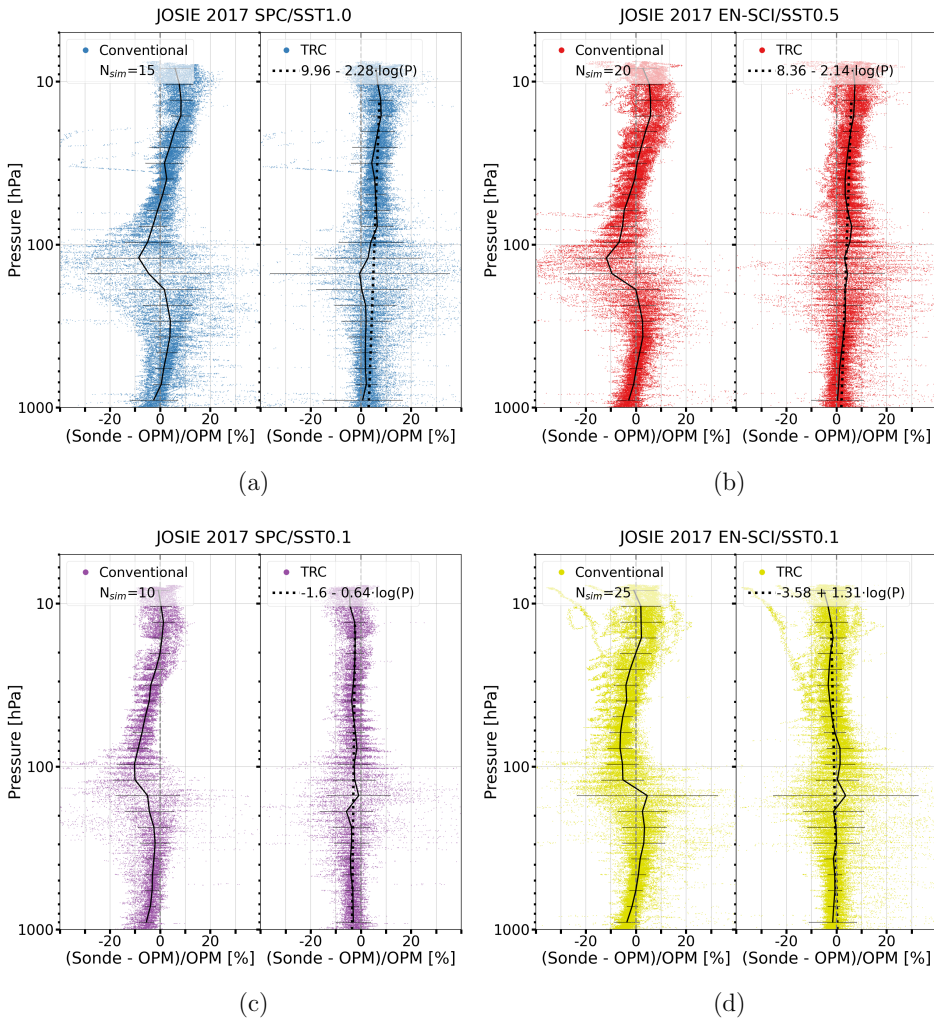
**Deleted:**

**Deleted:** 200

**Deleted:** ; t

**Deleted:** . The conventional method deviates strong from the OPM in the upper troposphere at about 100 hPa for the tropical ECC ozone profiles.

**Deleted:** For both SPC and EN-SCI, SST0.1 ozone measures about 10% lower than OPM in the stratosphere, compared to the recommended SOP (SPC/SST1.0 and EN-SCI/SST0.5). ...



905  
 906 **Figure 7.** JOSIE 2017: Differences with the OPM for the conventionally (left) and TRC (right) processed ozonesonde  
 907 profiles for the four sonde-SST pairs as scatter plots: SPC6A/SST1.0 (a: blue dots), EN-SCI/SST0.5 (b: red dots),  
 908 SPC6A/SST0.1 (c: purple dots), EN-SCI/SST0.1 (d: yellow dots). In each diagram for both methods, mean and  $1\sigma$ -standard  
 909 deviations are solid black lines. The black dashed lines in the TRC-diagrams are the linear regressions of the sonde-OPM  
 910 differences as a function of the pressure on a  $\log$  scale. A summary plot appears in Fig. S6 and absolute differences are in  
 911 Fig. S5 of Supplementary material.

912  
 913 When comparing the mean relative OPM offsets after processing the ozonesonde measurements with TRC methodology for  
 914 the two JOSIE campaigns, i.e. Figs. 6 and 7 (also in Figs. S4 and S6), we note that the network standards SPC/SST1.0 and  
 915 EN-SCI/SST05 are a few percent larger in the stratosphere for the “tropical” JOSIE 2017 campaign. That is, those mean  
 916 relative differences are manifest in both cases as a slightly decreasing relative bias with increasing pressure during both

Deleted: arithmic

Formatted: Superscript

Formatted: Left

918 campaigns. These differences are independent of post-ozone exposure and profile type (mid-latitude or tropical), in contrast  
919 to the conventional methodology which exhibits this past ozone memory effect. A striking disagreement between the profile-  
920 OPM offsets between JOSIE 2009/2010 and 2017 occurs at the lowest pressure range, lower than ~13 hPa. For the JOSIE  
921 2009/2010 data, the mean relative differences with the OPM display a stronger pressure dependence in this lowest pressure  
922 range, distinctly different for both sonde types, in contrast to the JOSIE 2017 mean relative OPM differences. The origin of  
923 this different behaviour above 13 hPa lies most likely in pump temperature differences between the simulated profiles.  
924 Whereas the mean pump temperature is close to 21°C in this pressure range in JOSIE 2009/2010, it is around 15°C for the  
925 tropical profiles in JOSIE 2017. Simultaneous temperature measurements during JOSIE 2017 revealed that the cell  
926 temperatures are about 5 to 10°C lower than the corresponding pump temperatures, depending on the sonde type.  
927 Specifically, the differences between pump and cell temperature are more at the high end range of this temperature interval  
928 for EN-SCI sondes, and at the low end range for the SPC due to differences in thermal contact between cells and pump. With  
929 these cell temperatures and taking the boiling temperatures at those low pressures into account, it turns out that the solutions  
930 in the SPC sondes tested in JOSIE 2009/2010 may already start boiling at higher ambient air pressures than during JOSIE  
931 2017. Cell weights were measured before and after all simulations for both campaigns. The weight loss due to  
932 evaporation/boiling of the sensing solution was considerably higher during JOSIE 2009/2010 than in JOSIE 2017: about a  
933 factor of 2 for EN-SCI/SST0.5 and even a factor of 3 for SPC/SST1.0. Although at these reduced ambient air pressures the  
934 absorption efficiency is not critical (Tarasick et al., 2021), the sensing solutions losses of the sondes may have become so  
935 large during JOSIE 2009/2010 that the absorption efficiency has non-negligibly declined. This may explain the  
936 underestimation of the ozone concentrations at low pressures for the JOSIE 2009/2010 profile simulations, in particular for  
937 SPC ozonesondes.

Deleted: near

Deleted: been

Deleted: ¶  
¶

## 938 5 Conversion Efficiency of TRC Method Calibrated to OPM

### 939 5.1 Differences Between Different Pairs of Sonde Type and SST

940 In the previous section it was shown that the TRC-method resolves the dependence of the measured ozonesonde profile from  
941 the past ozone exposure, whereas the deconvolution of the remaining fast ozone sensor current resolves effectively the  
942 impact of gradients in the profile caused by the 20-30 sec time response of the ECC-sensor. The sonde to OPM comparisons  
943 presented in section 4 for the mid-latitude profiles of JOSIE 2009/2010 (Fig. 6) and tropical profiles of JOSIE 2017 (Fig. 7)  
944 demonstrate that the TRC results are independent of the shape of the simulated ozone profiles, in contrast to the results  
945 obtained by the conventional method (e.g. Smit et al., 2007; Deshler et al., 2008, 2017; Thompson et al., 2019).  
946 For each pair of ozone sonde type and SST for JOSIE 2009/2010, JOSIE 2017 and combined JOSIE 2009/2010 and 2017  
947 (for SPC/SST1.0 and EN-SCI/SST0.5) a linear regression has been calculated as a function of pressure on a logarithmic  
948 scale for the TRC sonde-OPM relative differences within ±30% for pressures up to 13 hPa. These linear regression lines are  
949 shown in Figs. 6 and 7 as black dashed curves in the TRC diagrams for the different sonde-SST pairs; they agree well with  
950 the corresponding averages (black solid lines in TRC diagrams). All TRC-sonde/SST pair relative difference scatterplots  
951 display variations within 3-7% with altitude between the surface at P=1000 hPa and the upper end of the profile at P=10 hPa,  
952 as can be seen in Table 3 that displays the relative sonde-OPM differences at the intercepts P=1000 hPa and P=10 hPa of the  
953 linear regression. Table 3 illustrates the same typical differences of 3-5% for the same sonde type but different SST1.0 or  
954 SST0.5, as first observed in JOSIE 2000 (Smit et al., 2007). Figures S4 (a & b) and S6 (a and b) show the persistence of  
955 these systematic differences in detail for the conventional and TRC method as function of pressure (i.e. altitude). The low  
956 buffered (SST0.1) EN-SCI or SPC-6A sondes slightly underestimate ozone by a few percent compared to the OPM. It is  
957 noteworthy that the EN-SCI/SST0.1 OPM offsets decrease over the course of the sounding, in contrast to all other sonde-  
958 SST pairs for which the relative differences increase (Table 3: last column).

Deleted: 4.3 Differences Between Different Pairs of Sonde Type and SST ¶

For each pair of ozone sonde type and SST for JOSIE 2009/2010, JOSIE 2017 and combined JOSIE 2009/2010 and 2017 (for SPC/SST1.0 and EN-SCI/SST0.5) a linear regression has been calculated as a function of pressure on a logarithmic scale for the TRC sonde-OPM relative differences within ±30% for pressures up to 13 hPa. These linear regression lines are shown in Figs. 6 and 7 as black dashed curves in the TRC diagrams for the different sonde-SST pairs; they agree well with the corresponding averages (black solid lines in TRC diagrams). All TRC-sonde/SST pair relative difference scatterplots display variations within 3-7% with altitude between the surface at P=1000 hPa and the upper end of the profile at P=10 hPa, as can be seen in Table 3 that displays the relative sonde-OPM differences at the intercepts P=1000 hPa and P=10 hPa of the linear regression. Table 3 illustrates the same typical differences of 3-5% for the same sonde type but different SST1.0 or SST0.5, as first observed in JOSIE 2000 (Smit et al., 2007). Figures S4 (a & b) and S6 (a and b) show the persistence of these systematic differences in detail for the conventional and TRC method as function of pressure (i.e. altitude). The low buffered (SST0.1) EN-SCI or SPC-6A sondes slightly underestimate ozone by a few percent compared to the OPM. It is noteworthy that the EN-SCI/SST0.1 OPM offsets decrease over the course of the sounding, in contrast to all other sonde-SST pairs for which the relative differences increase (Table 3: last column). ¶



993 **Table 3.** Relative differences of the sonde to the OPM at the P= 1000 hPa and P=10 hPa intercepts of the linear regression as  
 994 a function of  $\text{Log}_{10}(P)$  obtained from the different JOSIE data sets (Figs. 6-7) and for the sonde pairs SPC-6A and EN-SCI  
 995 with different sensing solutions SST1.0, STT0.5 and SST0.1. Included are also the relative differences between EN-SCI and  
 996 SPC6A sondes when operated at the same SST (last three rows).

Data set	Number of Samples	Rel. Differences in % Sonde to OPM at intercept P=1000 hPa	Rel. Differences in % Sonde to OPM at intercept P=10 hPa	Rel. Differences in % Sonde to OPM between P is 1000 and 10 hPa
<b>SPC-6A /SST1.0</b>				
JOSIE 2009/2010	23	1.69	5.47	3.8
JOSIE 2017	11	3.12	7.68	4.6
JOSIE 2009/2010 + 2017	34	2.26	6.44	4.2
<b>SPC-6A /SST0.5</b>				
JOSIE 2009/2010	20	-2.0	3.62	5.6
<b>SPC-6A /SST0.1</b>				
JOSIE 2017	6	-3.52	-2.24	1.8
<b>EN-SCI /SST1.0</b>				
JOSIE 2009/2010	25	3.89	11.26	7.4
<b>EN-SCI /SST0.5</b>				
JOSIE 2009/2010	15	1.35	8.30	7.0
JOSIE 2017	20	1.93	6.21	4.3
JOSIE 2009/2010 + 2017	35	1.72	7.02	5.3
<b>ENSCI /SST0.1</b>				
JOSIE 2017	20	0.35	-2.27	-2.6
<b>SST EN-SCI – SPC6A</b>				
SST1.0		1.63	4.82	3.2
SST0.5		3.92	3.40	-0.5
SST0.1		3.87	0.03	-3.4

999 Further, the TRC results show a strong consistency of the mean relative differences with the OPM for the different sonde  
 1000 types-SST combinations across the different (grouped) JOSIE campaigns (see also Figs. S4 and S6). Therefore, those relative  
 1001 mean differences can be characterized by the linear regression curves as a function of  $\text{Log}_{10}(P)$  in Figs 6-7 and directly  
 1002 linked to the OPM. As such, these linear regression lines (hereafter referred to as “calibration curves”) could be applied as  
 1003 the final correction step of the TRCC methodology, tracing the ozonesonde measurements back to the OPM as the reference  
 1004 instrument.  
 1005  
 1006

Deleted: ¶

Deleted:

**Moved down [1]:** In the previous section it was shown that the TRC-method resolves the dependence of the measured ozonesonde profile from the past exposure of ozone, whereas the deconvolution of the remaining fast ozone sensor current resolves effectively the impact of gradients in the profile caused by the 20-30 sec time response of the ECC-sensor. The sonde to OPM comparisons presented in section 4 for the mid-latitude profiles of JOSIE 2009/2010 (Fig. 6) and tropical profiles of JOSIE 2017 (Fig. 7) demonstrate that the TRC results are independent of the shape of the simulated ozone profiles, in contrast to the results obtained by the conventional method (e.g. Smit et al., 2007; Deshler et al., 2008, 2017; Thompson et al., 2019). In the previous section it was shown that the TRC-method resolves the dependence of the measured ozonesonde profile from the past exposure of ozone, whereas the deconvolution of the remaining fast ozone sensor current resolves effectively the impact of gradients in the profile caused by the 20-30 sec time response of the ECC-sensor. The sonde to OPM comparisons presented in section 4 for the mid-latitude profiles of JOSIE 2009/2010 (Fig. 6) and tropical profiles of JOSIE 2017 (Fig. 7) demonstrate that the TRC results are independent of the shape of the simulated ozone profiles, in contrast to the results obtained by the conventional method (e.g. Smit et al., 2007; Deshler et al., 2008, 2017; Thompson et al., 2019). Further, the TRC results show a strong consistency of the mean relative differences with the OPM for the different sonde types-SST combinations across the different (grouped) JOSIE campaigns (see also Figs. S4 and S6). Therefore, those relative mean differences can be characterized by the linear regression curves as a function of  $\text{Log}_{10}(P)$  in Figs 6-7 and directly linked to the OPM. As such, these linear regression lines (hereafter referred to as “calibration curves”) could be applied as the final correction step of the TRC methodology, tracing the ozonesonde measurements back to the OPM as the reference instrument.

Moved (insertion) [1]

Deleted: .....Page Break.....

**5 Conversion Efficiency of TRC Method Calibrated to OPM¶**

In the previous section it was shown that the TRC-method resolves the dependence of the measured ozonesonde profile from the past exposure of ozone, whereas the deconvolution of the remaining fast ozone sensor current resolves effectively the impact of gradients in the profile caused by the 20-30 sec time response of the ECC-sensor. The sonde to OPM comparisons presented in section 4 for the mid-latitude profiles of JOSIE 2009/2010 (Fig. 6) and tropical profiles of JOSIE 2017 (Fig. 7) demonstrate that the TRC results are independent of the shape of the simulated ozone profiles, in contrast to the results obtained by the conventional method (e.g. Smit et al., 2007; Deshler et al., 2008, 2017; Thompson et al., 2019). In the previous section it was shown that the TRC-method resolves the dependence of the measured ozonesonde profile from the past exposure of ozone, whereas the deconvolution of the remaining fast ozone sensor current resolves effectively the impact of gradients in the profile caused by the 20-30 sec time response of the ECC-sensor. The sonde to OPM comparisons presented in section 4 for the mid-latitude profiles of JOSIE 2009/2010 (Fig. 6) and tropical profiles of JOSIE 2017 (Fig. 7) demonstrate that the TRC results are independent of the shape of the simulat... [1]

Formatted: Font: Italic

Formatted: Normal

1113 **5.2 Parameterisation of the Overall Conversion Efficiency  $\eta_c$**

1114 The linear regressions of the relative differences of the sonde to the OPM (Figs. 6-7) of the TRC method can be interpreted  
1115 as the correction term of the overall conversion efficiency  $\eta_c$  when deviating from one for each of the different pairs of  
1116 sonde type and SST. The overall conversion efficiency  $\eta_c$  in Eq. (6) can be expressed as a function of the ambient air  
1117 pressure of the vertical sounding:

1118 
$$\eta_c(P) = 1 + F_c(P) \tag{17}$$

1119 where  $F_c(P)$  is the so-called correctional term of  $\eta_c$  as a function of the ambient air pressure  $P$ , which is parameterised by  
1120 the linear regression fit of the relative sonde-OPM deviations as a function of  $\text{Log}_{10}(P)$  and substituted in Eq. (17). This  
1121 means that the overall conversion efficiency  $\eta_c(P)$ , calibrated to the OPM, has the following parameterisation

1122 
$$\eta_c(P) = 1 + a + b \cdot \text{Log}_{10}(P) \tag{18}$$

1123 The linear regression curves derived for the different pairs of SPC-6A, EN-SCI with SST1.0, SST0.5, or SST0.1 obtained  
1124 for the different JOSIE campaigns are shown in the TRC diagrams of Figs. 6-7 by the **black dashed line**. From Fig. 6-7 and  
1125 Table 3, it is obvious that the relative OPM offsets (and the resulting linear regressions) for the same pairs of sondes and  
1126 SST05 or SST1.0 are very similar in JOSIE 2009/2010 and JOSIE 2017. Thus, to achieve the best statistics, the results for  
1127 those campaigns are lumped together in Fig. 8.

1129 The results of the parameterisation of  $\eta_c(P)$ , i.e. the offset  $a$  and the slope  $b$  (Eq.18), including their uncertainties  $\Delta a$  and the  
1130 slope  $\Delta b$ , respectively, are listed for the different pairs of sonde type and SSTs as JOSIE (2009/2010 + 2017) in Table 4. The  
1131 sonde/SST pairs operated with SST0.5 and SST1.0 cover mid-latitude as well as tropical ozone profile conditions, i.e. the  
1132 resulting  $\eta_c(P)$  functions are independent of the ozone profile. Based on this, we expect that the  $\eta_c(P)$  for the SST0.1, which  
1133 could only be derived in this study for the tropical JOSIE-2017 conditions, can also be applied to non-tropical ozone profiles.  
1134 Likewise, we expect that the  $\eta_c(P)$  determined from JOSIE 2009 only for the SPC/SST0.5 and EN-SCI/SST1.0 pairs are  
1135 valid for tropical ozone profiles. **Of course, the derived linear regression coefficients for the calibration functions are  
1136 directly linked to the pump efficiency values used, and it is assumed here that the used average pump efficiency values from  
1137 Nakano and Morofuji (2023) in Table 1 are correct within their uncertainties and representative for this study. However, if  
1138 these pump efficiency values might change over time (see Nakano and Morofuji, 2023), the calibration functions must be  
1139 adjusted accordingly.**

1141 The calibration functions are presented here (Table 4) as a function of pressure, but this does not mean that they are really  
1142 pressure dependent. However, the goal is to provide a practical empirical representation of the overall performance of the  
1143 ozonesonde, ascending with a balloon at  $\sim 5\text{m/s}$ . The calibration functions can thus be interpreted as the correction term of  
1144 the overall conversion efficiency of the ECC sonde when deviating from one, but **their origin is still unclear**. Most likely this  
1145 term relates to the unknown stoichiometry of the fast chemical reactions converting ozone into free iodine, in other words,  
1146 the fast ECC current  $I_f$ . This is supported by the shape of the vertical profiles of the absolute  $\text{PO}_3$ -differences of the ECC  
1147 sonde compared to the OPM for the TRC, shown for the JOSIE 2009/2010, JOSIE 2017 and for the JOSIE 1996-2002 data  
1148 (described in section 5.3), in the middle diagrams of Figures S3, S5 and S7, respectively. Indeed, in the middle stratosphere,  
1149 the shapes of the residual currents compared to the OPM are more or less in phase with the simulated ozone profiles. This is  
1150 most pronounced for the JOSIE-2017 tropical profiles (Fig. S5) and might indicate that these residual currents result from  
1151 the fast chemical conversion and not from the 25-min delayed slow reaction. In the latter case, a phase shift between the  
1152 residual currents and the ozone profile would be expected. The observed increase with altitude of typical 3-7% in the  
1153 calibration functions (Tables 3 & 4) might **be explained** from a small slightly increasing change of the stoichiometry of the  
1154 fast  $\text{O}_3$  conversion due to an increase of KI concentration and buffer strength caused by evaporation during the sounding.

Deleted: 1

Formatted: Font: Italic

Formatted: Font: Italic

Formatted: Font: Italic

Formatted: Font: Italic

Deleted: black

Formatted: Font: Italic

Formatted: Font: Italic

Deleted:

Formatted: Font: Italic

Deleted: ¶

Deleted: the

Deleted: s

Deleted: are

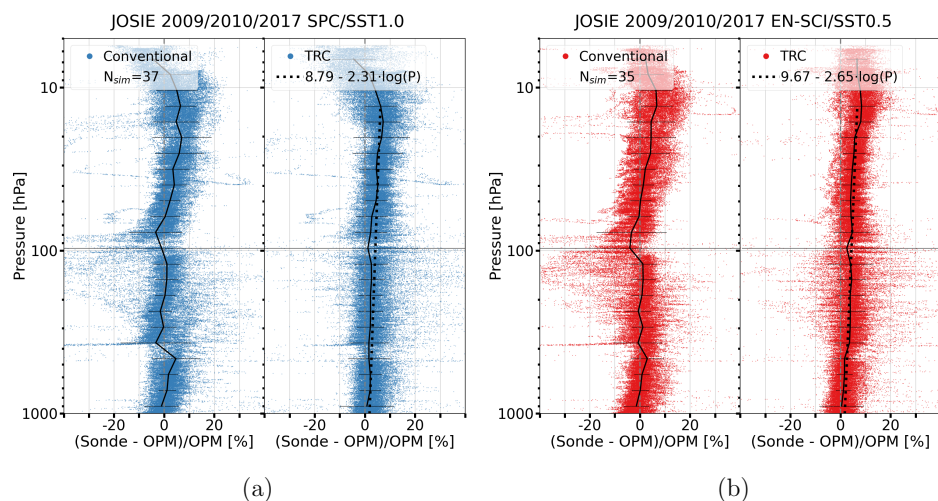
Deleted: certain

Deleted: e

Deleted: 2

Deleted: derive



1167  
1168

1169 **Figure 8.** JOSIE 2009/2010 and 2017: Relative differences with the OPM for the conventional (left diagrams of panels (a)  
 1170 and (b)) and TRC (right diagrams of panels (a) and (b)) processed ozonesonde profiles for two pairs of sonde type and SST  
 1171 shown as scatterplots for SPC6A/SST1.0 (a: blue dots) and EN-SCI/SST0.5 (b: red dots), respectively. In each diagram for  
 1172 both methods the mean and  $1\sigma$ -standard deviation are included (solid black line). The black dashed lines in the TRC-  
 1173 diagrams are the linear regressions of the differences of the ozonesonde to the OPM as function of the pressure (on a  $10^{\log}$   
 1174 scale).

1175

1176 Although the cell temperatures of the ozonesondes (both SPC6A/SST1.0 and EN-SCI/SST0.5) in JOSIE. 2009/2010 were  
 1177 about 10 °C higher than in JOSIE 2017 there are no direct indications that there is any cell temperature dependence of the  
 1178 calibration functions. This is demonstrated by the fact that SPC6A/SST1.0 and EN-SCI/SST0.5 for both campaigns show  
 1179 very similar OPM deviations over the course of the sounding when compared at the intercept points at  $P=1000$  and 10 hPa  
 1180 (Table 3). However, temperature dependence cannot be completely excluded, in as much as the chemical reactions involved  
 1181 in the  $KI+O_3$  chemistry may have significant temperature dependencies. Again, further in-depth investigations are needed.

1182

1183

1184 **Table 4.** Parameterisation (offset  $a$  and slope  $b$ ) of the calibrated conversion efficiency  $\eta_c(P)$  (Eq. 18) for the different pairs  
 1185 of SPC-6A or ENSCI with SST1.0, SST0.5, or SST01 derived from the results of JOSIE 2009/2010 and JOSIE 2017.

1186 Included are the  $1\sigma$ -uncertainties  $\Delta a$  and  $\Delta b$  of the offset  $a$  and slope  $b$  in Eq. 18, respectively. The parameterisation of  $\eta_c$   
 1187 ( $P$ ) is valid from  $P=1000$  hPa until  $P=13$  hPa ( $Z\approx 30$  km) for SPC, and for EN-SCI to 10 hPa ( $Z\approx 32-33$ km).

1188

Deleted:

Deleted: arithmetic

Formatted: Superscript

Deleted:

Deleted: 5

Sonde Type / SST	Number of Samples	TRC-Conversion Efficiency $\eta_c(P) = 1 + a + b \cdot \text{Log}_{10}(P)$ Eq. (18)		JOSIE Data Set
		Offset $a \pm \Delta a$	Slope $b \pm \Delta b$	
SPC-6A /SST1.0	37	$(8.79 \pm 0.07) \times 10^{-2}$	$(-2.32 \pm 0.03) \times 10^{-2}$	JOSIE (2009/2010 + 2017)
SPC-6A /SST0.5	20	$(6.43 \pm 0.08) \times 10^{-2}$	$(-2.81 \pm 0.04) \times 10^{-2}$	JOSIE 2009
SPC-6A /SST0.1	10	$(-1.60 \pm 0.12) \times 10^{-2}$	$(-0.64 \pm 0.05) \times 10^{-2}$	JOSIE 2017
EN-SCI /SST1.0	25	$(14.94 \pm 0.07) \times 10^{-2}$	$(-3.68 \pm 0.03) \times 10^{-2}$	JOSIE 2009
EN-SCI /SST0.5	35	$(9.67 \pm 0.06) \times 10^{-2}$	$(-2.65 \pm 0.03) \times 10^{-2}$	JOSIE (2009/2010 + 2017)
EN-SCI /SST0.1	20	$(-3.58 \pm 0.09) \times 10^{-2}$	$(1.31 \pm 0.04) \times 10^{-2}$	JOSIE 2017

Deleted: 4

Deleted: 53

Deleted: 09

Deleted: 6

### 5.3 Application to JOSIE 1996 + 1998 + 2000 + 2002 data

The calibrated  $\eta_c(P)$  functions derived from JOSIE 2009/2010 and JOSIE 2017 (Table 4) for the different sonde/SST pairs are applied to TRC processed ozonesonde data of JOSIE 1996 + 1998 + 2000 + 2002, in Figure 9, again as relative differences to the OPM. In the remainder of this paper, we will use the abbreviation TRCC to denote that the TRC method has been applied with additional application of the calibration functions. The JOSIE 1996 + 1998 + 2000 datasets and results were described in detail by Smit and Kley (1998) and Smit and Sträter (2004a, 2004b) and analysed by Smit et al. (2007). For JOSIE 1996, we excluded data from NOAA and CNRS because their operating procedures deviated too greatly from the Komhyr (1986) procedures; JOSIE 2002 was a small campaign in which only 3 simulation runs were made with 10 SPC/SST1.0 sondes. The setup of the earlier campaigns was similar to the JOSIE 2009/2010 or JOSIE 2017 experiments. In the earlier campaigns mostly mid-latitude ozone profiles were simulated with the same four combinations of EN-SCI or SPC with either SST0.5 or SST1.0 (although the sample sizes with SST0.5 were rather small). The largest difference between JOSIE 2009/2010 and the early JOSIE campaigns lies in the preparation of the ozonesondes: in JOSIE 2009/2010, the same SOPs were followed by the three operators; ozonesondes “flown” in the earlier JOSIE-campaigns being prepared by different teams of people with a variety of SOPs.

Deleted: 2

Deleted:

The comparisons with the OPM in Fig.9 are displayed for the TRC results, hence not calibrated ( $\eta_c(P) = 1.00$ , middle diagrams) and for the TRCC corrections, i.e. calibrated ( $\eta_c(P)$  from Table 4, right diagrams), while the results for the conventional method (left diagrams) are also included. From the figure it is obvious that independent of the sonde type (SPC-6A or EN-SCI) or sensing solution type (SST1.0, SST0.5), after applying  $\eta_c(P)$  the residual average curves (black solid lines) are within less than  $\pm 1\%$  deviation from the “zero” over the entire vertical profile until 7-10 hPa. This means that with the TRCC, i.e. TRC combined with the use of the specific  $\eta_c(P)$  for the various sonde-SST pairs, there are no longer systematic bias effects in the measured vertical ozonesonde profiles with respect to the OPM as a function of pressure (i.e. altitude). The use of the TRCC can be a powerful tool to homogenize long term ozone records in the global ozonesonde network, so that these are now traceable to one reference standard, i.e. the OPM at the WCCOS. The application of the TRCC with the use of the calibration functions on the JOSIE 2009/2010 and JOSIE 2017 datasets is also illustrated in the figures S3, and S5 in the Supplementary Material, showing the vertical profiles of the absolute differences of the sondes with the OPM for the conventional method, TRC and TRCC. This information is also provided for the absolute differences for the early JOSIE campaigns in Fig. S7.

Deleted: once

Deleted: once

Deleted: (

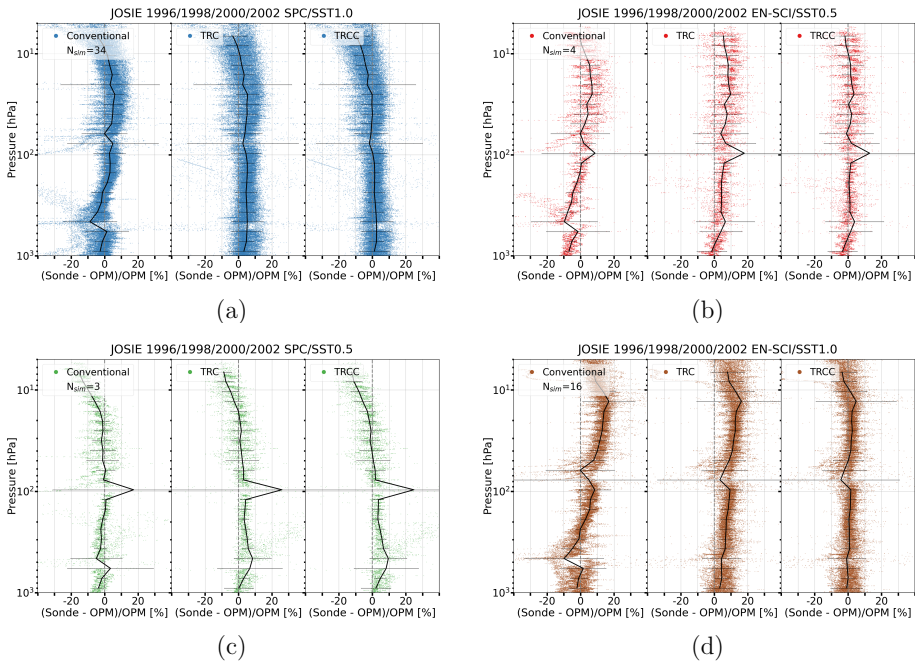
Deleted: arc

Deleted:

Deleted: calibrated

Deleted:

Deleted: + Calibration



1238  
 1239  
 1240  
 1241  
 1242  
 1243  
 1244  
 1245  
 1246  
 1247  
 1248

**Figure 9.** JOSIE 1996 + 1998 + 2000 + 2002: Relative differences [%] with the OPM for the “conventional” (left diagrams of panels a-d), “TRC” (middle diagrams of panels a-d), and “TRCC” (= TRC + application of calibration functions) (right diagrams of panels a-d) processed ozonesonde profiles for four pairs of sonde type and SST, shown as scatter plots in four different colors in the panels a-d: SPC6A/SST1.0 (a: blue dots), EN-SCI/SST0.5 (b: red dots), SPC6A/SST0.5 (c: green dots), and EN-SCI/SST1.0 (d: brown dots), respectively. In each diagram for both methods the mean and 1 $\sigma$ -standard deviation of the relative differences are included (solid black line). The absolute difference plots are available in the Supplementary Material (Fig. S7), and a summary plot of the relative differences in Fig. S8.

1249 **6. Contribution Individual Correction Steps and Uncertainty Budget of the TRCC Method**

1250 In this section we quantify the impact of the individual corrections made in the TRCC method and estimate their uncertainty  
1251 contributions to the overall uncertainty of the ozone partial pressure derived from the measured ECC-ozone sensor current.

Deleted:  
Deleted:

1253 **6.1 Contribution of Correction Steps of TRC-Method for Mid-Latitude and Tropical Conditions**

1254 To derive from the measured cell current  $I_M$  the partial ozone pressure in the ambient air the TRCC method includes five  
1255 different corrections: (i) constant background current  $I_{B0}$ ; (ii) slow cell current  $I_S$ ; (iii) time lag of fast current  $I_F$ : deconvolved  
1256 fast cell current (incl. smoothing); (iv) true pump efficiency (Nakano and Morofuji, 2023); (v) calibrated conversion  
1257 efficiency  $\eta_c(P)$  (Eq. 18 and Table 4). The impact of the different corrections on the measured cell current as a function of  
1258 pressure (i.e.  $\log^{10}(P)$ ) is shown in Figure 10 for mid-latitude (JOSIE 2009/2010) and tropical (JOSIE 2017) vertical profile  
1259 conditions for the standard sonde type –SST pairs, SPC6A/SST1.0 and EN-SCI/SST0.5, respectively; included are in  
1260 addition examples of the different corrections made using the conventional method for JOSIE 2009/2010 and JOSIE 2017,  
1261 respectively.

Deleted: four  
Deleted: new  
Formatted: Not Highlight  
Deleted: are  
Deleted: .

1263 A first, obvious, observation to make is that the corrections for a decreasing pump efficiency are for all sonde type- SST  
1264 pairs identical and at pressures smaller than 100 hPa increase slowly but significantly from 1 % at  $P=100$  hPa to 12% at  $P =$   
1265 10 hPa and to almost 20 % at  $P = 5$  hPa. In the upper part of the profile (above 25 hPa) it is the dominating correction. In the  
1266 lower part, below 100 hPa, the constant background  $I_{B0}$  (brown line) and the past ozone dependent slow cell current  $I_S$   
1267 (yellow line) are the major corrections, particularly in the upper tropical troposphere, with its very low ozone concentrations  
1268 (diagrams f and g). Here, those corrections can amount up to about 10-15%, depending on e.g. the amplitude of the measured  
1269  $I_{B0}$  values. In this context, we also note that, because of the larger  $S_S$  values for SPC6A/SST1.0, the past ozone dependent  
1270 slow current ( $I_S$ ) correction will be about a factor of 2 larger than the  $I_S$  correction for the ENSCI/SST0.5, in all diagrams of  
1271 Fig. 10. On top of this effect, for SPC6A/SST1.0 JOSIE 2009/2010 (diagram b in Fig. 10), above 10 hPa, the relative  $I_S$   
1272 correction is even rapidly increasing in absolute value due to the limited performance of the SPC6A sonde due to substantial  
1273 losses of the sensing solution caused by boiling effects, as explained before in section 4.2. The impact of the time lag  
1274 correction of the fast current is of the order of  $\pm 5\%$ , and of course strongly dependent on the local vertical ozone gradient.  
1275 Therefore, it can even become the dominant correction in the tropical UTLS region (between 5-10%), with its strong vertical  
1276 ozone gradient (diagrams f-g). Finally, we mention that very similar results are obtained for the ozonesonde types combined  
1277 with SST0.1, which are shown in the supplementary material (Fig. S9).

Deleted: panels  
Deleted: E  
Deleted: F

1278 All individual corrections of the TRCC method are based on known physical and chemical processes, with one exception  
1279 being the remaining conversion efficiency, which was derived from calibration of the TRC-corrected probe readings with the  
1280 OPM reference instrument. This contrasts with the corrections made in the conventional method (Fig.10-d, g), which were  
1281 empirically derived to achieve a total ozone normalization factor close to one. Therefore, the following corrections are  
1282 applied: (i) an empirical effective efficiency function (Fig. 10, blue line in graphs (d) and (g)) that represents the estimation  
1283 of a decreasing pump efficiency and an increasing conversion efficiency (i.e. increasing stoichiometry of  $O_3+KI$  redox  
1284 reaction (R1) at lower pressures); (ii) a background current  $I_{B1}$  correction that compensates for excessive ozone levels near  
1285 the surface. However, in the tropics the  $I_{B1}$  correction is too large (Fig. 10-g: brown line) and leads to significantly too low  
1286 ozonesonde values in the troposphere (Fig. S9-f in the Supplement).

Deleted: e  
Deleted: f

Formatted: Subscript  
Formatted: Font: Italic  
Formatted: Subscript  
Formatted: Font: Italic  
Formatted: Subscript  
Formatted: English (US)

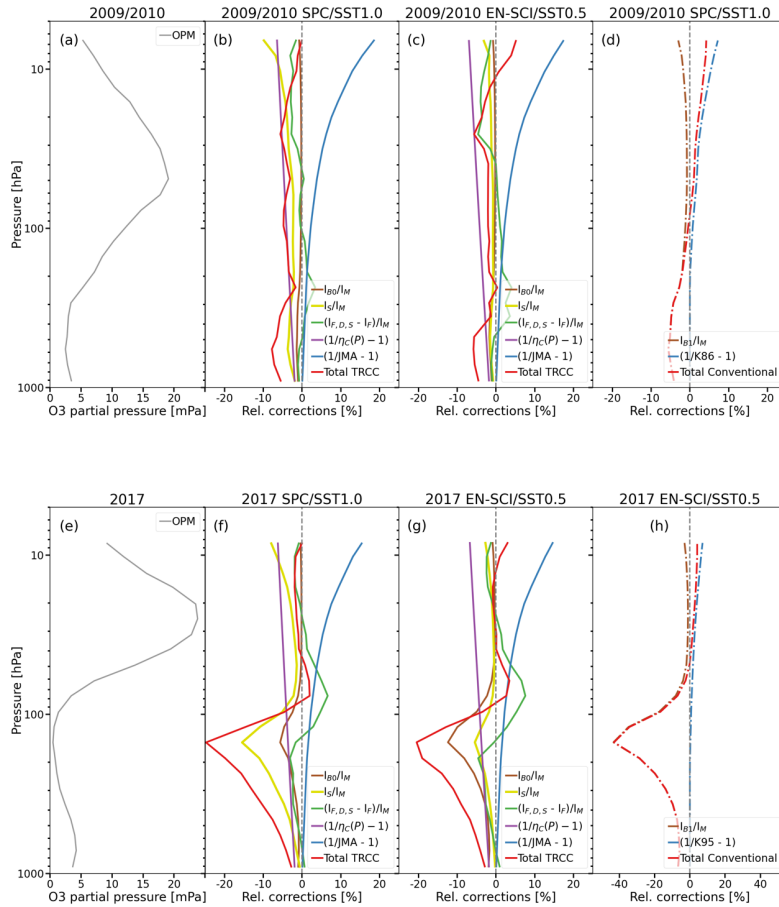


**Figure 10.** Relative corrections of TRCC method for typical mid-latitude (upper diagrams (a), (b), (c); JOSIE 2009/2010) and tropical (diagrams (e), (f), (g); JOSIE 2017) ozonesonde profiles, respectively, showing the influence of the different correction steps for the new TRCC method for SPC/SST1.0 (diagrams (b) and (f)) and EN-SCI/SST0.5 (diagrams (c) and (g)). The total correction (red line) consists of: (i)  $I_{B0}$  (brown line); (ii)  $I_s$  (yellow line); (iii) De-convolved and smoothed  $I_F$  (green line); (iv) True pump efficiency (blue line: Nakano and Morofuji, 2023); (v) Calibrated conversion efficiency (purple line). Diagrams (d) and (h) show the relative corrections of the conventional method for JOSIE 2009/2010 (SPC/ SST1.0) and JOSIE 2017 (EN-SCI/SST0.5), respectively; total correction (red line) consists of: (i)  $I_{B1}$  (brown line); (ii) empirical effective efficiency (blue line: Komhyr (1986) for SPC and Komhyr et al (1995) for EN-SCI, respectively).

- Deleted: A
- Deleted: B
- Deleted: C
- Deleted: d
- Deleted: e
- Deleted: f
- Deleted:
- Deleted: e
- Deleted:
- Deleted: f
- Deleted: w/green
- Deleted: convolution
- Deleted:
- Deleted: i
- Deleted: P

1330 **6.2 Uncertainty Budget of the TRC Method**

1331 For the conventional method a detailed uncertainty budget has been studied by Tarasick et al. (2021) and described in detail  
 1332 in the GAW 268 Report (Eq. E-3-1), together with practical guidelines to determine the overall uncertainty from the  
 1333 individual instrumental and procedural contributions. It is assumed that the uncertainties are random, uncorrelated, and  
 1334 normally distributed and following Gaussian statistics. In case of the TRCC, the overall relative uncertainty of  $P_{O_3}$  is derived  
 1335 from Eq. (6), which has slightly changed compared to formula E-3-1 in GAW#268 (2021) as follows:

$$1336 \frac{\Delta P_{O_3}}{P_{O_3}} = \sqrt{\left(\frac{\Delta \eta_P}{\eta_P}\right)^2 + \left(\frac{\Delta \eta_A}{\eta_A}\right)^2 + \left(\frac{\Delta \eta_C}{\eta_C}\right)^2 + \left(\frac{\Delta I_F}{I_F}\right)^2 + \left(\frac{\Delta T_P}{T_P}\right)^2 + \left(\frac{\Delta \Phi_{P_0}}{\Phi_{P_0}}\right)^2 + \sum \varepsilon_i^2} \quad (19)$$

1337 The additional term  $\varepsilon_i$  represents additional random uncertainties (Tarasick et al., 2021); in case of the TRCC these can be  
 1338 e.g. the relative uncertainty contributions by the used numerical schemes of either the convolution to obtain  $I_S(t)$  or the  
 1339 deconvolution of  $I_F(t)$  and its additional smoothing.

1340 To determine the uncertainty budget for TRCC in Eq. (19) the uncertainty contributions  $\Delta \eta_P$ ,  $\Delta \eta_A$ ,  $\Delta \eta_C$ ,  $\Delta I_F$ ,  $\Delta T_P$ , and  $\Delta \Phi_{P_0}$   
 1341 are exactly the same as in GAW Report No. 268 (2021) following the guidelines in its Annex-C. However, the recipes to  
 1342 determine the uncertainty contributions of the time varying  $I_F(t)$ , and the pressure dependent  $\eta_C(P)$  (see Table 4) differ from  
 1343 GAW#268:

1344 Uncertainty contribution  $\Delta I_F$ :

1345 From Eq. (7) the relative uncertainty of the fast sensor current  $I_F(t)$  can be derived:

$$1346 \frac{\Delta I_F(t)}{I_F(t)} = \sqrt{\frac{(\Delta I_M)^2 + (\Delta I_{B_0})^2 + (\Delta I_S)^2}{(I_M - I_{B_0} - I_S)^2}} \quad (20)$$

1347 Here  $\Delta I_{B_0} \approx 0.01 \mu A$ , obtained from the  $I_{B_0}$  time series from Uccle.  $I_S(t)$  estimations by varying the slow time constant with  
 1348  $\Delta \tau_S = \pm 5$  minutes has shown that  $\Delta \tau_S$  only has a minor contribution to  $\Delta I_S(t)$  of less than 1%, while a potential contribution  
 1349 of the numerical convolution scheme itself is vanishing small. It is obvious that  $\Delta I_S(t)$  is predominantly determined by the  
 1350 uncertainty  $\Delta S_S$  of the stoichiometry  $S_S$  of the slow reaction path (Table 2) as:

$$1351 \Delta I_S(t) \approx \frac{\Delta S_S(t)}{S_S(t)} \cdot I_S(t) \quad (21)$$

1352 The impact of the slow time constant  $\tau_S$  on the stoichiometry  $S_S$  and its uncertainty  $\Delta S_S$  is also insignificant, as we assessed  
 1353 by varying  $\Delta \tau_S = \pm 5$  minutes. Further, any contribution of the numerical schemes of deconvolution and its additional  
 1354 smoothing to the uncertainty of  $I_F$  have been checked and appeared to be vanishingly small (< 0.5%).

1355 Uncertainty contribution  $\Delta \eta_C$ :

1356 The conversion efficiency  $\eta_C(P)$  (Eq. 18) has been calibrated to the OPM such that its uncertainty  $\Delta \eta_C(P)$  includes also the  
 1357 uncertainty of the  $P_{O_3,OPM}$  measurement by the OPM as follows

$$1358 \frac{\Delta \eta_C(P)}{\eta_C(P)} = \sqrt{\frac{(\Delta a)^2 + (\text{Log}_{10}(P) \cdot \Delta b)^2}{(\eta_C(P))^2} + \left(\frac{\Delta P_{O_3,OPM}(P)}{P_{O_3,OPM}(P)}\right)^2} \quad (22)$$

1359 Hereby  $\frac{\Delta P_{O_3,OPM}(P)}{P_{O_3,OPM}(P)}$  is the relative uncertainty of the  $P_{O_3,OPM}$  measurement of the OPM which is estimated to be better than 2  
 1360 % at  $P > 10$  hPa, and with lower pressures slightly increasing to 3 % until  $P = 5$  hPa through potential small wall losses at  
 1361 these pressures. The reported relative uncertainty values here for the OPM are about 1.5 % better than the values mentioned  
 1362 before by Proffitt et al. (1983) because of the seven times smaller uncertainty of the new UV-absorption cross-section  
 1363 (Hodges et al., 2019) compared to the former cross-section (Hearn et al., 1961) that was used before to derive the  $P_{O_3}$   
 1364 measurement of the OPM.

1365  
 1366 The overall uncertainty budget for the TRCC method is summarized in Table 5. Figure 11 shows the contributions of the  
 1367 different uncertainty sources to the uncertainty budgets for the SPC6A/SST1.0 and EN-SCI/SST0.5 when applying the

Deleted: 7

Formatted: Font: Italic

Formatted: Font: Italic

Formatted: Font: Italic

Formatted: Font: Italic

Formatted: Font: Italic

Formatted: Font: Italic

Formatted: Font: Italic

Formatted: Font: Italic

Deleted: S

Formatted: Font: Italic

Formatted: Font: Italic

Formatted: Font: Italic

Formatted: Font: Italic

Formatted: Font: Italic

Formatted: Font: Italic

Deleted: with

Deleted: t

1372 TRCC method for a typical mid-latitude and tropical ozone profile as used in JOSIE 2009/2010 and JOSIE 2017,  
 1373 respectively. The results for SPC6A/SST0.5 and EN-SCI/SST1.0 for JOSIE 2009/2010 and the low buffered SPC6A/SST0.1  
 1374 and EN-SCI/SST0.1 for JOSIE 2017 are shown in Figure S10 in Supplementary Material. For the sake of clarity, the  
 1375 uncertainty contributions due to (i) ascent rate variation, (ii) pressure uncertainty, (iii) total ozone normalization factor are  
 1376 not included here, as these are beyond the scope of this study. However, the characteristics of these uncertainty  
 1377 contributions, as reported by Tarasick et al. (2021) and GAW Report No. 268, would not change the uncertainty budget of  
 1378 the TRC method itself.

1380 **Table 5.** Sources of ozonesonde profile uncertainty and their estimated magnitudes for the TRCC method. All quoted  
 1381 uncertainties are one standard deviation ( $1\sigma$ ). (\*) To approximate  $\Delta S_s$  as a one standard deviation uncertainty the MAD  
 1382 values (only covering 25-75 percentiles) in Table 2 have been multiplied by 1.5 to become compatible with the Gaussian  
 1383 error propagation applied here.

Source	Uncertainty	Reference
Pump flow rate $\Phi_{p0}$	$\Phi_{p0}$ [E-3-3] and $\Delta\Phi_{p0}$ [E-3-9]: $\frac{\Delta\Phi_{p0}(P)}{\Phi_{p0}(P)} = 1\%$	GAW Report No. 268 (2021)
Pump temperature $T_P$	$T_P$ : $\frac{\Delta T_P}{T_P} = 0.25\%$	GAW Report No. 268 (2021)
Pump efficiency $\eta_P(P)$	$\eta_P(P)$ and $\Delta\eta_P(P)$ in Table 1: JMA-efficiency	Nakano and Morofuji (2023)
Absorption efficiency $\eta_\lambda$	$\eta_\lambda = 1.00$ and $\Delta\eta_\lambda = 0.01$	GAW Report No. 268 (2021)
Measured cell current $I_M(t)$	$\Delta I_M(t) = \pm 0.005 \mu\text{A}$ at $I_M(t) < 1.00 \mu\text{A}$ $\Delta I_M(t) = \pm 0.5\%$ of $I_M(t)$ at $I_M(t) > 1.00 \mu\text{A}$	GAW Report No. 268 (2021)
Background current $I_{B0}$	$I_{B0} = 0$ to $0.03 \mu\text{A}$ and $\Delta I_{B0} = 0.01 \mu\text{A}$	GAW Report No. 268 (2021)
Slow cell current $I_S(t)$	Different sonde type and SST: $\Delta I_S(t) = \frac{\Delta S_S(t)}{S_S(t)} \cdot I_S(t)$ from Eq. (21) $S_S$ and $\Delta S_S$ from Table 2 (*)	This study
Fast cell current $I_F(t)$	$I_F(t)$ from Eq. (7) and $\frac{\Delta I_F}{I_F}$ from Eq. (20)	This study
Conversion efficiency $\eta_C(P)$	Different sonde type and SST: $\eta_C(P)$ from Table 3 and $\frac{\Delta\eta_C(P)}{\eta_C(P)}$ from Eq. (22) $\cong 2\%$	This study
Partial pressure ozone by OPM: $P_{O_3, OPM}$	$\Delta P_{O_3, OPM} : 2\%$ at $P > 10 \text{ hPa}$ $2\%$ to $3\%$ at $P$ from $10 \text{ hPa}$ to $5 \text{ hPa}$	This study

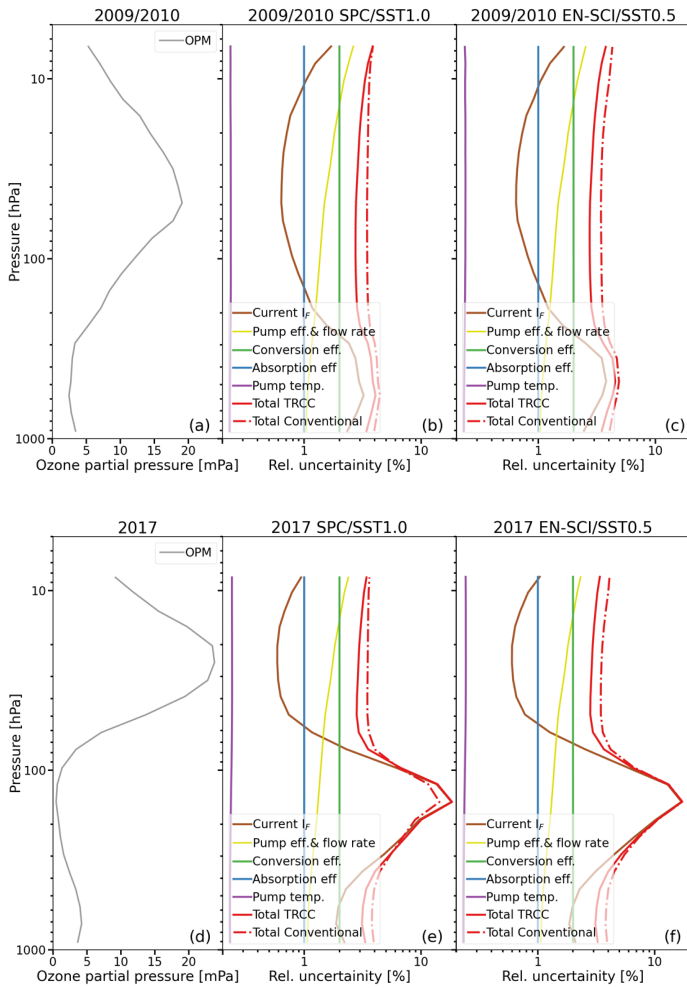
1385  
 1386  
 1387 In both the mid-latitude and tropical case (Fig. 11) it is seen that the (“background”) current in the troposphere and the  
 1388 conversion efficiency in the stratosphere are the dominant uncertainty sources. For the conventional method the conversion  
 1389 efficiency assumes that the overall stoichiometry factor is 1.00 with an uncertainty of 0.03 (Dietz et al. 1973), and obviously  
 1390 also the dominant uncertainty source in the stratosphere. However, in this study we have shown that the overall stoichiometry  
 1391 can significantly differ from unity, which makes the overall uncertainty for the conventional method rather optimistic. For the  
 1392 TRCC-method  $\Delta\eta_C(P)$  is mostly determined by the 2-3% uncertainty of the OPM as the reference to obtain the  $\eta_C(P)$   
 1393 calibration functions (Table 4). In the troposphere, the contribution of  $I_S$  correction in the TRCC method is mostly smaller than  
 1394 the  $I_{B1}$  correction in the conventional method, particularly in the tropics.

Formatted: Not Superscript/ Subscript

Deleted: T

Deleted: is based on the assumption





- Deleted: c
- Formatted: Not Highlight
- Formatted: Not Highlight
- Formatted: Not Highlight
- Formatted: Not Highlight
- Formatted: Not Highlight
- Formatted: Not Highlight
- Deleted: c
- Formatted: Not Highlight
- Formatted: Not Highlight
- Formatted: Not Highlight
- Formatted: Not Highlight
- Formatted: Not Highlight
- Formatted: Not Highlight
- Formatted: Not Highlight
- Formatted: Not Highlight
- Deleted: brown
- Deleted:  $I_M-I_{B0}-I_S$
- Deleted: Pump flow
- Deleted: w/green
- Formatted: Not Highlight
- Formatted: Not Highlight
- Formatted: Font: Italic, Not Highlight
- Formatted: Not Highlight
- Formatted: Font: Italic, Not Highlight
- Formatted: Not Highlight
- Deleted: flow rate + efficiency
- Deleted: iii
- Deleted: )
- Deleted: (iv) Absorption efficiency (blue line);
- Formatted: Font: Italic
- Formatted: Font: Italic
- Formatted: Not Highlight
- Formatted: Font: Italic
- Formatted: English (US)
- Formatted: Not Highlight
- Formatted: Font: Italic, Not Highlight
- Formatted: Not Highlight
- Deleted: purple
- Deleted: (
- Deleted: )
- Formatted: Font: Italic, English (US)
- Formatted: Not Highlight

1397

1398

1399

1400

1401

1402

1403

1404

1405

**Figure 11.** Uncertainty budgets of a mid-latitude (diagrams a, b, c: JOSIE 2009/2010) and tropical (diagrams (d), (e), (f): JOSIE 2017) ozonesonde profile, showing the influence of the different uncertainty source terms listed in Table 5 for the TRCC method for SPC/SST1.0 (diagrams (b) and (e)) and EN-SCI/SST0.5 (diagrams (c) and (f)). Total uncertainty (red solid line) consists of (i) Corrected cell current (brown line:  $\Delta I_{FDS}$ , (TRC)); (ii) Pump efficiency & flow rate (yellow line:  $\Delta \eta(P)$  &  $\Delta \phi_0$ ); (iii) Absorption efficiency (blue line:  $\Delta \eta_{A_{\lambda}}$ ); (iv) Conversion efficiency (green line:  $\Delta \eta(P)$ ); (v) Pump temperature (purple line:  $\Delta T_p$ ). In addition, the total uncertainty of the conventional method is shown by the dashed red line.



1419 However, both their contributions to the uncertainty are of the order of 0.01-0.02  $\mu\text{A}$ , but on a relative scale they become  
1420 strongly dependent on the magnitude of the ozone partial pressures, particularly in the upper tropical troposphere. In the  
1421 stratosphere the contributions of the different uncertainties do not vary much, and the overall uncertainty stays well below  
1422 5%.

1423 It is to be noted that in the remote Tropics in the upper troposphere the partial pressure of ozone  $P_{\text{O}_3}$  can be very low of the  
1424 order of 0.1-0.3 mPa while the detection limit of the ECC-sensor is of the order of 0.01-0.02  $\mu\text{A}$ , which corresponds to  
1425 ozone levels of about 0.04-0.08 mPa. It is obvious that at these very low ozone levels the ECC-sonde performance is  
1426 strongly determined by its detection limit, which of course can have a significant and large impact on the overall uncertainty  
1427 of the  $P_{\text{O}_3}$  ozonesonde measurements.

1428

## 1429 7. Implementation of the TRCC Into Field Operation

1430 A detailed procedure for applying the TRCC method in practice is described in Appendix C. In this section, we apply the  
1431 methodology developed in the previous sections to ozonesonde profile data from three different stations: (i) a mid-latitude  
1432 site (Uccle); (ii) a tropical station (American Samoa), and (iii) an ozone hole profile from the South Pole station in the  
1433 Antarctic. At those sites, we selected ascent and the corresponding descent profiles, such that the methodology to resolve  
1434 time response effects in the ECC signal can be assessed by comparing the ascent and descent profile of the same flight.  
1435 For the ozonesonde profiles of the three stations, we first determined the slow component  $I_S(t)$  by convolution of the  
1436 measured cell current  $I_M(t)$  with an exponential decay with a time constant  $\tau_s = 25$  minutes (Eq. 10) and conversion  
1437 efficiencies  $S_S = 0.018$  for SST0.5 (Uccle) and  $S_S = 0.023$  for SST0.1 (Samoa & South Pole). For the  $I_S$  at time  $t = 0$  of the  
1438 launch, (i) zero is used at Uccle, as the last exposure to ozone usually occurs at least one hour prior to launch and the  
1439 measured value will fall back to  $I_{B0}$ , and (ii) we use  $I_{B1}-I_{B0}$  multiplied by the exponential decay factor  $X_S = \text{Exp}[-\Delta t/\tau_s]$ , for the  
1440 other two stations, with  $\tau_s = 25$  min and  $\Delta t = 30$  min (South Pole) and 90 min (Samoa). Those time intervals are the typical  
1441 time differences between the  $I_{B1}$  measurement and launch time at those sites. This slow component is then subtracted from  
1442 the measured cell current  $I_M$ , together with the background current  $I_{B0}$ . The remaining signal is the fast component, which is  
1443 deconvolved to correct for the fast time response  $\tau_F$ . For this latter, the time lag measurements before launch at the stations  
1444 (e.g. time to drop from 4 to 1.5  $\mu\text{A}$ ) are taken. The smoothing of  $I_{FD}$  is done by applying a Gaussian filter prior to the time  
1445 lag correction using a width equal to 20% of the fast time lag constant (as in Vömel et al., 2020). The final currents are then  
1446 converted to ozone partial pressures using the calibration functions in Table 4 as conversion efficiency, taking the Nakano  
1447 and Morofuji (2023) true pump efficiency correction factors into account, correcting the pump temperature and the pump  
1448 flow rates as in GAW#268 (2021). For the conventional method, the GAW recommendations have been followed rigorously,  
1449 instead of subtracting  $I_{B0}$  (Uccle) and  $I_{B2}$  (Samoa and South Pole) as background currents.

1450

1451 In Fig. 12, the profiles corrected with the conventional method are on the left side, while the implementation of the TRCC on  
1452 the profiles is shown on the right side. It should immediately strike the eye that the agreement between the ascent and  
1453 descent profiles is much improved after applying in particular the fast time response deconvolution with the new method,  
1454 and this for the three different sites. But also the profile shape, e.g. around the ozone peak maximum at the Uccle and Samoa  
1455 profiles, corresponds much better with each other for the ascent and descent profiles for the new method. The slow time  
1456 response correction contributes to a certain extent as well to this better profile shape agreement.

1457

Deleted: our

Deleted: target

Deleted: in remote air conditions

Deleted: restricted

Deleted: to

Deleted: New Time Responses Correction

Deleted: new

Deleted: new

Deleted: occurs

Deleted: "new"

Deleted: + calibration function



1475 A nice illustration of the impact of the slow time response correction is also found in the upper troposphere of the Samoa  
1476 ozone profile. The upper tropospheric ozone concentrations are significantly decreased in both the ascent and descent  
1477 profiles after applying this correction, while still agreeing very well. The strong reduction of upper-tropospheric ozone  
1478 concentrations can be ascribed to correct for previous exposure to relatively high ozone amounts from the lower troposphere  
1479 plus the (artificial) ozone spike for the ascent profile and from the ozone maximum for the descent profile.

1480  
1481 The TRCC figures are remarkable in amplifying the features after correcting for the fast time constant. We already **observed**  
1482 that **the TRCC** method is able to resolve some features in the ozonesonde data that were effectively present in the (faster)  
1483 OPM ozone measurements in the JOSIE simulations. As **mentioned** by Vömel et al. (2020), the noise amplitude of the fast  
1484 response time-lag-corrected data is comparable to that of the original data, but its spectral characteristics are different  
1485 because of the smoothing algorithm. As a result, individual data points are heavily influenced by the noise characteristics of  
1486 the smoothed data. This is demonstrated by the ozone spike in the Samoa ascent, which has a larger peak amplitude for the  
1487 **TRCC** method.

Deleted: noted

Deleted: this new

Deleted: noted

Deleted: new

## 1489 8. Summary and Conclusions

1490 The ECC ozonesonde, in principle an absolute measuring device, encounters in the course of its flight several imperfections,  
1491 e.g. changing pump and conversion efficiency, that need to be corrected for. In the actual processing chain, the used  
1492 **“empirical effective efficiency”** tables (Komhyr 1986, Komhyr et al., 1995) in fact represent an overall correction,  
1493 empirically tweaked to coincident total ozone measurements, that includes both a measured pump flow efficiency and an  
1494 estimate of the stoichiometry increase over the flight (GAW Report No.268, 2021). However, the availability of recent  
1495 measured **true** ECC pump flow efficiencies (Nakano & Morofuji, 2023), confirming earlier measurements, together with the  
1496 knowledge that the ECC sonde response (chemical reactions pathways) is driven by a slow and fast component (Vömel et  
1497 al., 2020, Tarasick et al., 2021), call for a new approach. Vömel et al. (2020) also questioned the term “background current”  
1498 in the ECC processing.

Deleted: pump efficiency

1500 This study describes the concepts and the development of an updated methodology of ECC sonde data processing that  
1501 applies a better correction of the ozone exposure dependent stoichiometry of the  $O_3+KI$  titration reaction in the  
1502 electrochemical cell of the ECC-sonde **using true pump efficiencies combined with resolving the time responses of the slow**  
1503 **( $\approx 25$  min) and fast ( $\approx 20-25$  sec) components of the measured ECC-ozone sensor current. Experimental evidence is given to**  
1504 treat the measured ECC-sensor current as the superposition of a (i) dominant fast ozone current  $I_F$ ; (ii) slow time-variant,  
1505 past ozone-exposure dependent, current  $I_S$ ; (iii) a constant ozone-independent background current  $I_{B0}$ .

Deleted: through the use of

Deleted:

1507 The Time Responses Correction **plus Calibration (TRCC)** method developed here is briefly described in three steps:

1508 I. The slow cell current component as a function of flight time is determined from the measured ozone sensor current,  
1509 after correction for the constant background current  $I_{B0}$ , by using a first order numerical convolution scheme (Eq.  
1510 (10). Hereby, the in-flight time response tests of JOSIE 2009/2010 have been used to quantify the stoichiometry  
1511 ( $O_3/I_2$ ) factors  $S_S$  (and their uncertainties) of the slow reaction pathways for both sonde types, SPC and EN-SCI, and  
1512 two different sensing solution types, SST0.5 and SST1.0. In separate laboratory upward and downward response  
1513 time experiments  $S_S$  and  $\Delta S_S$  of the low buffered combination of EN-SCI with SST0.1 have been determined using  
1514 the same approach as in JOSIE 2009/2010 **(see Appendix B). Depending on the buffer strength the slow current**

Deleted:

1523  
1524  
1525  
1526  
1527  
1528  
1529  
1530  
1531  
1532  
1533  
1534  
1535  
1536  
1537  
1538  
1539  
1540  
1541  
1542  
1543  
1544  
1545  
1546  
1547  
1548  
1549  
1550  
1551  
1552  
1553  
1554  
1555  
1556  
1557  
1558  
1559  
1560  
1561  
1562  
1563  
1564  
1565

typically amounts to about 1-4% of measured cell current  $I_M$  for SST0.5 or SST0.1 and about 2-8% for SST1.0. However, in regions with very low ozone it can reach up to 10-15 %.

- II. By subtracting the constant background current before exposure of ozone ( $I_{B0}$ ) and the time variant slow sensor current  $I_S$  from the measured ECC-sensor current  $I_M$ , the remaining fast sensor current  $I_F$  has been resolved from the 20-30 sec. time response by using a first order deconvolution scheme (Eq. 12). Essential for this procedure is that the resulting deconvolved fast current  $I_{F,D}$  has to be smoothed adequately to eliminate high frequency noise.
- III. From  $I_{F,D,S}$  and using the correct true pump efficiencies (Table 1: Nakano and Morofuji, 2023) the partial pressure of ozone measured by the ECC-sonde is determined (Eq. 6). Additionally, using the conversion efficiency in Table 4 ("calibration functions"), the ozonesonde measurement is referred to the reference of the ozonesonde network, i.e. the photometer in the simulation chamber of the WCCOS in Jülich

Because the numerical convolution scheme used here is a recursive expression, the initial condition of  $I_S$  at the launch carries the past ozone exposure of the pre-launch preparations. In laboratory experiments it was shown that after  $I_{B1}$  has been recorded during the pre-flight preparation  $I_S(t)$  will further decay exponentially at the slow time constant  $\tau_S=25$  min. By knowing the time span between recording of  $I_{B1}$  and turning-on the pump just before launch  $I_{B1}$  can be used to derive the initial value of  $I_S$  at the launch. Therefore, it is essential that during the pre-flight preparations both background currents before ( $I_{B0}$ ) and after ( $I_{B1}$ ) exposure of ozone are being recorded, including the timestamp at recording  $I_{B1}$  and activating the pump just before launch of the sonde. Similarly, our understanding of this slow time constant justifies the use of limiting values for  $I_{B0}$  and after  $I_{B1}$  in the operational preparation of ozone soundings (see GAW Report No. 268, 2021), with filters providing a good quality zero ozone air source.

The slow stoichiometry factor  $S_S$  of the slow background due to the conversion of  $O_3$  into  $I_2$  and their Mean Absolute Deviation (MAD)-uncertainties (Table 2) are each based on a statistically relevant number of samples.  $S_S$  depends on the different SSTs used (Table 2), but is not dependent on the sonde type, which indicates that the secondary reaction pathway is not responsible for the systematic 4-5 % relative differences between EN-SCI and SPC when operating with the same SST. However, a direct quantitative relation of the buffer strength and the magnitude of  $S_S$  only holds for the full buffered SST1.0 ( $S_S \approx 0.046-0.050$ ) and the half-buffered SST0.5 ( $S_S \approx 0.017-0.018$ ), but not for the low-1/10<sup>th</sup> buffered SST0.1 ( $S_S \approx 0.023$ ). For SST0.1 significant lower  $S_S$  values might be expected, which might indicate that, in lower buffered sensing solutions, another competing chemical reaction scheme may occur that also produce free iodine at a 25 minute time scale and contributes to  $I_S$ . This may be the reason that for non-buffered or low-buffered sensing solutions  $I_{B1}$  values of 0.01-0.04  $\mu A$  are still recorded.

$S_S$  values reported in Table 2 are significantly smaller than the so-called "steady bias factor" values applied by Vömel et al. (2020), which are the overall excess stoichiometry derived from steady state experiments under ozone exposure (Vömel and Diaz, 2010). The difference may be explained by the overall excess stoichiometry originating from the secondary reaction pathway that only contributes partly to the slow  $I_S$  while the other part still contributes to the fast  $I_F$  (Appendix A). Further, in contrast to this study, Vömel et al. (2020) do not correct for  $I_{B0}$  before determining  $I_S$  and calculating  $I_F$ . These two different approaches in the methodology (e.g.  $I_{B0}$  subtraction and different stoichiometry factors  $S_S$  for the slow current  $I_S$ ) will of course lead to different results when comparing the sondes to the OPM. To demonstrate the impact of these different assumptions between both correction schemes we have processed the JOSIE 2009/2010 and JOSIE 2017 according to the TRC-scheme used by Vömel et al. (2020). The comparisons are shown in the supplementary material in the figures S4 and S6 for JOSIE 2009/2010 and JOSIE 2017, respectively. The impact of subtracting  $I_{B0}$  is generally small and only significant in the upper troposphere in the Tropics, where including subtraction of  $I_{B0}$  leads to better agreement with the OPM. The

Formatted: Font: Italic  
Formatted: Subscript  
Deleted: thereby  
Deleted: is  
Deleted: the  
Deleted: into  $I_{F,D,S}$ .  
Deleted: y  
Deleted: t  
Deleted: and the ECC pump is not running anymore,  
Deleted: existing  
Deleted: would be  
Deleted: also  
Deleted: s  
Deleted: is  
Deleted: only  
Deleted: contributing  
Deleted: and the  
Deleted: is  
Deleted: ing  
Deleted: of  
Deleted: ce  
Deleted: the  
Deleted: subtracting

1587 impact of larger  $S_s$  values for SST1.0 and SST0.5 will lower the differences to the OPM above 100 hPa, but there still  
1588 remains a significant deviation from the OPM. In the upper troposphere, the larger  $S_s$  gives negative deviations, particularly  
1589 in the Tropics.

1590  
1591 Different JOSIE data sets (JOSIE 2009/2010, JOSIE 2017, and JOSIE 1996 + 1998 + 2000 + 2002) have been used to  
1592 compare the relative differences of the sonde to the OPM obtained with the Time Responses Correction (TRC) versus the  
1593 conventional methodology of post flight data processing (GAW Reports No. 201 and 268). Hereby, it is very important to  
1594 mention that, in contrast to the conventional methodology, the relative differences obtained with TRC are almost  
1595 independent of the ozone profile type (e.g. mid-latitude or tropical). In other words, the observed relative differences with  
1596 TRC are independent of the past ozone exposure and increase only a few percent with altitude (or lower pressure). This is  
1597 most pronounced in the tropical ozone profiles at 200-100 hPa pressure in the upper troposphere with very low ozone values  
1598 and the steep vertical ozone gradient when entering the lower stratosphere. The typical systematic relative differences of 3-  
1599 5% for the same sonde type but different SST1.0 or SST0.5 as observed since JOSIE 2000 are still preserved in the TRC.

1600  
1601 The different behavior between JOSIE2009/2010 and JOSIE2017 in the relative differences of the TRC corrected sonde  
1602 profiles with the OPM for pressures smaller than about 13 hPa is ascribed to different pump temperatures used for the mid-  
1603 latitude and tropical profiles in the respective campaigns. During JOSIE2009/2010, the higher pump temperatures led to a  
1604 higher boiling rate in this pressure range, confirmed by the higher solution weight losses.

1605 The TRC mean relative differences of the sonde with the OPM show a strong consistency for the different pairs of sonde  
1606 type and SST and can be therefore represented by a linear regression as a function of  $\text{Log}_{10}$  of the pressure. This linear  
1607 regression can be interpreted as the calibration function for the conversion efficiency which is not quite equal to one (Eq.  
1608 18). The calibration functions introduced here for the various sonde-SST combinations, parameterized as a function of  
1609 ambient air pressure in Table 4, are independent of the ozone exposure, and thus invariant to the measured ozone profile  
1610 itself. The use of these calibration functions makes the global ozonesonde records traceable to one common standard, i.e. the  
1611 OPM of the WCCOS. The origin of these calibration functions remains speculative, but there are some experimental  
1612 indications that they are linked to the unknown stoichiometry of the fast chemical conversion of  $\text{O}_3$  into  $\text{I}_2$  and not caused by  
1613 an underestimation of the slow cell current  $I_s$ . It is to be noted that the here reported calibration functions are directly linked  
1614 to the average pump efficiency values from Nakano and Morofuji (2023) as in Table 1, however, if these pump efficiency  
1615 values might change over time (see Nakano and Morofuji, 2023), the calibration functions must be adjusted accordingly.

1616  
1617 The overall uncertainty of combining the TRC with the calibration functions (TRCC) is about 3-4 % throughout the entire  
1618 ozone profile, except for the upper troposphere, where the overall uncertainty can increase up to 10% for very low ozone  
1619 amounts, particularly in the tropics. The major uncertainty sources in the upper troposphere are the constant background  
1620 current  $I_{B0}$  and the slow current  $I_s$  (i.e.  $S_s$ ).

1621  
1622 The TRCC have been tested in practice (practical guidelines in Appendix C) for three different vertical ozone profiles  
1623 measured during ascent and descent at a mid-latitude site, a tropical station and during an ozone hole at the South Pole. The  
1624 resolving power of the fast deconvolution numerical scheme is clearly demonstrated by removing the strong delay shift in  
1625 the descent ozone profile compared with the ascent ozone profile before and after applying the TRCC. However, the  
1626 examples also clearly demonstrate the importance of careful and proper smoothing of the deconvolved ozone profile. To  
1627 apply the TRCC method to the time series of an ozonesonde site, a proper determination of  $I_{B0}$  and  $I_{B1}$  is required. Imperfect  
1628 or defective zero ozone air filters might increase those background currents by several orders of magnitude, compromising  
1629 the subtraction by the (too high)  $I_{B0}$  value throughout the entire profile and at the beginning of the profile due to the high

Formatted: Not Highlight

Deleted: s

Deleted: into

Deleted: can be

Deleted: .

Deleted: which has been observed

Deleted: of the correctional term of

Deleted: when deviating from one

Deleted: will allow us to get

Deleted: the use of

Deleted: , despite the correction of the slow current for the past ozone exposure in the TRC

Deleted:

Deleted: thereby

Deleted: resolving

Deleted: Improper

1645 initial value for  $I_s(t_0)$ . Some more analysis is needed to formulate alternative approaches for these cases. As stated also by  
1646 ASOPOS 2.0 (GAW Report No. 268) the use of proper gas filters to provide ozone free, dry and purified air in practice at the  
1647 sounding site, is very essential in general, but also when applying the TRCC data processing.

1649 An important outcome of this study is also that the contribution of the slow current  $I_s$  is not as large as previously thought  
1650 (Vömel et al. 2020), because TRC demonstrates that the secondary pathway involving the buffer can also contribute to the  
1651 fast stoichiometry factor to increase the fast current  $I_f$  so that the uncalibrated conversion efficiency exceeds one, which is  
1652 most likely the case for SST1.0 and SST0.5. This in contrast to SST0.1, where the slow current has most likely a different  
1653 chemical origin and not an additional contribution to  $I_f$ , so that the fast stoichiometry (i.e. conversion efficiency) does not  
1654 exceed one and is even a few percent lower. The underlying chemical mechanisms remain speculative in some cases and the  
1655 stoichiometry of the fast  $O_3+KI$  chemistry cannot be quantified explicitly but only expressed implicitly in the conversion  
1656 efficiency with the introduction of calibration functions (Table 4). These calibration functions can improve the  
1657 homogenization of long term ozonesonde records of the global network, making the data traceable to one ozone standard, the  
1658 OPM at the WCCOS at Jülich (Germany). Our OPM reference values have been scaled up 1.23% compared to earlier JOSIE  
1659 publications because of the revised UV ozone absorption cross-section at 254 nm (BIPM, 2022; Hodges et al., 2019). The  
1660 latter adjustment is being introduced in the global ozone network in 2024/2025.

1662 Finally, we list some specific recommendations for further research include:

- 1663 1. Regular JOSIE-campaigns at WCCOS (Jülich, Germany) are essential to check the long-term stability of the  
1664 calibration functions reported in this study (Table 4) and to guarantee the long-term traceability of global  
1665 ozonesonde records to the OPM-standard.
- 1666 2. More research is needed to understand the slow stoichiometry  $S_s$  factors in more detail, particularly for the low or  
1667 no buffered sensing solutions for which the underlying chemical processes are not understood at all. A key question  
1668 hereby is also the role of KBr in the sensing solutions. This should be in conjunction with understanding the  
1669 differences observed between the methods to derive  $S_s$  from either a zero-ozone or ozone exposure time response  
1670 experiment. Dedicated laboratory experiments in the WCCOS simulation chamber can accomplish this.
- 1671 3. More detailed understanding of the chemical reaction mechanisms that are responsible for the fast and slow cell  
1672 current response of the ECC-sensor, and their interaction. This should include determining the temperature  
1673 dependency of the  $KI+O_3$  chemistry.
- 1674 4. Better knowledge of the time behaviour of the high background currents  $I_{B0}$  and  $I_{B1}$  that are often measured in  
1675 practice at the sounding sites when not using proper gas filters. Experiments are necessary to describe and  
1676 eventually correct for this high  $I_{B0}$  and  $I_{B1}$  caused by using inadequate gas filters. This is essential as re-processing  
1677 ozonesonde records often goes hand in hand with correcting very high  $I_{B0}$  and  $I_{B1}$ .

1679 This study did not solve the systematic 3-5% offsets in measured ozone concentrations between EN-SCI and SPC  
1680 instruments when operating with the same SST. However, we showed that the  $S_s$  values are comparable for both sondes with  
1681 the same SST, which means the differences are not caused by the slow chemistry. More research here is essential.

1683 Both the TRCC and the conventional method are post-flight data processing methods that assume the following three basic  
1684 QA criteria are met: (i) best operating practices at the ozone monitoring stations in the global network (GAW Report No.  
1685 268, 2021) ; (ii) high-quality balloon instruments (e.g. ozone and radiosondes) and ground equipment; (iii) well-trained  
1686 operators at the sounding site. Even small imperfections in these QA criteria can result in significant degradation in the  
1687 quality of recorded ozonesonde data, such as the recently observed sudden drop in the total column ozone (TCO)

Deleted: prominent

Deleted: occurs

Deleted: Some

Deleted: specific

Deleted: s

Deleted:

Deleted: because

Deleted: means

1696 [measurements of ozonsondes compared to other TCO-measuring instruments \(e.g. satellites\) \(Stauffer et al., 2020\). Neither](#)  
1697 [the TRCC nor the conventional method can avoid these inconveniences. However, it highlights the future need for QA](#)  
1698 [monitoring of ozonsonde data in quasi-real time and comparing it with satellite and ground based \(e.g. Lidar or](#)  
1699 [Dobson/Brewer\) data to detect potential artifacts \(e.g. Stauffer et al. 2022\).](#)

#### 1700 Acknowledgements

1701 For the JOSIE 2009/2010 we are very grateful to Marcel Berg (FZJ/IEK-8, Germany) and Dr. Johannes Stauffer (ETHZ,  
1702 Switzerland) for the pre-flight preparation of the ozonsondes. Many thanks to Dr. Holger Vömel for stimulating discussions  
1703 in preparing the manuscript. Also, many thanks to the people who supplied ECC-sondes to be “flown” in the simulation  
1704 chamber in JOSIE 2009/2010 and 2017. For JOSIE 2009/2010 we thank: Dr. Bryan Johnson (NOAA-GML, USA), Francis  
1705 Schmidlin (NASA/Goddard/Wallops Flight Facility, USA), Dr. Hugo De Backer (RMI, Belgium), Dr. Rene Stübi (Meteo  
1706 Suisse., Switzerland), Dr. Rigel Kivi (FMI, Finland), Dr. Richard Querel (NIWA, New Zealand), Dr. Matt Tully (BOM,  
1707 Australia), Dr. Emilio Cuevas (AEMET, Spain). Sondes for JOSIE-2017 were supplied by FZJ/IEK-8, NOAA/GML and  
1708 NASA/Goddard. Researchers from FZ-J, NASA/Goddard, NOAA/GML, MeteoSwiss, RMI (Belgium), KNMI  
1709 (Netherlands), JMA (Japan), Environment & Climate Change Canada along with 8 SHADOZ operators contributed time to  
1710 JOSIE-2017. We thank the United Nations Environmental Programme, WMO, EN-SCI and SPC for supporting the  
1711 participation of the SHADOZ personnel in JOSIE-2017. JOSIE 2009/2010 and 2017 were sponsored by WMO/GAW,  
1712 [Forschungszentrum Jülich \(FZJ\) and NASA/GSFC.](#)

Deleted: and

#### 1713 Competing interests

1714 R. Van Malderen is a member of the editorial board of Atmospheric Measurement Techniques. The peer review process will  
1715 be guided by an independent editor. The authors have no other competing interests to declare.

#### 1716 References

1717 Ancellet, G., Godin-Beekmann, S., Smit, H. G. J., Stauffer, R. M., Van Malderen, R., Bodichon, R., and Pazmiño, A.:  
1718 Homogenization of the Observatoire de Haute Provence electrochemical concentration cell (ECC) ozonsonde data record:  
1719 comparison with lidar and satellite observations, *Atmos. Meas. Tech.*, 15, 3105–3120, [https://doi.org/10.5194/amt-15-3105-](https://doi.org/10.5194/amt-15-3105-2022)  
1720 [2022](https://doi.org/10.5194/amt-15-3105-2022), 2022.  
1721 BIPM, 2022: [https://www.bipm.org/documents/20126/27085544/RapportBIPM-2022-02.pdf/f93def70-2544-ff13-ae63-](https://www.bipm.org/documents/20126/27085544/RapportBIPM-2022-02.pdf/f93def70-2544-ff13-ae63-3bc73f36688e)  
1722 [3bc73f36688e](https://www.bipm.org/documents/20126/27085544/RapportBIPM-2022-02.pdf/f93def70-2544-ff13-ae63-3bc73f36688e).  
1723 Crutzen, P.J.: The influence of nitrogen oxides on the atmospheric ozone content, *Quart. J. Roy. Met. Soc.*, 96, No. 408, 320–  
1724 325, <https://doi.org/10.1002/qj.49709640815>, 1970.  
1725 Davies, J., McElroy, C.T., Tarasick, D.W., and Wardle, D.I.: Ozone capture efficiency in ECC ozonsondes: Measurements  
1726 made in the laboratory and during balloon flights, EAE03-A-13703, in *Geophysical Research Abstracts*, Vol. 5, 13703, EGS-  
1727 AGU-EUG Joint Assembly, Nice, France, 6–11 April 2003, 2003.  
1728 De Muer, D., & Malcorps, H.: The frequency response of an electrochemical ozone sonde and its application to the  
1729 deconvolution of ozone profiles, *J. Geophys. Res.*, 89, 1361–1372, 1984.  
1730 Deshler, T., Mercer J., Smit, H.G.J., Stübi, R., Levrat, G., Johnson, B.J., Oltmans, S.J., Kivi, R., Davies, J., Thompson, A.M.,  
1731 Witte, J., Schmidlin, F.J., Brothers, G., Sasaki, T.: Atmospheric comparison of electrochemical cell ozonsondes from  
1732 different manufacturers, and with different cathode solution strengths: The Balloon Experiment on Standards for  
1733 Ozonsondes, *J. Geophys. Res.*, 113, D04307, <https://doi.org/10.1029/2007JD008975>, 2008.



1735 Deshler, T., Stübi, R., Schmidlin, F. J., Mercer, J. L., Smit, H.G.J., Johnson, B.J., Kivi, R. and Nardi, B., 2017: Methods to  
1736 homogenize ECC ozonesonde measurements across changes in sensing solution concentration or ozonesonde manufacturer,  
1737 *Atm. Meas. Tech.*, 10, 2012–2043, doi:10.5194/amt-10-2021-2017, 2017.

1738 Dietz, R. N., Pruzansky, J., & Smith, J. D.: Effect of pH on the stoichiometry of the iodometric determination of ozone. *Anal.*  
1739 *Chem.*, 45, 402–404, 1973.

1740 Farman, J.C., Gardener, B.G., and Shanklin, J.D.: Large Losses of total ozone in Antarctica reveal seasonal ClO<sub>x</sub>/NO<sub>x</sub>  
1741 interaction, *Nature*, 315, 207-210, 1985.

1742 Garner, G. G., and Thompson, A. M.: Ensemble statistical post-processing of the National Air Quality Forecast Capability:  
1743 Enhancing ozone forecasts in Baltimore, Maryland. *Atmos. Environ.*, 81, 517–522, doi:10.1016/j.atmosenv.2013.09.020,  
1744 2013.

1745 GAW Report No. 104: Report of the Fourth WMO Meeting of Experts on the Quality Assurance/Science Activity Centres  
1746 (QA/SACs) of the Global Atmosphere Watch, WMO Global Atmosphere Watch Report Series, No. 104, World  
1747 Meteorological Organization, Geneva, 1995.

1748 GAW Report No. 201, Smit, H.G.J., and the ASOPOS Panel: Quality Assurance and Quality Control for Ozonesonde  
1749 Measurements in GAW, WMO Global Atmosphere Watch Report Series, No. 201, World Meteorological Organization,  
1750 Geneva, [Available online at [https://library.wmo.int/doc\\_num.php?explnum\\_id=7167](https://library.wmo.int/doc_num.php?explnum_id=7167)], 2014.

1751 GAW Report No. 268, Smit, H.G.J., Thompson, A.M., and the ASOPOS 2.0 Panel: Ozonesonde Measurement Principles and  
1752 Best Operational Practices, WMO Global Atmosphere Watch Report Series, No. 268, World Meteorological Organization,  
1753 Geneva, [Available online at [https://library.wmo.int/doc\\_num.php?explnum\\_id=10884](https://library.wmo.int/doc_num.php?explnum_id=10884)], 2021.

1754 ~~Haagen-Smit, A.J.: Chemistry and physiology of Los Angeles smog. *Indust.Eng. Chem.*, 44, 1342-1346, 1952.~~

1755 Hearn, A.G.: Absorption of ozone in ultraviolet and visible regions of spectrum, *Proc. Phys. Soc.*, 78, 932–940, 1961.

1756 Hodges, J.T., Viallon, J., Brewer, P.J., Drouin, B.J., Gorshchev, V., Janssen, C., Lee, S., Possolo, A., Smith, M.A.H., Walden,  
1757 J., Wielgosz, R.I.: Recommendation of a consensus value of the ozone absorption cross-section at 253.65 nm based on a  
1758 literature review, *Metrologia*. 56: 034001. <https://iopscience.iop.org/article/10.1088/1681-7575/ab0bdd>, 2019.

1759 Huang, L.J., Chen, M.J., Lai, C.H., Hsu, H.T. and Lin, C.H.: New Data Processing Equation to Improve the Response Time  
1760 of an Electrochemical Concentration Cell (ECC) Ozonesonde. *Aerosol Air Qual. Res.* 15: 935-944.  
1761 <https://doi.org/10.4209/aaqr.2014.05.0097>, 2015.

1762 Imai, K., Fujiwara, M., Inai, Y., Manago, N., Suzuki, M., Sano, T., Mitsuda, C., Naito, Y., Hasebe, F., Koide, T., Shiotani,  
1763 M.: Comparison of ozone profiles between Superconducting Submillimeter-Wave Limb-Emission Sounder and worldwide  
1764 ozonesonde measurements, *J. Geophys. Res. Atmos.*, 118, 12,755– 12,765, doi:10.1002/2013JD021094, 2013.

1765 IPCC-Climate Change 2013: The Physical Science Basis. Contribution of Working Group I to the Fifth Assessment Report  
1766 of the Intergovernmental Panel on Climate Change [Stocker, T.F., Qin, D. , Plattner, G.-K., Tignor, M., Allen, S.K.,  
1767 Boschung, J., Nauels, A., Xia, Y., Bex, V. and Midgley, P.M. (eds.)]. Cambridge University Press, Cambridge, United  
1768 Kingdom and New York, NY, USA, 1535 pp, 2013.

1769 IPCC-Climate Change 2021: The Physical Science Basis. Contribution of Working Group I to the Sixth Assessment Report  
1770 of the Intergovernmental Panel on Climate Change [Masson-Delmotte, V., Zhai, P., Pirani, A., Connors, S.L., Péan, C.,  
1771 Berger, S., Caud, N., Chen, Y., Goldfarb, L., Gomis, M.I., Huang, M., Leitzell, K., Lonnoy, E., Matthews, J.B.R., Maycock,  
1772 T.K., Waterfield, T., Yelekçi, O., Yu, R., and Zhou, B. (eds.)]. Cambridge University Press, Cambridge, United Kingdom and  
1773 New York, NY, USA, In press, doi:10.1017/9781009157896, 2022.

1774 Johnson, B.J., S.J. Oltmans, Vömel, H., Smit, H.G.J., Deshler, T. and Kroeger, C.: ECC Ozonesonde pump efficiency  
1775 measurements and tests on the sensitivity to ozone of buffered and unbuffered ECC sensor cathode solutions, *Journal of*  
1776 *Geophysical Research*, 107, D19, <https://doi.org/10.1029/2001JD000557>, 2002.

1777 Komhyr, W.D.: Nonreactive gas sampling pump, *Rev. Sci. Instr.*, 38, 981–983, 1967.

Formatted: English (US)

Formatted: English (US)

Formatted: English (US)

Deleted: -

1779 Komhyr, W.D.: Electrochemical concentration cells for gas analysis, *Ann. Geoph.*, 25, 203–210, 1969

1780 Komhyr, W.D. and T.B. Harris: Development of an ECC Ozonesonde, NOAA Technical Report, ERL 200-APCL 18, 1971.

1781 Komhyr, W.D.: Operations handbook - Ozone measurements to 40 km altitude with model 4A-ECC ozone sondes, NOAA

1782 Technical Memorandum, ERL-ARL-149, 1986.

1783 Komhyr, W.D., Barnes, R.A., Brothers, G.B., Lathrop, J.A. and Opperman, D.P.: Electrochemical concentration cell

1784 ozonesonde performance evaluation during STOIC 1989, *J. Geophys. Res.*, 100, 9231–9244, 1995.

1785 Lovelock, J.E., Maggs, R.J., Wade, R.J.: Halogenated Hydrocarbons in and over the Atlantic, *Nature*, 241, 194–196,

1786 <https://doi.org/10.1038/241194a0>, 1973.

1787 Miloshevich, L. M., Paukkunen, A., Vomel, H., and Oltmans, S. J.: Development and validation of a time lag correction for

1788 Vaisala radiosonde humidity measurements, *J. Atm. Ocean. Tech.*, 21, 1305–1327, 2004.

1789 Mills, G, Pleijel, H., Malley, C.S., Sinha, B., Cooper, O.R., Schultz, M.G., Neufeld, H.S., Simpson, D., Sharps, K., Feng, Z.,

1790 Gerosa, G., Harmens, H., Kobayashi, K., Saxena, P., Paoletti, E., Sinha, V. and Xu, X.: Tropospheric Ozone Assessment

1791 Report: Present-day tropospheric ozone distribution and trends relevant to vegetation. *Elem Sci Anth*, 6: 47. DOI:

1792 <https://doi.org/10.1525/elementa.302>, 2018.

1793 Molina, M., Rowland, F. Stratospheric sink for chlorofluoromethanes: chlorine atom-catalysed destruction of

1794 ozone. *Nature* 249, 810–812, <https://doi.org/10.1038/249810a0>, 1974.

1795 Nakano, T. and Morofuji, T.: Development of an automated pump-efficiency measuring system for ozonesondes utilizing an

1796 airbag-type flowmeter, *Atm. Meas. Tech.*, 16, 1583–1595, <https://doi.org/10.5194/amt-16-1583-2023>, 2023.

1797 Newton, R., Vaughan, G., Ricketts, H.M.A., Pan, L.L., Weinheimer, A. J. and Chemel, C., 2016: Ozonesonde profiles from

1798 the West Pacific Warm Pool: Measurements and validation, *Atm. Chem. Phys.*, 619–634, [doi:10.5194/acp-16-619-2016](https://doi.org/10.5194/acp-16-619-2016),

1799 2016.

1800 Proffitt, M.H. and McLaughlin, R.J.: Fast response dual-beam UV-absorption photometer suitable for use on stratospheric

1801 balloons, *Rev. Sci. Instr.*, 54, 1719–1728, 1983.

1802 Reid, S.J., Vaughan, G., Marsh, A.R. and Smit, H.G.J.: Intercomparison of ozone measurements by ECC sondes and

1803 BENDIX chemiluminescent analyser, *J. Atmos. Chem.*, 25, 215–226, 1996.

1804 Saltzman, B.E. and Gilbert, N.: Iodometric micro-determination of organic oxidants and ozone, resolution of mixtures by

1805 kinetic colorimetry, *Anal. Chem.*, 31, 1914–1920, 1959.

1806 Seinfeld, J.H., Pandis, S.N.: *Atmospheric Chemistry and Physics (From Air Pollution to Climate Change, 3<sup>rd</sup> Edition, 1152*

1807 *pp., ISBN-13: 978-111894740, John Wiley and Sons, Inc., New York, 2016.*

1808 Smit, H.G.J., Sträter, W., Kley, D. and Proffitt, M.H.: The evaluation of ECC ozonesondes under quasi flight conditions in the

1809 environmental simulation chamber at Jülich, in *Proceedings of Eurotrac symposium 1994*, edited by P.M. Borell et al., SPB

1810 Academic Publishing B.V., The Hague, The Netherlands, 349–353, 1994.

1811 Smit H.G.J and Kley, D.: JOSIE: The 1996 WMO International Intercomparison of Ozonesondes Under Quasi Flight

1812 Conditions in the Environmental Simulation Chamber at Jülich, *WMO Global Atmosphere Watch Report Series, No. 130,*

1813 *WMO/TD No. 926, World Meteorological Organization, Geneva, 1998.*

1814 Smit H.G.J., Sträter, W., Helten, M. and Kley, D.: *Environmental Simulation Facility to Calibrate Airborne Ozone and*

1815 *Humidity Sensors. Jül Berichte, No. 3796, Forschungszentrum Jülich, 2000.*

1816 Smit, H.G.J.: Ozonesondes, in *Encyclopedia of Atmospheric Sciences, Second Edition*, edited by G.R. North, J.A. Pyle, and

1817 F. Zhang, Vol 1, pp. 372–378, Academic Press, London, 2014.

1818 Smit, H.G.J., and Sträter, W.: JOSIE-1998, Performance of ECC Ozone Sondes of SPC-6A and ENSCI-Z Type, *WMO*

1819 *Global Atmosphere Watch Report Series, No. 157, WMO/TD No. 1218, World Meteorological Organization, Geneva, 2004a.*

1820 Smit, H.G.J., and Sträter, W.: JOSIE-2000, Jülich Ozone Sonde Intercomparison Experiment 2000, *The 2000 WMO*

1821 *International Intercomparison of Operating Procedures for ECC Ozonesondes at the Environmental Simulation Facility at*

1822 Jülich, WMO Global Atmosphere Watch Report Series, No. 158, WMO TD No. 1225, World Meteorological Organization,  
1823 Geneva, 2004b.

1824 Smit, H.G.J.: Tropospheric Ozone as a Tracer to Investigate Deep Convection and its Influence on the Humidity in the  
1825 Marine Tropics, PhD Thesis, University of Wuppertal, [on-line available: [https://elekpub.bib.uni-](https://elekpub.bib.uni-wuppertal.de/ubwhsmig/content/titleinfo/3555358)  
1826 [wuppertal.de/ubwhsmig/content/titleinfo/3555358](https://elekpub.bib.uni-wuppertal.de/ubwhsmig/content/titleinfo/3555358)], 2004c.

1827 Smit, H.G.J., Sträter, W., Johnson, B.J., Oltmans, S.J., Davies, J., Tarasick, D.W., Högger, B., Stübi, R., Schmidlin, F.J.,  
1828 Northam, T., Thompson, A.M., Witte, J.C., Boyd, I. and Posny, F.: Assessment of the performance of ECC ozonesondes  
1829 under quasi-flight conditions in the environmental simulation chamber: Insights from the Jülich Ozone Sonde  
1830 Intercomparison Experiment (JOSIE), *Journal of Geophysical Research*, 112, D19306, [doi:10.1029/2006JD007308](https://doi.org/10.1029/2006JD007308), 2007.

1831 Smit, H.G.J., and O3S-DQA Panel: Guidelines for Homogenization of Ozonesonde Data, SI2N/O3S-DQA Activity as part of  
1832 “Past Changes in the Vertical Distribution of Ozone Assessment”, available at <https://www.wccos-josie.org/en/o3s-dqa/>,  
1833 2012.

1834 Stauffer, R.M., Thompson, A.M., Kollonige, D.E., Tarasick, D.W., Van Malderen, R., Smit, H.G.J.: An examination of the  
1835 recent stability of ozonesonde global network data. *Earth and Space Science*, 9, e2022EA002459.  
1836 <https://doi.org/10.1029/2022EA002459>, 2022.

1837 Steinbrecht W., Schwartz, R. and Claude, H.: New pump correction for the Brewer-Mast ozone sonde: Determination from  
1838 experiment and instrument intercomparisons, *J. Atm. Ocean. Tech.*, 15, 144–156, 1998.

1839 Sterling, C.W., Johnson, B.J., Oltmans, S.J., Smit, H.G.J., Jordan, A.F., Cullis, P.D., Hall, E.G., Thompson, A.M. and Witte,  
1840 J.C.: Homogenizing and estimating the uncertainty in NOAA's long-term vertical ozone profile records measured with the  
1841 electrochemical concentration cell ozonesonde, *Atm. Meas. Tech.*, 11, 3661–3687, [https://doi.org/10.5194/amt-11-3661-](https://doi.org/10.5194/amt-11-3661-2018)  
1842 [2018](https://doi.org/10.5194/amt-11-3661-2018), 2018.

1843 Stolarski, R. S. and Cicerone, R. J.: Stratospheric Chlorine: a Possible Sink for Ozone, *Can. J. Chem.*, 1610-1615,  
1844 <https://doi.org/10.1139/v74-233>, 1974.

1845 Tarasick, D.W., Jin, J.J., Fioletov, V.E., Liu, G., Thompson, A.M., Oltmans, S.J., Liu, J., Sioris, C.E., Liu, X., Cooper, O.R.,  
1846 Dann, T. and Thouret, V.: High-resolution tropospheric ozone fields for INTEX and ARCTAS from IONS ozonesondes, *J.*  
1847 *Geophys. Res.*, 115, D20301, <https://doi.org/10.1029/2009JD012918>, 2010.

1848 Tarasick, D.W., Davies, J., Smit, H.G.J. and Oltmans, S.J.: A re-evaluated Canadian ozonesonde record: measurements of the  
1849 vertical distribution of ozone over Canada from 1966 to 2013, *Atm. Meas. Tech.*, 9, 195–214, [doi:10.5194/amt-9-195-2016](https://doi.org/10.5194/amt-9-195-2016),  
1850 2016.

1851 Tarasick, D., Galbally, I.E., Cooper, O.R., Schultz, M.G., Ancellet, G., Leblan, T., Wallington, T.J., Ziemke, J., Liu, X.,  
1852 Steinbacher, M., Staehelin, J., Vigouroux, C., Hannigan, J.W., García, O., Foret, G., Zanis, P., Weatherhead, E.,  
1853 Petropavlovskikh, I., Worden, H., Osman, M., Liu, J., Chang, K.-L., Gaudel, A., Lin, M., Granados-Muñoz, M., Thompson,  
1854 A.M., Oltmans, S.J., Cuesta, J., Dufour, G., Thouret, V., Hassler, B., Trickl, T. and Neu, J.L.: Tropospheric Ozone  
1855 Assessment Report: Tropospheric ozone from 1877 to 2016, observed levels, trends and uncertainties. *Elementa: Science of*  
1856 *the Anthropocene*, 7:39. <https://doi.org/10.1525/elementa.376>, 2019.

1857 Tarasick, D.W., Smit, H.G.J., Thompson, A.M., Morris, G.A., Witte, J.C., Davies, J., Nakano, T., Van Malderen, R., Stauffer,  
1858 R.M., Deshler, T., Johnson, B.J., Stübi, R., Oltmans, S.J. and Vömel, H., 2021: Improving ECC ozonesonde data quality:  
1859 Assessment of current methods and outstanding issues, *Earth and Space Science*, 8, e2019EA000914,  
1860 <https://doi.org/10.1029/2019EA000914>, 2021.

1861 Thompson, A.M.: The oxidizing capacity of the Earth's atmosphere: Probable past and future changes. *Science*, 256, 1157–  
1862 1165, <https://doi.org/10.1126/science.256.5060.1157>, 1992.

1863 Thompson, A.M., Stone, J.B., Witte, J.C., Miller, S.K., Pierce, R.B., Chatfield, R.B., Oltmans, S.J., Cooper, O.R., Loucks,  
1864 A.L., Taubman, B.F., Johnson, B.J., Joseph, E., Kucsera, T.L., Merrill, J.T., Morris, G.A., Hersey, S., Forbes, G., Newchurch,

1865 M.J., Schmidlin, F.J., Tarasick, D.W., Thouret, V. and Cammas, J.-P.: Intercontinental Chemical Transport Experiment  
1866 Ozonesonde Network Study (IONS) 2004: 1 Summertime upper troposphere/lower stratosphere ozone over northeastern  
1867 North America, *J. Geophys. Res.*, 112, D12S12, [doi:10.1029/2006JD007441](https://doi.org/10.1029/2006JD007441), 2007a.

1868 Thompson, A.M., Witte, J.C., Smit, H.G.J., Oltmans, S.J., Johnson, B.J., Kirchhoff, V.W.J.H. and Schmidlin, F.J.: Southern  
1869 Hemisphere Additional Ozonesondes (SHADOZ) 1998–2004 tropical ozone climatology: 3. Instrumentation, station-to-  
1870 station variability, and evaluation with simulated flight profiles, *J. Geophys. Res.*, 112, D03304, [doi:10.1029/2005JD007042](https://doi.org/10.1029/2005JD007042),  
1871 2007b.

1872 Thompson, A.M., Oltmans, S.J., Tarasick, D.W., von der Gathen, P., Smit, H.G.J. and Witte, J.C.: Strategic ozone sounding  
1873 networks: Review of design and accomplishments, *Atm. Env.*, 45, 2145–2163, [doi:10.1016/j.atmosenv.2010.05.002](https://doi.org/10.1016/j.atmosenv.2010.05.002), 2011.

1874 Thompson, A.M., Witte, J.C., Sterling, C., Jordan, A., Johnson, B.J., Oltmans, S.J., Fujiwara, M., Vömel, H., Allaart, M.,  
1875 PETERS, A., Coetzee, G.J.R., Posny, F., Corrales, E., Andres Diaz, J., Félix, C., Komala, N., Lai, N., Maata, M., Mani, F.,  
1876 Zainal, Z., Ogino, S.-Y., Paredes, F., Luiz Bezerra Penha, T., da Silva, F.R., Sallons-Mitro, S., Selkirk, H.B., Schmidlin, F.J.,  
1877 Stübi, R. and Thiongo, K.: First reprocessing of Southern Hemisphere Additional Ozonesondes (SHADOZ) ozone profiles  
1878 (1998–2016). 2. Comparisons with satellites and ground-based instruments, *J. Geophys. Res.*, 122,  
1879 <https://doi.org/10.1002/2013JD019771>, 2017.

1880 Thompson, A.M., Smit, H.G.J., Witte, J.C., Stauffer, R.M., Johnson, B.J., Morris, G.A., von der Gathen, P., Van Malderen,  
1881 R., Davies, J., PETERS, A., Allaart, M., Posny, F., Kivi, R., Cullis, P., Nguyen T.H. Ahn, Corrales, E., Machinini, T., DaSilva,  
1882 F.R., Paiman, G., Thiong'o, K., Zainal, A., Brothers, G.B., Wolff, K.R., Nakano, T., Stübi, R., Romanens, G., Coetzee,  
1883 G.J.R., Diaz, J.A., Mitro, S., 'bt Mohamad, M. and Ogino, S.-Y.: Ozonesonde quality assurance: The JOSIE-SHADOZ  
1884 (2017) experience, *Bull. Amer. Met. Soc.*, 100, <https://pubmed.ncbi.nlm.nih.gov/33005057/>, 2019.

1885 Thompson, A.M., Stauffer, R.M., Wargan, K., Witte, J.C., Kollonige, D.E., and Ziemke, J.R.: Regional and Seasonal Trends  
1886 in Tropical Ozone From SHADOZ Profiles: Reference for Models and Satellite Products, *J. Geophys. Res.*, 126,  
1887 <https://doi.org/10.1029/2021JD03469>, 2021.

1888 Thompson, A.M., Smit, H.G.J., Kollonige, D.E., Stauffer, R.M.: Ozonesondes: Instrumentation and Data Application, In:  
1889 Field Measurements for Passive Environmental Remote Sensing (Ed. Nalli, N.R.), 458 pp., 1<sup>st</sup> Edition, ISBN 13- 978-  
1890 0128239537, Elsevier, Amsterdam, 2022.

1891 Thornton, D.C., and Niazzy, N.: Sources of background current in the ECC ozonesonde: Implication for total ozone  
1892 measurements, *J. Geophys. Res.*, 87, 8943–8950, 1982.

1893 Thornton, D.C. and Niazzy, N.: Effects of solution mass transport on the ECC ozonesonde background current, *Geophys. Res.*  
1894 *Let.*, 10, 148–15, 1983.

1895 UNEP-Ozone Secretariat, Handbook for the Montreal Protocol on Substances that Deplete the Ozone Layer, 14<sup>th</sup> Edition,  
1896 ISBN: 978-9966-076-79-3, [on-line available [https://ozone.unep.org/sites/default/files/Handbooks/MP-Handbook-2020-  
1897 English.pdf](https://ozone.unep.org/sites/default/files/Handbooks/MP-Handbook-2020-English.pdf)], 2020.

1898 Van Malderen, R., Allaart, M.A.F., De Backer, H., Smit, H.G.J., De Muer, D.: On instrumental errors and related correction  
1899 strategies of ozonesondes: possible effect on calculated ozone trends for the nearby sites Uccle and De Bilt, *Atm. Meas.*  
1900 *Tech.*, 9, 3793–3816, doi:10.5194/amt-9-3793-2016/, 2016.

1901 Vömel, H. and Diaz, K.: Ozone sonde cell current measurements and implications for observations of near-zero ozone  
1902 concentrations in the tropical upper troposphere, *Atm. Meas. Tech.*, 3, 495–505, doi:10.5194/amt-3-495-2010,  
1903 <http://www.atmos-meas-tech.net/3/495/2010/>, 2010.

1904 Vömel, H., Smit, H.G.J., Tarasick, D.W., Johnson, B.J., Oltmans, S.J., Selkirk, H.B., Thompson, A.M., Stauffer, R.M., Witte,  
1905 J.C., Davies, J., Van Malderen, R., Morris, G.A., Nakano, T. and Stübi, R.: A new method to correct the ECC ozone sonde  
1906 time response and its implications for “background current” and pump efficiency, *Atm. Meas. Tech.*, 13, 5667–5680,  
1907 <https://amt.copernicus.org/articles/13/5667/2020/>, 2020.

1908 Wang, H. J. R., Damadeo, R., Flittner, D., Kramarova, N., Taha, G., Davis, S., Thompson, A.M., Strahan, S., Wang, Y.,  
1909 Froidevaux, L., Degenstein, D., Bourassa, A., Steinbrecht, W., Walker, K.A., Querel, R., Leblanc, T., Godin-Beekmann, S.,  
1910 Hurst, D., Hall, E.: Validation of SAGE III/ISS solar occultation ozone products with correlative satellite and ground based  
1911 measurements, *J. Geophys. Res.*, 125, e2020JD032430, <https://doi.org/10.1029/2020JD032430>, 2020.  
1912 Witte, J.C., Thompson, A.M., Smit, H.G.J., Fujiwara, M., Posny, F., Coetzee, G.J.R., Northam, E.T., Johnson, B.J., Sterling,  
1913 C.W., Mohamad, M., Ogino, S.-Y., Jordan, A. and da Silva, F.R.: First reprocessing of Southern Hemisphere Additional  
1914 Ozonesondes (SHADOZ) profile records (1998–2015): 1. Methodology and evaluation, *J. Geophys. Res.*, 122, 6611–6636,  
1915 <https://doi.org/10.1002/2016JD026403>, 2017.  
1916 Witte, J.C., Thompson, A.M., Smit, H.G.J., Vömel, H., Posny, F. and Stübi, R.: First reprocessing of Southern Hemisphere  
1917 Additional Ozonesondes profile records: 3. Uncertainty in ozone profile and total column. *J. Geophys. Res.*, 123, 3243–  
1918 3268. <https://doi.org/10.1002/2017JD027791>, 2018.  
1919 Witte, J.C., Thompson, A.M., Schmidlin, F.J., Northam, E.T., Wolff, K.R. and Brothers, G.B.: The NASA Wallops Flight  
1920 Facility digital ozonesonde record: Reprocessing, uncertainties, and dual launches. *J. Geophys. Res.*, 124, 3565–3582,  
1921 [doi:10.1029/2018JD030098](https://doi.org/10.1029/2018JD030098), 2019.  
1922 WMO/UNEP: Scientific Assessment of Ozone Depletion: 2022, Ozone Research and Monitoring – GAW Report No. 278,  
1923 World Meteorological Organization, Geneva, 2023.  
1924 Xu, X., Muller, R.P., Goddard, W.A.: The gas phase reaction of singlet dioxygen with water: A water-catalyzed mechanism,  
1925 *PNAS*, 99 (6), 3376–3381, <https://doi.org/10.1073/pnas.052710099>, 2002.  
1926 Zhang, J., Xuan, Y., Yan, X., Liu, M., Tian, H., Xia, X., Pang, L. and Zheng, X.: Development and preliminary evaluation of  
1927 a double-cell ozonesonde, *Adv. Atm. Sci.*, 31, 938–947, 2014a.  
1928 Zhang, J.-Q., Xuan, Y.-J., Xia, X.-A., Liu, M.-Y., Yan, X.-L., Pang, L., Bai, Z.-X., and Wan, X.-W.: Performance evaluation  
1929 of a self-developed ozonesonde and its application in an intensive observational campaign, *Atm. Ocean. Sci. Lett.*, 7, 175–  
1930 179, <https://doi.org/10.3878/j.issn.1674-2834.13.0089>, 2014b.  
1931

1932 **Appendix A: KI + O<sub>3</sub> Chemistry in Presence of Phosphate-Buffer (NBKI after Saltzman & Gilbert, 1959)**

1933 Iodometric determination of ozone and the underlying oxidation of iodide ion by ozone to liberate iodine has long been  
 1934 subject of controversy. The reaction of KI with O<sub>3</sub> may proceed through a variety of chemical pathways strongly depending  
 1935 on pH, KI and O<sub>3</sub> concentrations, whether or not in presence of a pH-buffer. In this study the focus is on the neutral buffered  
 1936 potassium iodide (NBKI) method and its application in the ECC-ozone sensor. Experimentally it was shown by several  
 1937 investigators (e.g. Saltzman and Gilbert, 1959; Flamm and Anderson, 1975) that iodate (IO<sub>3</sub><sup>-</sup>) as intermediate can be  
 1938 excluded as long as ozone partial pressures in the air are well below 100 mPa. This makes it most likely that much of the  
 1939 behaviour of the ECC and its slow and fast sensor currents may be explained by the chemical reaction mechanisms for the  
 1940 NBKI and the impact of the phosphate buffer as postulated by Saltzman and Gilbert (1959). It was experimentally shown  
 1941 that the fast and slow reactions increase as KI concentrations increase, whereby the slow reactions increase with the buffer  
 1942 concentration. Buffered solutions with no KI show no evidence of gaseous O<sub>3</sub> uptake into the sensing solution, indicating  
 1943 that the additional reactions with O<sub>3</sub> are secondary reactions after the initial O<sub>3</sub> + KI reaction.

Deleted:

Deleted: (Neutral Buffered KI)

Deleted: its

Deleted: s

Formatted: English (US)

Deleted: , JGR

1944  
 1945 Primary reaction pathway:



1947 In ion-notation:



1949 Or in detail (postulated after Saltzman & Gilbert, 1959) :

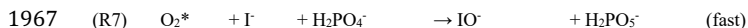


1953 Losses of IO<sup>-</sup>, i.e. I<sub>2</sub>:



- 1956 • If all O<sub>3</sub> would be absorbed and react with KI in this primary reaction pathway, it would be expected that the
- 1957 stoichiometry for O<sub>3</sub>/IO<sup>-</sup> i.e. O<sub>3</sub>/I<sub>2</sub> in neutral/acid solution is equal to one.
- 1958 • However, self-reaction of IO<sup>-</sup> (R6) can be a loss mechanism, competing with the formation of I<sub>2</sub> (R4).
- 1959 • In general, loss mechanisms of IO<sup>-</sup> might compete with (R4) and then the stoichiometry of the primary reaction pathway
- 1960 is less than one.
- 1961 • ECC shows for 1% KI and no buffer a stoichiometry less than one (Johnson et al., 2002).
- 1962 • Dismutation (disproportioning) of IO<sup>-</sup> into iodate (IO<sub>3</sub><sup>-</sup>) and I<sup>-</sup> is extremely slow and is of no importance in case of the
- 1963 ECC-sensor. Iodate-chemistry plays first a role at significantly higher KI or O<sub>3</sub> concentrations than are used in the ECC-
- 1964 sensor or encountered in the atmosphere, respectively.

1965  
 1966 Secondary Reaction Pathway: Impact of Phosphate Buffer



1970 But also losses of I<sub>2</sub> iodine (via IO<sup>-</sup> losses):



- 1973 • R7 is the key reaction to form extra IO<sup>-</sup> that can react via (R4) into I<sub>2</sub> and is contributing in addition to the fast reaction
- 1974 pathway and thus adding to the stoichiometry causing the fast ECC signal.

- 1980 •  $\text{H}_2\text{PO}_5^-$  can be seen as the interim reactant that is formed fast but via (R8) decaying slowly to form extra  $\text{IO}^-$ . This latter
- 1981 can produce in addition extra  $\text{I}_2$  which is causing the slow part of the ECC current.
- 1982 • It is known that  $\text{H}_2\text{PO}_5^-$  reacts similar as  $\text{H}_2\text{O}_2$  to form  $\text{IO}^-$ , i.e.  $\text{I}_2$  with typical time constant of about 25 minutes: this fits
- 1983 to the slow, secondary response time of ECC of typical 25 minutes.

#### 1984 Appendix B: Laboratory Experiments to Determine $S_s$ for EN-SCI SST0.1

1985 As no time response tests are available during JOSIE campaigns for SST0.1 to determine  $S_s$ , we undertook laboratory

1986 measurements under room conditions in Uccle (Belgium). During the experiments, 4 ozonesondes were simultaneously

1987 exposed to ozone amounts generated by a photometric ozone calibrator Teledyne API T703 according to the following

1988 scheme (3 times): 30 minutes of exposure to a value of  $450 \mu\text{g}/\text{m}^3$  (around 225 ppb) ozone were preceded and succeeded by

1989 10 minutes of ozone-free air, see Fig. B1. The value of  $450 \mu\text{g}/\text{m}^3$  has been imposed by the upper limit ( $6.5 \mu\text{A}$ ) of the

1990 microcurrent meters used in the Forschungszentrum Jülich homemade ground calibration box for the 4 ozonesondes. These

1991 microcurrents were read out digitally and, as in the JOSIE experiments, the  $S_s$  values were again estimated as the average

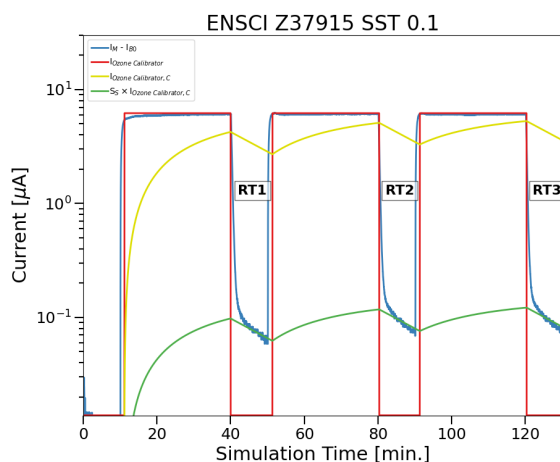
1992 over a 50 seconds time interval between 4 and 5 minutes after the end of the ozone exposure. As the time response test

1993 intervals in these laboratory measurements are twice as long (10 minutes) as in the JOSIE 2009/2010 campaigns, we tried

1994 different timings for the determination of the  $S_s$  values, but they did not give significantly different results for the slow

1995 stoichiometry coefficients. Again, the differences between the  $S_s$  values obtained from the different time response test

1996 intervals  $RT$  in one experiment were insignificant as well.



1997

1998 **Figure B1.** Example of a series of three upward and downward ozone steps generated by a photometric ozone calibrator

1999 Teledyne API T703 (represented by the generic  $I_{\text{Ozone Calibrator}}$ , red line) and the response of the measured cell current  $I_M - I_{B0}$

2000 (blue line) of an EN-SCI SST01 ozonesonde as function of time, the 25 min convolved  $I_{\text{Ozone Calibrator, C}}$  (yellow line) and the

2001 slow current after determination and application of  $S_s$  ( $S_s \times I_{\text{Ozone Calibrator, C}}$ : green line).

2002

2003 In total, we have 8  $S_s$  estimations with 4 EN-SCI ozonesondes filled with SST0.1 solutions coming from 3 different

2004 experiment runs: 2 runs with each 2 (new) EN-SCI ozonesondes (with SST0.1), and a run with all 4 (re-used) EN-SCI

2005 ozonesondes involved. These 4 ozonesondes, all with serial numbers Z379xxx, have been prepared by the same person,

2006 according to the SOPs defined in GAW Report No.268, 2021. The median value for  $S_s$  for the 8 experiments, each including



three-time intervals, is  $0.023 \pm 0.005$ . This value is very close to the value  $S_S=0.017$  found for SST0.5 during the JOSIE 2009/2010 campaign, whereas a smaller value could be expected due to the lower buffer amount in SST0.1 (see Johnson et al., 2002 and Sect. 3.2). However, the same Uccle experimental setup and method as described here above for EN-SCI SST0.1 have been used to determine the  $S_S$  coefficient for 4 EN-SCI ozonesondes filled with SST0.5 (serial numbers Z379xxx, but different from those used with SST0.1) during two experimental runs. The resulting median value,  $0.022 \pm 0.004$ , is again in close agreement with the value determined for EN-SCI SST0.5 with the JOSIE 2009/2010 ( $0.018 \pm 0.004$ ), confirming the consistency between the two instrumental setups to determine the stoichiometry coefficients. Nevertheless, a JOSIE campaign is foreseen in 2024 to determine the  $S_S$  factors for SST0.1 for both EN-SCI and SPC ozonesondes, using the same simulation setup as in JOSIE 2009/2010.

Deleted: 3

**Appendix C: How to use TRCC in practice: Practical Guidelines**

Deleted: + calibration functions

In this appendix, we give a schematic overview of the different steps that need to be taken to implement the TRCC in the data processing of an ozonesonde time series in practice, displayed schematically in the flow chart in Fig. C1.

Deleted: + calibration functions

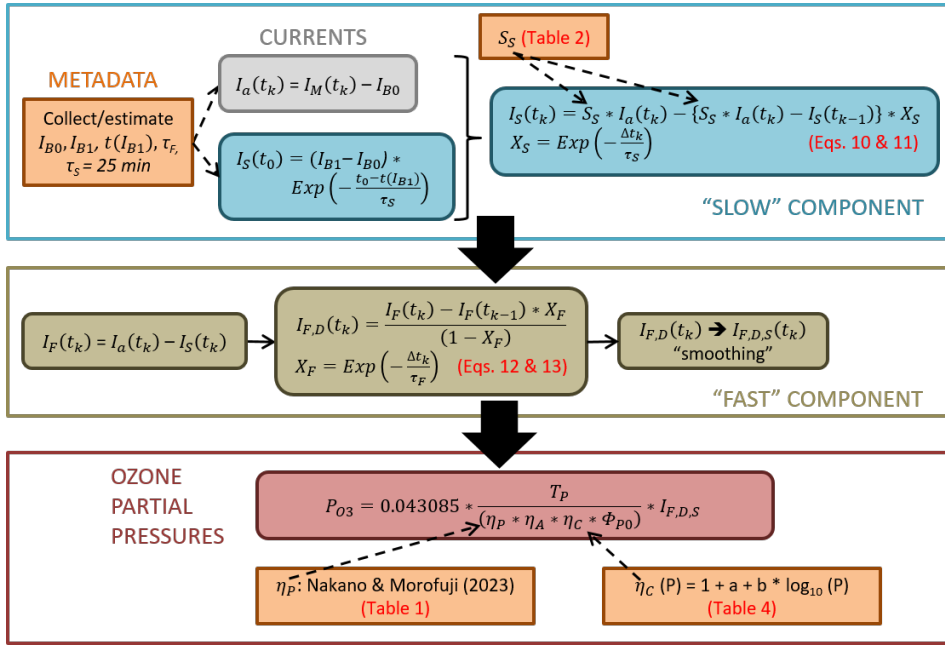


**Figure C1.** Flow chart summarizing the processing steps for the Time Responses Correction & Calibration (TRCC) method for correcting ozonesonde data. The table and equation numbers in red refer to these in this paper.

Deleted: Resolving

Deleted: Method

First, it should be noted that the TRC is applied on the currents measured by the ozonesonde. Hence, these ozonesonde's raw measurements should be available. Normally, when a site has been homogenized as part of the O3S-DQA activity, the currents have been made available or have been converted back from the ozone partial pressures. Secondly, the TRCC demands the knowledge of some metadata parameters that should have been measured during the preparation of the

2034 ozonesonde 0-1 day prior to launch (see also Fig. C1):  $I_{B0}$ ,  $I_{B1}$ , the time of the  $I_{B1}$  measurement (relative to the launch time),  
 2035 and the sensor fast response time  $\tau_F$ , measured as the time to drop from 4.0 to 1.5  $\mu\text{A}$  (after the 5  $\mu\text{A}$  test). If those metadata  
 2036 parameters are missing, these might be estimated as the means over a representative time period, e.g. using the same filter for  
 2037 determining the background currents, or the same batch of ozonesonde serial numbers or sensing solution for the fast  
 2038 response time.

2039 In a next step, the  $I_{B0}$  value is subtracted from the time series of measured currents of the sounding, resulting in  $I_a(t)$ , and all  
 2040 forthcoming calculations should be done with those currents  $I_a(t)$ . As the calculation for obtaining the slow component of  
 2041 the ECC signal is a recursive equation (Eq. 10), the slow component at launch time should be estimated first. Therefore, it  
 2042 suffices to start from the last measured value of the ozonesonde before launch, the  $I_{B1}$ , corrected for (i.e. subtract) the  $I_{B0}$   
 2043 value, and convolve it with an exponential decay function with a slow time constant of 25 minutes. Hereby, the time  
 2044 difference between the  $I_{B1}$  measurement and the launch is used. If this time difference is large enough (GAW Report No.  
 2045 268 recommends a minimum 30-min time window), the exponential decay function will be close to zero,  $I_{B1}$  will approach  
 2046 the  $I_{B0}$  value, and the slow component at launch time will be zero, which is the allowed lower limit. Now, for every time  
 2047 step, the slow component of the ECC signal can be calculated from equations (10) and (11), using the stoichiometry factor  $S_s$   
 2048 from the sonde-SST combination (see Table 2). This slow component can be seen as a time varying background current and  
 2049 should be subtracted from the currents  $I_a(t)$ , to be left over with the fast component  $I_F$  of the ECC signal.

2050 To eliminate the 20 to 25 seconds response delay in the fast component, the latter can be deconvolved (Eqs. 12 and 13), i.e.  
 2051 corrected for the exponential decay of the signal with the fast sensor response time, measured before launch. This  
 2052 deconvolution will introduce a lot of noise in the signal, and therefore, a smoothing of the current, either before or after the  
 2053 deconvolution, will be necessary. Different smoothing algorithms can be considered, with different filter widths and/or time  
 2054 windows (e.g. for running averages). The choice of the smoothing algorithm depends on the application, e.g., to resolve  
 2055 steep vertical gradients, on the profiles (smooth mid-latitude vs. upper-tropospheric tropical profile), as well as on the  
 2056 measurement time interval (10 s versus 1 s time resolution). At the end, a compromise between the smoothness of the profile  
 2057 and a full correction for the time response delay around strong vertical gradients should be sought.

2058 The smoothed, deconvolved time series of the fast component  $I_{F,D,S}$  of the ECC signal is then used in the basic equation of  
 2059 the ozonesonde signal, converting the current to ozone partial pressure. In this equation, the recommended corrections for  $T_F$ ,  
 2060  $\eta_A$ , and  $\phi_{P0}$  in GAW Report No. 268 should be implemented as well: the conversion to the piston pump temperature [E-3-  
 2061 15], a correction for the absorption efficiency if the cathode cell was only filled with 2.5  $\text{cm}^3$  of solution before launch [E-3-  
 2062 11-A&B], and the humidification [E-3-4] and pump temperature [E-3-7] corrections for the pump flow rate at the ground. In  
 2063 comparison with the recommended processing in GAW Report No. 268, the true pump efficiency corrections proposed by  
 2064 Nakano & Morofuji (2023) should now be used for all combinations of sonde type and SSTs, as these are the actual  
 2065 measured ones. The Komhyr (1986) and Komhyr et al. (1995) tables should be discarded, as these are empirical effective  
 2066 efficiency curves, as they actually combine pump efficiency and conversion efficiency. A last difference with the  
 2067 conventional method as proposed in GAW Report No. 268 is the use of the "calibration functions" defined in Sect. 6, Eq. 18:  
 2068  $\eta_C(P) = 1 + a + b * \log_{10}(P)$ , with the coefficients  $a$  and  $b$  determined for every sonde type and SST combination separately  
 2069 (see Table 4), for the conversion efficiency, instead of adopting the value  $\eta_C(P) = 1.00$ . Using the calibration functions, the  
 2070 ozone sounding measurement should be traceable to the common reference of the ozonesonde network, the ozone  
 2071 photometer OPM in the simulation chamber of the World Calibration Centre for Ozonesondes in Jülich.

2072

2073 To calculate the uncertainties associated with the ozone partial pressure measurements of an ozonesonde, corrected with  
 2074 TRC, the uncertainty equation E-3-1 in GAW Report No. 268 (2021) forms the basis. With respect to this formula, the  
 2075 uncertainty equation for the TRC (see also Fig. C2) has one changed term, and the meaning of a couple other terms has  
 2076 changed. We will only describe these 3 terms here.

Deleted:

Deleted:

Deleted: and

Deleted: correction

Deleted:  $p$

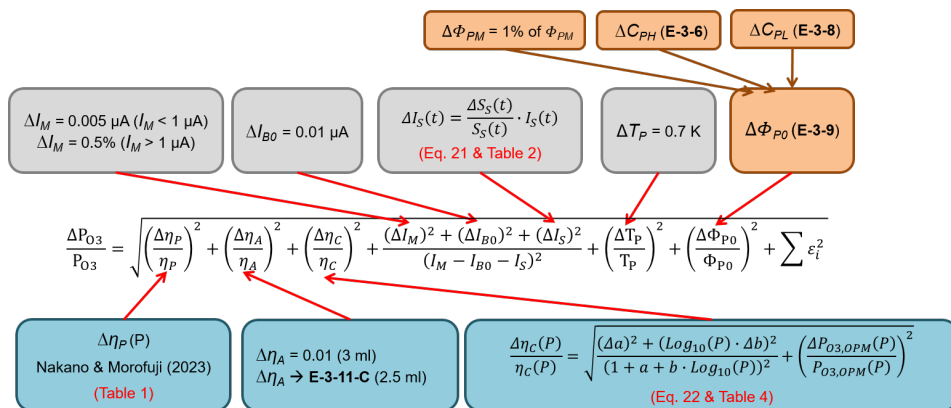
Deleted:  $p$

Deleted:  $p$

Deleted:

Deleted: + calibration functions,

2086  
2087



2088  
2089

**Figure C2.** Overview of the different data processing steps and input to derive the uncertainty of the ozone partial pressure measured with an ozonesonde, using the TRCC. Figure adapted from Fig. C-4 in GAW Report No. 268 (2021). The equation numbers also refer to equations in this GAW report. Table numbers in red refer to tables in the main text of this paper.

2093

First, as both the  $I_{B0}$  and slow component  $I_S$  are subtracted from the measurement background in the TRC, the uncertainties of the  $I_{B0}$  and  $I_S$  should be included now. For  $I_{B0}$ , the uncertainty is estimated to be  $0.01 \mu\text{A}$ , and the (relative) uncertainty of the slow component is, in a first order approximation, equal to the (relative) uncertainty of the stoichiometric coefficient  $S_S$ . The uncertainties of  $S_S$  for the different SSTs can be found in Table 2.

2098

For TRCC, the uncertainties of the pump efficiencies  $\Delta \eta_P(P)$  are now equal to the standard deviations of the true pump efficiency measurements reported in Nakano & Morofuji (2023), also shown in Table 1. Finally, the uncertainty of the conversion efficiency is no longer estimated as a fixed value  $\Delta \eta_C(P) = 0.03$ , but should take into account the uncertainty of the derived calibration functions  $\eta_C(P) = 1 + a + b \cdot \log_{10}(P)$  in Sect. 6 (see Table 4 for the uncertainties on the linear regression coefficients  $a$  and  $b$  for the different combinations of sonde type and SST), as well as the uncertainty of the photometer (OPM) to which the ozonesonde measurements are traced back. This latter (relative) uncertainty  $\frac{\Delta P_{O_3,OPM}(P)}{P_{O_3,OPM}(P)}$  is estimated to be around 2%.

2104  
2105

Deleted: + calibration functions

Deleted: y

Deleted: y

Deleted: a

Formatted: Font: Italic

Deleted: =

Formatted: Font: Italic

Formatted: Font: Italic

Deleted: p

Deleted: p

2113 **Appendix D: Nomenclature of parameters**

2114	$I_{B0}$	Background Current before exposure with ozone (after 10 min flushing cathode cell with “zero” air)
2115	$I_{B1}$	Background Current after exposure with ozone (after 10 min flushing cathode cell with “zero” air)
2116	$I_{B2}$	Background Current at launch site just before flight
2117	$I_B$	Background Current used in data processing in Eq. (1)
2118	$S_F$	Stoichiometry factor of fast reaction pathway of conversion of $O_3$ into $I_2$
2119	$S_S$	Stoichiometry factor of slow reaction pathway of conversion of $O_3$ into $I_2$
2120	$I_M$	Measured (cathode) cell current
2121	$I_{OPM}$	Ozone equivalent ECC current at time t derived from OPM
2122	$I_F$	Fast cell current
2123	$I_{F,D}$	Fast cell current, deconvolved
2124	$I_{F,D,S}$	Fast cell current, deconvolved, smoothed
2125	$I_S$	Slow cell current
2126	$P_{O_3}$	Ozone partial pressure
2127	$R$	Universal gas constant
2128	$F$	Faraday constant
2129	$T_P$	Pump temperature
2130	$\Phi_{P0}$	Pump flowrate
2131	$\eta_A$	Absorption efficiency
2132	$\eta_P$	Pump efficiency
2133	$\eta_C$	Conversion efficiency
2134	$\eta_T$	Total (overall) efficiency
2135	$\tau_F$	Response time of fast reaction pathway of conversion of $O_3$ into fast cell current component
2136	$\tau_S$	Response time of slow reaction pathway of conversion of $O_3$ into slow cell current component
2137	<b>RT1, RT2, RT3, RT4</b>	Response time tests in vertical ozone profile
2138		
2139		

Deleted: ¶

Deleted:

Deleted:

Deleted:

Deleted:

2145	<b>Appendix E: List of Abbreviations</b>	
2146	<b>ASOPOS</b>	Assessment of Standard Operating Procedures for OzoneSondes
2147	<b>BESOS</b>	Balloon Experiment on Standards for OzoneSondes
2148	<b>CMDL</b>	Climate Monitoring and Diagnostics Lab (formerly called GMD, now GML)
2149	<b>ECC</b>	Electrochemical Concentration Cell
2150	<b>EN-SCI</b>	Environmental Science Corporation; ECC ozonesonde manufacturer
2151	<b>ESRL</b>	Earth System Research Laboratories
2152	<b>FZJ</b>	ForschungsZentrum Jülich
2153	<b>GAW</b>	Global Atmosphere Watch
2154	<b>GML</b>	Global Monitoring Laboratory (division of NOAA's ESRL; formerly GMD)
2155	<b>H<sub>2</sub>O<sub>2</sub></b>	Hydrogen peroxide
2156	<b>IAP</b>	Institute of Atmospheric Physics, Beijing, China
2157	<b>IGACO</b>	<u>Integrated Global Atmospheric Chemistry Observations</u>
2158	<b>IOC</b>	<u>International Ozone Commission</u>
2159	<b>IPCC</b>	Intergovernmental Panel on Climate Change
2160	<b>JMA</b>	Japanese Meteorological Agency
2161	<b>JOSIE</b>	Jülich OzoneSonde Intercomparison Experiment
2162	<b>KI</b>	Potassium Iodide
2163	<b>NASA</b>	National Aeronautics and Space Administration
2164	<b>NBKI</b>	Neutral-Buffered Potassium Iodide
2165	<b>NDACC</b>	Network for the Detection of Atmospheric Composition Change
2166	<b>NOAA</b>	National Oceanic and Atmospheric Administration
2167	<b>NO<sub>x</sub></b>	Nitrogen Oxides
2168	<b>O3S-DQA</b>	OzoneSonde-Data Quality Assessment
2169	<b>OPM</b>	Ozone PhotoMeter instrument (used as <u>ozone UV-photometer</u> reference at WCCOS)
2170	<b>SHADOZ</b>	Southern Hemisphere ADDitional OZonesonde
2171	<b>SP<sup>2</sup>N</b>	Ozone trend assessment study supported by SPARC, IOC, IGACO, and NDACC
2172	<b>SOP</b>	Standard Operating Procedure
2173	<b>SPARC</b>	Stratosphere-troposphere Processes And their Role in Climate
2174	<b>SPC</b>	Science Pump Corporation; ECC ozonesonde manufacturer
2175	<b>SST</b>	Sensing Solution Type
2176	<b>SST0.1</b>	1.0% KI & 1/10th buffer solution
2177	<b>SST0.5</b>	0.5% KI & half pH-buffer solution
2178	<b>SST1.0</b>	1.0% KI & full pH-buffer solution
2179	<b>SST2.0</b>	2.0% KI & non-pH-buffered solution with no KBr
2180	<b>STP</b>	Standard Temperature (=273.15 K) and Pressure (=1013.25 hPa) conditions
2181	<b>TOAR</b>	Tropospheric Ozone Assessment Report
2182	<b>TRC</b>	Time Responses <u>Correction</u>
2183	<b>TRCC</b>	<u>TRC + Calibration</u>
2184	<b>UNEP</b>	United Nations Environment Programme
2185	<b>UV</b>	Ultraviolet
2186	<b>UWYO</b>	University of Wyoming
2187	<b>VOC</b>	Volatile Organic Compound

Deleted: (Green marked are mentioned in manuscript)

Deleted: ic

Deleted: Resolving

Deleted: Methodology

- 2192 **WCCOS** World Calibration Centre for OzoneSondes
- 2193 **WMO** World Meteorological Organization

